March 2005

PERFORMANCE-BASED SEISMIC DESIGN OF EBF USING TARGET DRIFT AND YIELD MECHANISM AS PERFORMANCE CRITERIA

by

Shih-Ho Chao
Subhash C. Goel

A report on research sponsored by the
American Institute of Steel Construction

Department of Civil and Environmental Engineering
The University of Michigan
Ann Arbor, MI 48109-2125

ACKNOWLEDGEMENT

The authors gratefully acknowledge partial financial support provided by the American Institute of Steel Construction for this study. The senior author also received a stipend from the G. S. Agarwal Fellowship Fund at the Department of Civil & Environmental Engineering while working on this project. The opinions and views expressed in the report are solely those of the authors and do not necessarily reflect those of the sponsors.

PERFORMANCE-BASED SEISMIC DESIGN OF EBF USING TARGET DRIFT AND YIELD MECHANISM AS PERFORMANCE CRITERIA

EXECUTIVE SUMMARY

Eccentric braced steel frames (EBFs) are very efficient structures for resisting earthquakes as they combine the ductility of that is characteristic of moment frames and the stiffness associated with braced frames. In the EBFs inelastic activity is confined to a small length of the floor beams which yields mostly in shear (therefore called the shear link). Capacity design approach is followed in an attempt to limit the inelastic activity to the shear links only while all other frame members are designed to behave elastically. Research work carried out during the seventies and eighties led to the formulation of design code provisions. However, current design practice generally follows elastic analysis procedures in proportioning the frame members. Therefore, it is possible that yielding in the shear links may not be uniformly distributed along the height of the structure and may be concentrated in a few floors causing excessive inelastic deformations at those levels.

In this study a new design procedure based on energy and plastic design concepts is applied to EBFs. The design approach was originally developed and successfully applied to steel moment frames. The procedure begins by selecting a desired yield mechanism for the structure. The design base shear and lateral forces are determined from input spectral energy for a given hazard level needed to push the structure in the yielded state up to a selected target drift. The frame members are then designed by following the plastic design method in order to develop the

needed strength and the intended yield mechanism.

Two EBFs (3-story and 10-story) were selected for this study. These frames have been used in a recent related study where they were designed by following current design practice and IBC 2000 provisions. Those frames were re-designed by the proposed performance-based design methodology by using the same basic design spectral values as used for the code designed frames. The proposed design procedure was validated by extensive non-linear analyses for a number of ground motion records. Comparisons are made between the responses of the code designed frames with the ones designed by the proposed method. The results confirm the validity of the proposed method for the study EBFs in terms of meeting all the performance design objectives, such as target drifts, intended yield mechanism, etc. The frames designed by the proposed method showed superior performance over the code designed frames, and the total weights of steel used in the frames designed by those two approaches were the same.

TABLE OF CONTENTS

LIST OF TABLES

Table

LIST OF FIGURES

Figure

CHAPTER 1

Introduction

1.1 General

While steel moment frames can exhibit stable inelastic and ductile behavior under cyclic seismic excitation, the concentrically braced frames usually possess greater lateral stiffness which can limit the damage due to drift. However, moment frames are relatively flexible and their design is usually governed by the drift limitations in order to control the damage. On the other hand, the ductility and energy dissipation capacity of concentrically braced frames can significantly deteriorate if braces buckle under seismic loading. Eccentrically braced frames (EBFs) successfully combine the advantages of the moment frames and concentrically braced frames, namely high ductility and lateral stiffness, while eliminating the shortcomings of those frames by limiting the inelastic activity to ductile shear links and keeping braces essentially elastic without buckling, thus maintaining high lateral stiffness during earthquake events.

EBFs are characterized by an isolated segment of beam, which is referred to as *link*. The diagonal brace, at least at one end, is connected to the end of the link rather than the beam-column joint. All inelastic activity is intended to be confined to the properly detailed links. Links act as structural fuses which can dissipate seismic input energy without degradation of strength and stiffness, thereby limiting the forces transferred to the adjacent columns, braces, and beam segments. Typical EBF configurations are illustrated in Figure 1.1; in which the link length e of each type in EBF is highlighted.

Link plastic rotation angle (γ_p) can be easily estimated by frame geometry assuming rigid-plastic behavior of the frame members. The relationship between plastic story drift angle and link plastic rotation angle for the three types of EBFs is shown in Figure 1.2 (AISC, 2002). Depending on the section properties of the link, link may yield either in shear extending over the full length of the link or in flexure at the link ends, or the combination of shear and flexural yielding. Note that link plastic rotation angle is the same whether the link yields in shear or in flexure. Yielding mechanism of links depends on material properties of links such as moment capacity, shear capacity, and strain hardening. Equations to determine the length ranges and allowable link inelastic rotation angles have been developed for W sections as specified in AISC Seismic Provisions (Kasai and Popov, 1986; AISC 2002):

- Short (Shear yielding) links:

$$e \le 1.6\frac{M_p}{V_p} \qquad \gamma_p = 0.08 \text{ radians} \tag{1.1}$$

- Long (flexural yielding) links:

$$e \ge 2.6\frac{M_p}{V_p} \qquad \gamma_p = 0.02 \text{ radians} \tag{1.2}$$

- Intermediate length (combination of shear and flexural yielding) links:

$$1.6\frac{M_p}{V_p} < e < 2.6\frac{M_p}{V_p} \qquad \gamma_p = \text{ interpolation between 0.08 and 0.02 radians} \tag{1.3}$$

where $M_p = ZF_y$ is the nominal plastic flexural strength; Z is the plastic section modulus; F_y is the specified minimum yield stress. $V_p = 0.6F_y(d_b - 2t_f)t_w$ is the nominal shear strength; d_b is the

overall beam depth; t_f and t_w are the thicknesses of flange and web, respectively. Note that a small *e/L* ratio (*L* is the span length of beam) does not necessarily imply a short link. As suggested in the foregoing length criteria, the beam section properties determine the link category rather than the *e/L* ratio.

Considerable research has been undertaken on EBFs since mid-1970's, beginning with pseudo-static tests on one-third scale three-story EBF (Roeder and Popov, 1977; Manheim, 1982), followed by a five-story one-third scale model tested on shaking table (Yang, 1982). Isolated link tests were performed by Hjelmstad and Popov (1983) and by Malley and Popov (1983, 1984). Extensive subassemblages consisting of link, beam, or slab were tested by Kasai and Popov (1986) and by Ricles and Popov (1987). The tests with short shear yielding links showed that EBFs are very ductile and stable frames for resisting seismic loading. However, the architectural openings available by using short links sometimes are not sufficient. As a consequence, long links with flexural yielding were developed and tests were carried out by Engelhardt and Popov (1989a, 1992), in which the subassemblages tested included link, beam, and brace. Pseudo-dynamic testing was conducted on a full-scale six-story EBF building as part of the US-Japan Cooperative Program (Roeder, Foutch, and Goel, 1987; Foutch, 1989). A 0.3-scale EBF building was tested on shaking table by Whittaker, Uang, and Bertero (1987). More recently, isolated short and long links made from A992 steel were tested at University of Texas, Austin (Arce, 2002; Gálvez, 2004); large scale welded built-up shear links for the San Francisco-Oakland Bay self-anchored suspension bridge were tested at University of California, San Diego (McDaniel, Uang, and Seible, 2003). All the experimental work done to date has demonstrated the superior seismic performance and led EBFs to be among the popular

seismic-resistant steel framing systems.

1.2 Design of EBFs

Although outstanding performance of shear links has been experimentally validated, the global behavior of EBFs can be poor such as concentration of inelastic deformation at a few floors or plastic activity in columns. The former results from poor proportioning of links (Popov, Ricles, and Kasai, 1992), and the latter is attributable to higher modes of structural vibration, as well as to prevailing elastic design methods which cannot accurately capture the distribution of lateral forces in the inelastic state. EBF design methodologies are diverse and can be basically categorized as elastic design method (Becker and Ishler, 1996; Bruneau, Uang, and Whittaker, 1998; SEAOC, 2000) and plastic design method (Roeder and Popov, 1977; Manheim, 1982; Kasai and Popov 1986a; Englekirk, 1994). A review of current EBF design criteria based on AISC Seismic Provision (AISC, 2002), the conventional elastic and plastic design method is briefly described in the following.

1.2.1 AISC Design Criteria

Key points for designing an EBF in accordance with the AISC Seismic Provisions (AISC, 2002) are summarized herein. Focus is kept on shear yielding links in this report.

(1) Inelastic action is intended to occur primarily within the shear links; therefore elements outside the links such as beam segment, diagonal brace, and column should be designed following capacity design approach. That is, these elements should remain essentially elastic

under the maximum forces that can be generated by the fully yielded and strain-hardened links. It should be noted that a soft story could form if formation of plastic hinges in columns are combined with the yielded links; therefore plastic hinges should be avoided in the columns.

(2) For shear links, the design shear strength is calculated as:

$$\phi V_n = 0.9V_p = 0.9(0.6F_yA_w) = 0.9\left[0.6F_y(d_b - 2t_f)t_w\right] \tag{1.4}$$

where ϕ is the resistance factor which is taken as 0.9. F_y is the specified minimum yield stress and shall not exceed 50 ksi because all the experiments conducted earlier used links with a specified minimum yield stress of 50 ksi or less. d_b is the overall beam depth; t_f is the thickness of flange; t_w is the thickness of web. In order to have shear yielding inelastic response, the link length should satisfy Eq. (1.1).

(3) Links should comply with the width-thickness ratio prescribed in Table I-8-1 in the AISC Seismic Provisions, namely:

- For flanges of I-shaped beams:

$$\frac{b_f}{2t_f} \le 0.30\sqrt{\frac{E_s}{F_y}} = \frac{52}{\sqrt{F_y}} \tag{1.5}$$

- For webs of I-shaped beams:

$$\frac{h}{t_w} \le 3.14\sqrt{\frac{E_s}{F_y}}\left(1-1.54\frac{P_u}{\phi_b P_y}\right) = \frac{535}{\sqrt{F_y}}\left(1-1.54\frac{P_u}{\phi_b P_y}\right) \quad \text{when} \quad \frac{P_u}{\phi_b P_y} \le 0.125 \tag{1.6.1}$$

$$\frac{h}{t_w} \le 1.12\sqrt{\frac{E_s}{F_y}}\left(2.33-\frac{P_u}{\phi_b P_y}\right) = \frac{191}{\sqrt{F_y}}\left(2.33-\frac{P_u}{\phi_b P_y}\right) \quad \text{when} \quad \frac{P_u}{\phi_b P_y} > 0.125 \tag{1.6.2}$$

The flange width-thickness ratio limitation is satisfied by most ASTM A36 rolled shapes (F_y = 36 ksi). However, for the current prevailing ASTM A992 rolled shapes (F_y = 50 ksi), at least 52 wide-flange shapes are prohibited by this limitation ($52/\sqrt{F_y}$ =7.35) due to higher specified minimum yield stress. In order to justify this limitation, Arce (2002) tested seven $W10\times33$ sections with lengths ranging from shear to flexure dominated yielding ($b_f/2t_f = 9.2$ which exceeds $52/\sqrt{F_y}$ =7.35) and two $W16\times36$ sections ($b_f/2t_f = 7.15$ which is smaller than $52/\sqrt{F_y}$ =7.35). Results showed that all $W10\times33$ sections achieved their target plastic rotation angles without strength degradation due to flange buckling, while only one $W16\times36$ section failed to achieve target plastic rotation. Consequently, a relaxation of width-thickness ratio from $52/\sqrt{F_y}$ to the AISC LRFD Specification (AISC, 2001) prescribed ratio, *i.e.*, $65/\sqrt{F_y}$ ($0.38\sqrt{E_s/F_y}$), was suggested (Arce, 2002; Arce, Okazaki, and Engelhardt, 2003).

(4) To assure that yielding and energy dissipation in an EBF occur primarily in the links, capacity design approach is adopted for design of the diagonal brace and the beam segment outside the link. That is, the diagonal brace and beam segment outside the link are designed to resist the forces generated by the fully yielded and strain hardened link. For short links ($e \leq 1.6M_p/V_p$), the generated forces can be calculated as:

$$\text{Link shear} = 1.25R_yV_p \quad (1.7)$$

$$\text{Link end moment at column} = R_yM_p \quad (1.8)$$

$$\text{Link end moment at brace} = [e(1.25R_yV_p) - R_yV_p] \geq 0.75R_yV_p \quad (1.9)$$

where R_y is the ratio of the expected yield strength to the minimum specified yield strength F_y prescribed in AISC Seismic Provisions Table I-6-1 (AISC 2002). For ASTM A992 steel, R_y = 1.1. This ratio is used to account for possible material overstrength. The shear strength is further increased by 1.25 to account for strain hardening. Based on results of 16 links made from A992 steel (Arce, 2002), the average strain hardening ratio was formed to be 1.28, with a variation ranging from 1.17 to 1.44. Therefore, the 1.25 strain hardening ratio specified in the AISC Seismic Provisions is reasonable for A992 rolled shapes. Unequal end moments of link at column and brace are specified based on the experimental results for short links (Kasai and Popov, 1986).

However, for the design of the beam segment outside the link, the required beam strength

based on only 1.1 times the link expected shear strength is allowed by the Provisions. Namely,

$$\text{Link shear} = 1.1R_yV_p \tag{1.10}$$

This relaxation on link ultimate forces results primarily from the recognition that beam strength will be considerably increased due to the presence of composite slab. Also, limited yielding is sometime unavoidable and will not cause deterioration of the energy dissipation as long as stability of the beam is assured. Usually, for EBFs in which the diagonal brace is connected to the lower flange of the beam, as shown in Figure 1.1, experimental results showed that only the upper flange would buckle out-of-plane (Engelhardt and Popov, 1989a) because the brace can provide some constraint to the lower flange. The presence of composite slab will offer substantial restraint against instability as well as the capacity to carry a portion of the axial load. For design, the required strength of the beam is computed first based on Eqs. (1.7) and (1.9), same as for the design of brace member, then the resulting axial force and flexural moment acting on the beam are reduced by a factor 1.1/1.25 = 0.88. If no composite slab is present, the required beam segment strength should be based on link strain hardening ratio of 1.25. Moreover, appropriate lateral support is necessary for both upper and lower beam flanges.

Due to the presence of high axial force and moment (Engelhardt and Popov, 1989b), both diagonal brace and beam segment outside the link are required by the Provisions to be designed as beam-column. However, it is very likely that the beam segment may not satisfy the AISC beam-column interaction equations, H1-1a or H1-1b (AISC 2001) because of the combined high axial force and moment. For such cases, increasing the size of the beam cannot solve this

problem. This is because the beam segment and link are usually made of the same section; thus increasing beam size will increase the ultimate link strength, which in turn will raise the demand on the beam segment. Special measures such as using diagonal brace with large flexural stiffness so that moment is drawn away from the beam segment, or providing cover plates on the beam could be considered. Other remedies to reduce the stress level in the beam segment can be found in the AISC Seismic Provisions. Diagonal brace is expected to remain essential elastic and design is performed according to AISC LRFD equations H1-1a or H1-1b (AISC, 2001). Same equations apply to hollow sections if adopted for diagonal braces (AISC, 2000). The width-thickness ratio of the braces should comply with the values in LRFD Specification Table B5.1.

(5) Columns of an EBF should be designed using capacity design approach. The AISC Seismic Provisions require that the columns should be able to resist the maximum expected forces generated by the fully yielded and strain hardened links. Nevertheless, Eq. (1.10) is allowed for column design rather than Eq. (1.7). This relaxation is because links above the considered column would not likely reach their maximum expected shear strength all at the same time. However, for low-rise EBF, such situation could occur and the strain hardening factor 1.25 is suggested.

1.2.2 Elastic Design Method for EBFs

Design of EBFs usually starts by selecting the length of links at all levels based on criteria such as architectural constraints. After sizing the links, the selected length of link should be checked using material properties in order to satisfy Eq. (1.1), (1.2), or (1.3) depending on

which category the link belongs to (shear yielding, flexural yielding, or combination of shear and flexural yielding). Methods of sizing link, beam segment, diagonal brace, and column using conventional elastic design procedure of EBFs can be summarized as follows:

(1) Sizing the links: This is the most important step of designing an EBF because strength and ductility of an EBF is closely related to the strength and ductility of the links, and ill-proportioned links along the height of structures can lead to concentration of large inelastic link deformations at some floor levels due to over-strengthening of links at some levels (Popov, Ricles, and Kasai, 1992). Furthermore, elements other than the links are designed based on the maximum expected strength of links thus, improper sizing of links can also cause unexpected yielding in those other elements. In general, there are two measures to size the links; the first one is to determine the required link strength based on elastic analysis (Becker and Ishler, 1996; Uang et al., 2001). Then links are designed in accordance with the load combination stipulated by the applicable building code; for instance, $V_u = 1.2V_D + 0.5V_L + 1.0V_E$ as specified in IBC 2000 or IBC 2003 (ICC, 2000 and 2003).

The second way to determine the required strength of links is based on the relationships between link shear force and frame shear force, which is directly associated with EBF geometry. This method was first proposed by Popov et al. (1986, 1987) and is applicable to the situation that link response is either elastic or inelastic. Figure 1.3 (a) illustrates this approach for a K-braced EBF. V_{link} expresses the required link strength and V_{cum} is the design story shear accumulated from the top story to the corresponding level. To simplify the calculation, moments acting at the upper and lower ends of the designated EBF panel (solid line) are neglected. By equating moments about point A, the required design strength of the link for a K-braced EBF can

be expressed as:

$$V_{link} = \frac{h}{L} V_{cum} \tag{1.11}$$

For a D-braced EBF as shown in Figure 1.3 (b), similar procedure can be carried out and the required link strength can be estimated as (Bruneau et al., 1998):

$$V_{link} = \frac{h}{L - e/2} V_{cum} \tag{1.12}$$

It is noted that in either method for proportioning the link, the capacity to demand ratio should be kept uniform at all levels to avoid concentration of large inelastic link deformation at some levels. That is,

$$\frac{\phi_v V_p}{V_u} = \lambda \geq 1.0 \text{ (suggest keeping constant for all links)} \tag{1.13}$$

where $V_u = V_{link}$ which is obtained from elastic analysis or Eq. (1.11) or (1.12); ϕ_v is the resistance factor for link; V_p is the nominal shear strength of links. It is noted that λ cannot be too large because in such case excess strength of link is provided, which in turn results in unnecessarily heavy sections of other elements outside the links.

(2) Design of diagonal brace and beam segment outside the link: This is done by following the criteria stated in Section 1.2.1.; i.e., the capacity design approach.

(3) Design of columns: The design column axial load and moment can be computed as (Becker and Ishler, 1996; SEAOC, 2000; Uang et al., 2001):

$$P_u = 1.2P_D + 0.5P_L + \left(1.1R_y\right)V_p \tag{1.14}$$

$$M_u = 1.2M_D + 0.5M_L + \left(1.1R_y\lambda\right)M_E \tag{1.15}$$

where P_u is the required axial strength for columns at a particular level; P_D and P_L are axial forces induced by dead load and live load, respectively; M_u is the required flexural strength; M_D and M_L are moments induced by dead load and live loads, respectively; M_E is the moment in the column obtained from elastic analysis using the design seismic lateral forces. λ is the capacity to demand ratio prescribed in Eq. (1.13). Eq. (1.15) is an indirect way to account for moments caused by the lateral forces when links are fully yielded and strain hardened. Note that the IBC load combination is adopted in Eqs. (1.14) and (1.15).

1.2.3 Plastic Design Method for EBFs

It has been shown that, during an earthquake, the distribution of internal forces when a structure yields is drastically different from that predicted by elastic analysis (Lee, 1996; Leelataviwat et al., 1998). Also, a global deformation mechanism which can be maintained during the entire seismic excitation is desirable. Therefore, considerable attention has been paid to the plastic design methodology because it provides internal force distribution at structural ultimate level corresponding to a selected global yield mechanism as well as realistic

representation of inelastic behavior of the structures. Since the principle of EBF design is to confine all the inelastic activities within links only, and the design is directly related to link forces in plastic state, the plastic design is considered as most rational approach for EBFs.

Plastic design concept for EBFs was first proposed by Roeder et al. (Roeder and Popov, 1977). Their technique is based on the moment balancing procedure. Assumed distribution of forces and moments must be given at the beginning then considerable amount of trial and error is performed. The second method proposed by Manheim (1982) is based on the upper bound solution satisfying the desired yield mechanism. By equating external work done by lateral forces to internal work done by the links, the required link strength at all levels can be obtained. In either one of the preceding methods it is difficult to reach an equilibrium solution for calculating the design column moments. Of greatest concern is that columns in taller frames tend to develop single curvature deformation, which in turn leads to unrealistically large moments in the columns. Other disadvantages of these methods include less accuracy and difficulty in application. Detailed review of these methods and their shortcomings can be found elsewhere (Kasai and Popov 1986a).

The third design approach was proposed by Kasai and Popov (1986a), which is more straightforward and simple to apply. The basic idea of this approach can be illustrated using a D-braced EBF free-body shown in Figure 1.4. The link shear strength, V_{link} , is first estimated by using the same procedure as shown Figure 1.3. Forces in other elements are computed through equilibrium relationships according to the expected shear force in links, unequal moments at link ends, the forces from upper story, and design lateral forces. Assumption of column inflection points is suggested to reduce the static indeterminacy of the structure and to stabilize the column

moment solutions. Because that the design has to be performed iteratively from top to the bottom of a structure, a computer program was also recommended to reduce the computational effort. It was shown that the problem of single curvature and thus large moments in the columns, as in the previous two plastic design approaches can be successfully solved by using this approach. It should be noted, however, that the design of links is not based on a selected yield mechanism, nor performed by using the conventional plastic design method, i.e., equating external work to internal work. Accordingly, the third method may be considered to a capacity design approach rather than a plastic design approach.

1.2.4 Remarks on EBF Design Approach and Research Scope

As pointed out earlier, the reason that inelastic activity should be limited within links is to prevent other elements from yielding. Experimental results have shown that well-detailed links can sustain large inelastic deformation reversals without losing strength and stiffness. Therefore global structural stability and performance will not be jeopardized if inelastic activity is confined only to links. Unintended yielding or buckling of braces or columns can result in undesirable response. Testing on weak-column strong-beam steel frames has shown that columns exhibit poor hysteretic behavior with rapid strength and stiffness deterioration if the axial load exceeds 25% of the nominal axial yield strength (Schneider and Roeder, 1993). Such unintended poor seismic behavior cannot be effectively predicted and prevented by conventional design methods. In particular, although the column design follows capacity design approach in an indirect way, the calculated design moments may not give actual distribution of moments when the yield mechanism is reached. In this regard, the design lateral forces acting on the frames should be increased in certain amount to account for the fully yielded and strain hardened links at all floor

levels. By using this treatment, the resulting distribution of moments in columns will be more realistic and, in conjunction with the amplified axial load, the capacity design can be achieved. This approach has never been used in any design procedure for EBFs.

In recent years, seismic design has been gradually moving towards performance-based design approach, which is intended to produce structures with predictable and controlled seismic performance. To achieve this goal, knowledge of the ultimate structural behavior, such as nonlinear relations between forces and deformation, yield mechanism of structural system are essential. Therefore, the global yield mechanism needs to be built into the design process.

Recently, various performance-based design methods have been developed such as capacity spectrum approach for determining the design lateral loads, displacement-based design procedure, and energy-based design procedure (Rai, 2000). The energy-based design procedure uses the balance relation between the input seismic energy and the energy dissipated by structures to predict the drift level a structure may undergo when subjected to a specified seismic hazard level. If the drift can be accurately determined at the design stage, then damage can be controlled, thus intended performance is achieved. This approach, together with the plastic design procedure, has been successfully developed and validated using steel moment frames (Leelataviwat, Goel, and Stojadinović, 1999, Lee and Goel, 2001). In this report, the same procedure was employed to design two EBFs with shear yielding links, one has three stories, and another has 10 stories. These two frames were previously designed by the AISC Steel Solution Center by conventional elastic design method. Nonlinear static pushover and dynamic time history analyses were conducted for all frames. Comparison between the responses of frames designed by two different methodologies is made in terms of drift, link deformation, energy

dissipation, and global performance.

1.3 AISC Testing Protocol for Short Links

Recently, ASTM 992 50 ksi steel has been increased used for seismic resistant structures; in fact, almost all the wide-flange shapes are currently available in A992 50 ksi steel. Increasing adoption of A992 steel is attributable to its specified maximum yield strength and maximum yield-to-tensile strength ratio. Moreover, due to the upper limit on yield strength, the possibility of the weld metal becoming under-matched is considerably reduced, thus lowering the potential for brittle fractures (Zoruba and Grubb, 2003). Current detailing requirements for links of EBFs in the AISC Seismic Provisions are mainly based on test results of links made from ASTM A36 36 ksi wide-flange shapes. Testing on various length of links made from A992 steel was conducted at the University of Texas, Austin (UTA) to investigate the adequacy of current requirements for EBF links with higher strength.

As shown in Figure 1.5, test results showed that a notable feature occurred in the shear yielding links, which was not found in the A36 shear links tested earlier, was the web fracture of the link initiating at the end of the stiffener weld. Due to this premature web fracture, most of the tested links could not achieve the target plastic rotation angles. The fractures could stem from the stiffener-to-web weld been terminated too close to the k-area (Arce, 2002), close stiffener spacing, or over stringent loading protocol for EBF links as required by the AISC Seismic Provisions (AISC, 2002). Richards and Uang (2003) analyzed the aforementioned two frames design by the AISC Steel Solution Center and concluded that the AISC loading protocol is overly conservative for short links in representing the design earthquake demands. They proposed a

revised loading protocol which required only 67% of the cumulative rotation specified by the AISC loading protocol, as well as fewer large inelastic cycles.

1.4 Organization of Report

This report is organized into six chapters. Details of each chapter are described in the following.

The overall proposed performance-based design procedure is presented in Chapter 2. A brief background regarding the design philosophy based on energy-balance principle is also given, along with two design flowcharts.

Chapter 3 presents the details of the design of study EBFs. A preliminary design based on an earlier study of SMRF was examined using non-linear dynamic analyses and a refinement was made for this study.

Chapter 4 gives the modeling details used in the Perform-3D program, as well as the earthquake records (10 % in 50 years and 2 % in 50 years SAC LA region ground motion) and the design spectra.

Chapter 5 describes the evaluation of the study EBFs using extensive non-linear pushover and dynamic analyses. The study parameters included: location of yield activity, maximum link plastic rotations, maximum relative story shear distribution, maximum interstory drifts, and peak floor accelerations.

Chapter 6 presents a brief summary of the study and important conclusions and recommendations based on the analysis results.

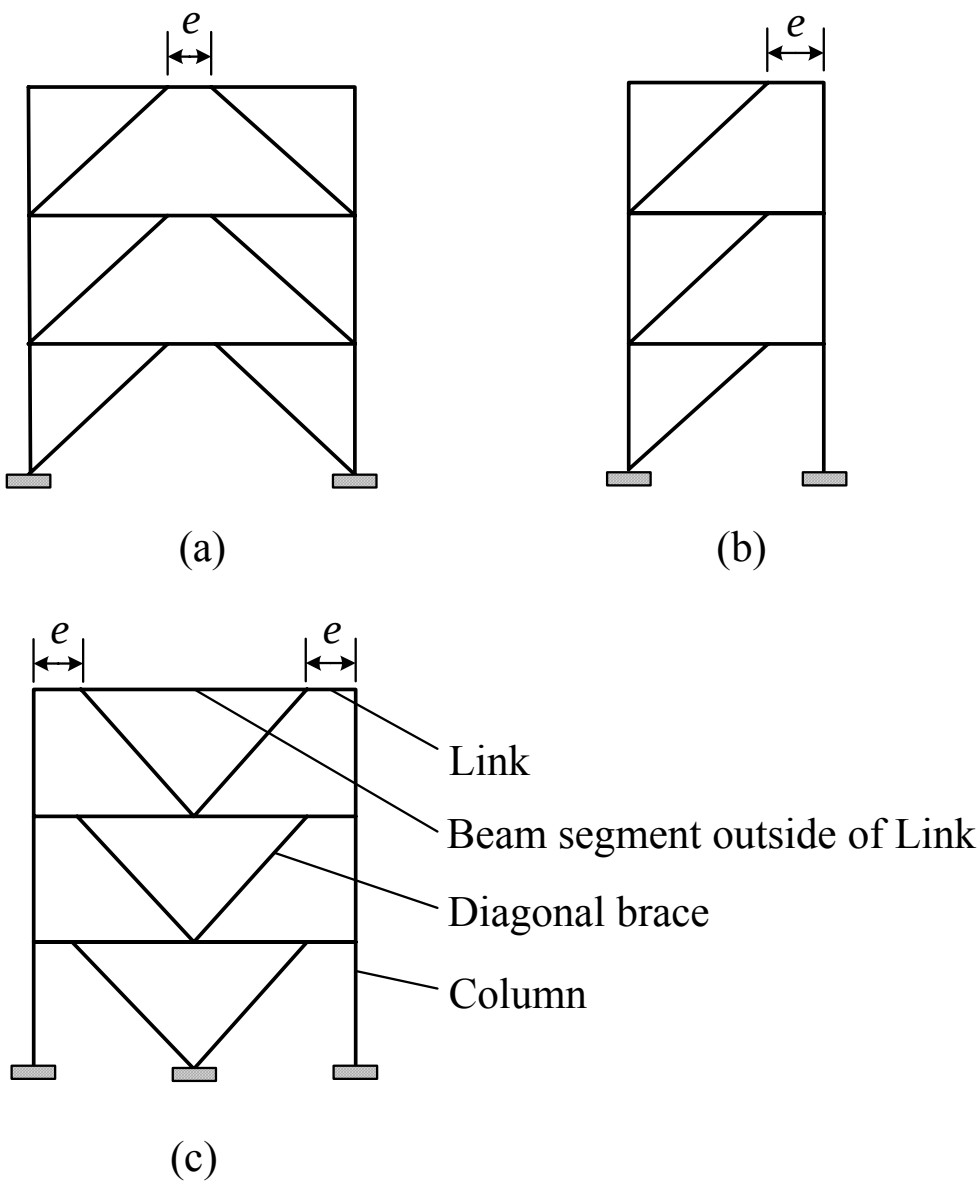

Figure 1.1 Typical eccentrically braced frames: (a) K-braced EBF; (b) D-braced EBF; (c) V-braced EBF

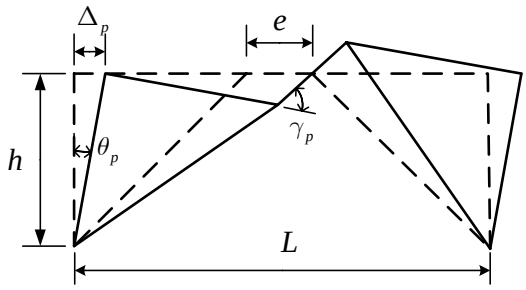

$$\gamma_p = \frac{L}{e}\theta_p$$

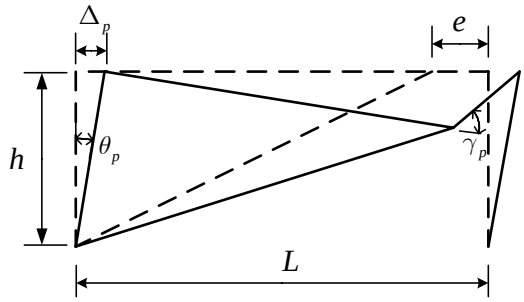

$$\gamma_p = \frac{L}{e}\theta_p$$

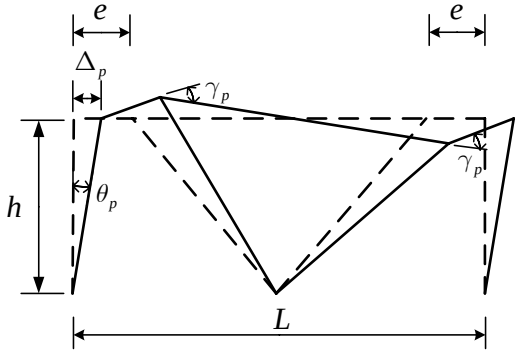

$$\gamma_p = \frac{L}{2e}\theta_p$$

L = Bay width

h = Story height

Δ_p = Plastic story drift (conservatively, take Δ_p equal to Design Story Drift)

θ_p = Plastic story drift angle, radians (= Δ_p / h)

γ_p = Link Rotation Angle, radians

Figure 1.2 Link rotation angle for various types of EBFs (AISC, 2002)

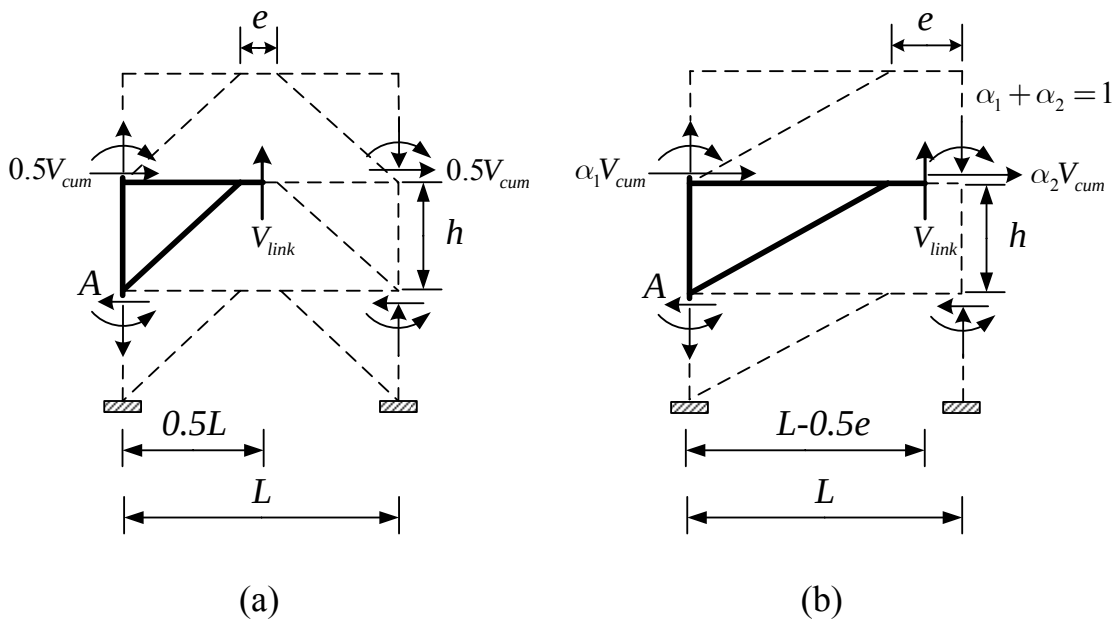

Figure 1.3 Link size proportion based on cumulative story shear and EBF configuration: (a) K-braced EBF (Popov et al., 1986, 1987); (b) D-braced EBF (Bruneau et al., 1998)

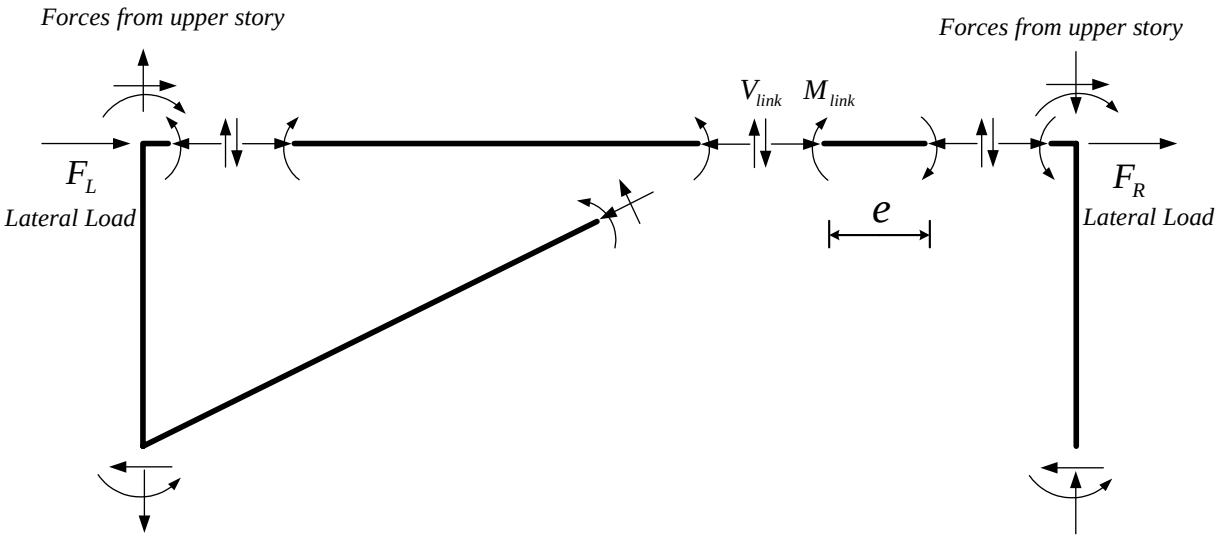

Figure 1.4 A free-body of D-braced EBF used in plastic design procedure proposed by Kasai and Popov (1986a)

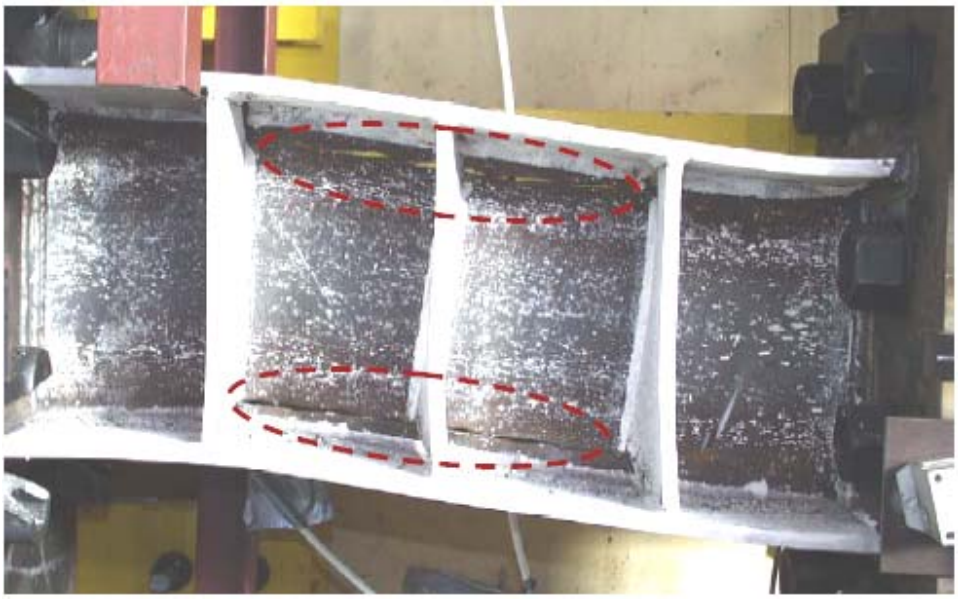

Figure 1.5 Web fractures initiating from the ends of stiffener-to-web welds in UTA short links (Specimen 4A, Arce, 2002)

CHAPTER 2

Performance-Based Seismic Design Procedure for EBF Using Pre-Selected Target Drift and Yield Mechanism

2.1 Introduction

It is desirable that structures are proportioned to yield at locations which are most capable of deforming into inelastic range and sustaining large cyclic inelastic deformations. Yielding in columns should be avoided or minimized because of the difficulty in detailing for ductile response in the presence of high axial loads and because of the possibility that excessive column yielding may result in formation of story mechanism which might cause collapse. Hence, for conventional special moment frames, capacity-design approach (strong column weak-beam) is usually employed to force plastic hinges developing at the beam ends. The strong column-weak beam design requirements in current codes, however, do not guarantee that plastic hinging would not occur in the columns during major earthquake events (Paulay and Priestley, 1992; Lee 1996). Yielding of columns may also be caused by higher modes of vibration, particularly in the upper stories, as well as due to prevailing elastic design methods which do not accurately capture the distribution of lateral forces in the inelastic range.

The performance-based design procedure, as briefly described herein, is aimed at achieving predictable and controllable behavior of structures during design level seismic events. Three major factors are essential in achieving this goal:

1) A design lateral force distribution which reflects realistic story shear distribution along

the height of the structure when subjected to severe earthquakes. The triangular force distribution used in most design codes is derived from elastic analysis and may not be valid in the inelastic state. Therefore, a design lateral force distribution derived from nonlinear dynamic analysis results and calibrated by representative ground motion records is more appropriate for performance-based design procedure.

2) A predictable global yield mechanism is more desirable so that the damage could be confined in pre-selected locations of the frame. In this regard, elastic design procedure cannot guarantee a predicable mechanism due to the predominantly inelastic nature of the structural response during severe earthquakes. Therefore, plastic design procedure is more suitable for purposes of performance-based seismic design because desirable yield mechanism is preselected. This design procedure was developed and successfully validated by Goel et al. through nonlinear dynamic analyses for the steel moment resistant frames (Leelataviwat, Goel and Stojadinović, 1999; Lee and Goel, 2001; Lee, Goel, and Chao, 2004).

3) A pre-designated target drift limit which can be incorporated in determination of the design base shear. To achieve the target building performance objectives (such as immediate occupancy, collapse prevention, etc.) for selected earthquake hazard levels the story drift is a good design parameter. Therefore, a design base shear based on selected target drift level, stiffness of the structure, ductility reduction factor, and structural ductility factor was used in this study. This design base shear was derived from modified energy balance equation and the proposed lateral force distribution (Leelataviwat, Goel and Stojadinović, 1999; Lee and Goel, 2001; Lee, Goel, and Chao, 2004).

The performance-based plastic design methodology which incorporates the above elements is briefly presented in the following for Eccentrically Braced Frames (EBFs).

2.2 Performance-based design procedure

2.2.1 Design Lateral Forces

The design lateral forces are determined by using the shear proportioning factor β_i (Lee and Goel, 2001) obtained by nonlinear time-history analyses. However, the shear proportioning factor was previously derived for moment frames. Therefore, β_i was re-calibrated through nonlinear dynamic analyses for EBFs in this study (see Chapter 3 for details) and can be expressed as:

$$\beta_i = \left(\frac{V_i}{V_n}\right)^{0.75T^{-0.2}} = \left(\frac{\sum_i^n w_i h_i}{w_n h_n}\right)^{0.75T^{-0.2}} \tag{2.1}$$

$$F_n = V\left(\frac{w_n h_n}{\sum_{j=1}^{n} w_j h_j}\right)^{0.75T^{-0.2}} \tag{2.2}$$

$$F_i = (\beta_i - \beta_{i+1})F_n \quad \text{when } i = n,\ \beta_{n+1} = 0 \tag{2.3}$$

where β_i is the shear proportioning factor at level i; V_i and V_n, respectively, are the story shear

forces at level *i* and at the top (*n*th)level; w_i and w_j are the weights of the structure at level *i* and *j*, respectively; h_i and h_j are the heights of story levels *i* and *j* from the ground, respectively; w_n is the weight of the structure at top level; h_n is the height of roof level from ground; *T* is the fundamental structure period obtained by code-specified methods; F_i and F_n are the lateral forces applied at level *i* and top level *n*, respectively; *V* is the design base shear (see next step).

2.2.2 Design Base Shear

2.2.2.1 Conventional Method

Design base shears in current seismic codes are calculated by reducing the elastic strength demands to the inelastic strength demands using the response modification factors. These inelastic strength demands are further increased according to the importance of specific structures using occupancy importance factor. Generally, the design base shear is determined form the code prescribed design acceleration spectrum and expressed in the following form:

$$V = C_s W = C_e \left(\frac{I}{R} \right) W \tag{2.4}$$

where C_s is the seismic response coefficient calculated based on specific design code; C_e is the normalized design pseudo-acceleration; *I* is the occupancy importance factor; *R* is the response modification factor (= 8 for EBF); and *W* is the total seismic weight.

After selecting the member sizes for required strengths (which is generally done by elastic

analysis) the calculated drift using elastic analysis is multiplied by deflection amplification factor, such as C_d given in the codes, and kept within specified drift limits (in the order of 2%).

2.2.2.2 Proposed Energy-Based Procedure

It should be noted that the response modification factors, *R*, specified in design codes for various structural systems are determined primarily based on engineering judgment. Moreover, as mentioned earlier, conventional design procedures are based on elastic force-based analysis methods rather than displacement-based methods, thus the inelastic response beyond the elastic limit for a structure cannot be predicted with good precision. A more rational design approach to overcome the shortcomings in the conventional approach was proposed by Leelataviwat (1998) and modified by Lee and Goel (2001), which uses energy balance equation as the design basis with the structure pushed monotonically up to a target drift after the formation of a selected yield mechanism. The amount of external work needed to do that is assumed as a factor γ times the elastic input energy $E(=\frac{1}{2}MS_v^2)$. The modification factor γ is dependent on the natural period of the structure which has significant influence on the earthquake input energy, as observed by many investigators (Uang and Bertero, 1988) Thus, the energy balance equation can be written as:

$$\gamma E = (E_e + E_p) \tag{2.5}$$

where E_e and E_p are, respectively, the elastic and plastic components of the energy needed as the structure is pushed up to the target drift. S_v is the design pseudo-velocity; *M* is the total mass of the system. The modification factor, γ, depends on the structural ductility factor (μ_s) and the

ductility reduction factor (R_μ), which is related to the structure's period. Figure 2.1 shows the relationship between the base shear (*CW*) and the corresponding drift (Δ) of an elastic system and an elastic-plastic system. From the geometric relationship the Eq. 2.5 can be written as:

$$\gamma\left(\frac{1}{2}C_{eu}W\Delta_{eu}\right)=\frac{1}{2}C_yW\left(2\Delta_{\max}-\Delta_y\right) \tag{2.6}$$

Using the expression for drifts (Δ), Eq. 2.6 can be rewritten as:

$$\gamma\frac{\Delta_e}{\Delta_y}=\frac{(2\Delta_{\max}-\Delta_y)}{\Delta_e} \tag{2.7}$$

where Δ_e and $\Delta_{\max}$ from Figure 2.1 are equal to $R_\mu\ \Delta_y$ and $\mu_s\Delta_y$, respectively. Substituting these terms into Eq. 2.7, the energy modification factor γ can be determined as:

$$\gamma=\frac{2\mu_s-1}{R_\mu^2} \tag{2.8}$$

where μ_s is the structural ductility factor which is equal to target drift divided by yield drift ($\Delta_{\max}/\Delta_y$); R_μ is the ductility reduction factor which can be determined based on the μ_s value. It can be seen from Eq. 2.8 that the energy modification factor γ is a function of the ductility reduction factor and the structural ductility factor. Using different approaches, many investigators have attempted to relate the ductility reduction factor and structural ductility factor (Miranda and Bertero 1994). In this study, the method proposed by Newmark and Hall (1982) is adopted to relate the ductility reduction factor and the structural ductility factor as shown in

Figure 2.2. The energy modification factor γ calculated based on Eq. 2.8 is shown in Figure 2.3.

The design elastic energy demand (E) can be determined from the elastic design pseudo-acceleration spectra as given in the building codes (CBC, IBC, UBC, or NEHRP). The design pseudo-acceleration based on the selected design spectrum for elastic systems can be specified as:

$$A = C_e g \tag{2.9}$$

where A is the design pseudo-acceleration, g is the acceleration due to gravity, and C_e is the normalized design pseudo-acceleration as defined in Eq. 2.4. Note that no occupancy importance factor is included in the design pseudo-acceleration for the approach proposed in this study. The occupancy importance factor, I, raises the design force level in an attempt to decrease the drift and ductility demand for the structure for a given level of ground shaking (SEAOC, 1999; NEHRP, 2001). However, that cannot be considered as a direct method to achieve the intended purpose such as damage control. The reduction of potential damage should better be handled by using appropriate drift limitations. In this regard, the approach of calculating the design base shear proposed in this study uses the target drift as an important parameter. It is assumed that the selected target drift will have the occupancy importance factor built into it. However, C_e can be further increased if other effects such as Spectral Ratio (CBC 1631A.5.4), near-fault effect, or possible torsion in the global structural system need to be considered.

The energy balance equation can be rewritten as:

$$(E_e + E_p) = \gamma\left(\frac{1}{2}MS_v^2\right) = \frac{1}{2}\gamma M\left(\frac{T}{2\pi}C_e g\right)^2 \tag{2.10}$$

Akiyama (1985) showed that the elastic vibrational energy (E_e) can be calculated by assuming that the entire structure can be reduced into a single-degree-of-freedom system, *i.e.*,

$$E_e = \frac{1}{2}M\left(\frac{T}{2\pi}\cdot\frac{V}{W}\cdot g\right)^2 \tag{2.11}$$

where V is the yield base shear and W is the total seismic weight of the structure ($W=Mg$). Substituting Eq. 2.11 into Eq. 2.10 and rearranging the terms gives:

$$E_p = \frac{WT^2 g}{8\pi^2}\left(\gamma C_e{}^2 - \left(\frac{V}{W}\right)^2\right) \tag{2.12}$$

By using a pre-selected yield mechanism as shown in Figure 2.4 and equating the plastic energy term E_p to the external work done by the design lateral forces shown in Eq. 2.3 gives:

$$E_p = \sum_{i=1}^{n} F_i h_i \theta_p \tag{2.13}$$

where θ_p is the global inelastic drift of the structure, which is the difference between the pre-selected target drift(θ_u) and yield drift(θ_y). The yield drift of an EBF was assumed as 0.5% for design purposes.

Substituting Eqs. 2.3 and 2.12 into Eq. 2.13 , and solving for *V/W* gives:

$$\frac{V}{W} = \frac{-\alpha + \sqrt{\alpha^2 + 4\gamma C_e^2}}{2} \tag{2.14}$$

where V is the design base shear and α is a dimensionless parameter, which depends on the stiffness of the structure, the modal properties and the intended drift level, and is given by:

$$\alpha = \left(\sum_{i=1}^{n} (\beta_i - \beta_{i+1}) h_i \right) \cdot \left(\frac{w_n h_n}{\sum_{j=1}^{n} w_j h_j} \right)^{0.75T^{-0.2}} \cdot \left(\frac{\theta_p 8\pi^2}{T^2 g} \right) \tag{2.15}$$

It should be noted that the required design base shear given in Eq. 2.14 is related to the lateral force distribution, the intended target drift, θ_p , and pre-selected yield mechanism. Also note that in Eq. 2.15 when $i = n$, $\beta_{n+1} = 0$.

It can be seen that the proposed method for determining lateral design forces is based on principles of structural dynamics, while ensuring formation of selected yield mechanism and drift control at the same time. There is no need for using response modification factor (*R*) and displacement amplification factor (such as C_d), which are required in current practice and are largely based on engineering judgment.

2.3 Proposed Design Procedure for EBFs

2.3.1 Pre-Selected Yield Mechanism

Figure 2.4 shows EBFs subjected to design lateral forces and pushed to its maximum drift state. All the inelastic deformations are intended to be confined within the shear links in the form of shear yielding. Since the plastic hinges developed at the column bases are almost inevitable in a major earthquake, the desired global yield mechanism of an EBF is formed by yielding (due to shear force) of the shear links plus the plastic hinges at the column bases. The gravity loads (dead load and live load) are assumed uniformly distributed and no pattern loading is considered for live loads.

2.3.2 Proportioning of Shear Links

The primary purpose of using plastic design procedure is to ensure the formation of intended yield mechanism. For EBFs, the inelastic actions are intended to occur only in the shear links and column bases. Earlier studies have shown that it is desirable to have the distribution of shear link strength along the building height closely follow the distribution of story shears derived by using shear proportioning factor (β_i) which is obtained and calibrated by nonlinear dynamic time-history analyses (namely, the lateral force distribution proposed in this study). This helps to distribute the yielding more uniformly along the height, thereby, preventing excessive yielding from concentrating at a few levels. Referring to the D-braced EBF in Figure 2.5, only one bay of the frame and the corresponding portion of lateral forces are shown for illustration of the design procedure. It should be noted that using all the bays gives the same required shear link

strength.

By using the principle of virtual work and equating the external work to the internal work, as is commonly done for plastic analysis by mechanism method and knowing that the link plastic rotation angle is $\gamma_p = \frac{L}{e}\theta_p$ for a D-braced EBF (Figure 1.2), following equation can be obtained:

$$\sum_{i=1}^{n} F_i h_i \theta_p + \frac{1}{2}\sum_{i=1}^{n} w_{iu} L \theta_p (L-e) = 2M_{pc}\theta_p + \sum_{i=1}^{n} \beta_i V_{pr} L \theta_p \qquad (2.16)$$

where L is the span length; e is the length of shear link. It is noted that, for practical design purposes, the shear link length used herein includes half depth of the connected column. It will not alter the final require shear strength. However, the half column depth cannot be included in the value of e when Eqs. 1.1, 1.2, and 1.3 are used to classify the links. V_{pr} is the required shear strength of links at the top level and the only unknown variable in Eq. 2.16. The required link shear strength (plastic shear capacity) at level i can be determined by multiplying V_{pr} by the shear proportioning factor β_i at level i, namely, $\beta_i V_{pr}$. M_{pc} is the required plastic moment of columns in the first story as shown in Figure 2.5. Note that due to the deformed shape of beam segment and shear link of a D-braced EBF (as shown in Figures 2.4 and 2.5), as well as the uniformly distributed gravity loads as assumed, the external work done by the gravity loads leads to the second term on left side of Eq. 2.16.

The required plastic moment of columns in the first story, M_{pc}, needs to be determined

before using Eq. 2.16. Leelataviwat et al. (1999) suggested that M_{pc} can be chosen in such a way that no soft story mechanism would occur when a factor of 1.1 times the design lateral forces are applied on the frame as shown in Figure 2.6. Thus, the plastic moment of the first-story columns can be computed as:

$$M_{pc} = \frac{1.1V'h_1}{4} \tag{2.17}$$

where V' is the base shear for one bay only, which is equal to V divided by the number of bays; h_1 is the height of the first story; and the factor 1.1 is the overstrength factor accounting for possible overloading due to stain hardening and uncertainty in material strength. Substituting Eqs. 2.16 into 2.17, the required link hear strength at any level i can be determined as:

$$\beta_i V_{pr} = \beta_i \cdot \frac{\left(\sum_{i=1}^{n} F_i h_i + \frac{1}{2} L \cdot (L-e) \sum_{i=1}^{n} w_{iu} - 2M_{pc}\right)}{L \cdot \sum_{i=1}^{n} \beta_i} \tag{2.18}$$

Eq. 2.18 is used to determine the required shear strength of shear links at any level for a D-braced EBF with fixed column bases and uniformly distributed gravity loading. In the case when EBF is located at the perimeter of a structure, the gravity loading is relatively small and can be ignored, Eq. 2.18 can be reduced to:

$$\beta_i V_{pr} = \beta_i \cdot \frac{\left(\sum_{i=1}^{n} F_i h_i - 2M_{pc}\right)}{L \cdot \sum_{i=1}^{n} \beta_i} \tag{2.19}$$

If the column bases can be treated as hinge supports, Eq. 2.19 is further reduced to:

$$\beta_i V_{pr} = \beta_i \cdot \frac{\sum_{i=1}^{n} F_i h_i}{L \cdot \sum_{i=1}^{n} \beta_i} \tag{2.20}$$

For the K-braced and V-braced EBFs illustrated in Figures 1.2 and 2.4, it can be easily shown that the required shear strength can also be calculated using Eq. 2.19. No external work done by the gravity loading needs to be included for these two type EBFs due to the antisymmetric deformed shape as shown in Figure 2.4.

The design of shear links is performed using Eq. 1.4:

$$\phi V_n = 0.9 V_p = 0.9(0.6 F_y A_w) = 0.9\left[0.6 F_y (d_b - 2t_f) t_w\right] \geq \beta_i V_{pr} \tag{2.21}$$

If the required axial strength P_u in a shear link exceeds $0.15P_y$, where P_y is equal to $F_y A_g$, the effect of axial force on the link design shear strength should be considered and the shear link design strength becomes:

$$\begin{aligned} \phi V_n &= 0.9 V_p \sqrt{1 - \left(P_u / P_y\right)^2} \\ &= 0.9\left[0.6 F_y (d_b - 2t_f) t_w\right] \cdot \sqrt{1 - \left(P_u / P_y\right)^2} \geq \beta_i V_{pr} \end{aligned} \tag{2.22}$$

In general, the effect of axial load on the shear capacity is negligible except for a modified

EBF configuration that leads to large axial forces. Indeed, as demonstrated by the nonlinear dynamic analysis in this study, even under a major earthquake, almost all the shear links have axial forces generated in the range of $0.03P_y \sim 0.10P_y$. Further investigation of the only link with required axial strength exceeding $0.15P_y$ shows that the reduction of shear strength is insignificant. Consequently, no axial load effect needs to be considered when designing the shear links.

Link section should also satisfy the width-thickness limitations given in AISC Seismic Provisions Table I-8-1 (Eqs. 1.5 and 1.6); however, as suggested by Arce et al. (2003), sections with flange slenderness ratio not exceeding $65/\sqrt{F_y}$ ($0.38\sqrt{E_s/F_y}$) were also accepted in this study.

2.3.3 Design of Members outside the Links

The design of elements outside the shear links, including beam segments, braces, and columns, is performed based on the capacity design approach. That is, elements outside the shear links should have a design strength to resist the combination of factored gravity loads and the maximum expected shear forces as well as moments developed in the shear links. The maximum expected shear forces (V_u) can be considerably higher than the plastic shear strength (V_p) resulting primarily from material overstrength, strain-hardening, and the development of shear resistance in the link flanges. V_u is calculated using Eq. 1.7 as specified by the code (AISC, 2002). By the same reasoning, maximum link moments at column side (M_C) and brace side

(M_B) are calculated according to Eqs. 1.8 and 1.9, respectively. Note that the shear link length, *e*, specified in Eq. 1.9, should be the actual length of the links.

Once the maximum expected link shear forces and moments are determined, the frame can be cut into several free bodies, *i.e.*, columns with associated beam segments and braces. An example 3-story EBF and the corresponding column free bodies are illustrated in Figures 2.7, 2.8 and 2.9. This is done so that the elements outside the shear links are designed based on the maximum expected strength of the shear links as well as the updated lateral forces as described below, thus confining all inelastic activity to the shear links while keeping the other elements essentially elastic when subjected to a major earthquake.

2.3.4 Design of Columns with Associated Beam Segments and Braces

The design procedure is illustrated using an example 3-story D-braced EBF shown in Figure 2.7. Due to the presence of pin connections, the exterior columns are designed using gravity loads only, whereas the interior columns need to be designed based on the capacity approach. The free bodies of interior column 2 and 1 are shown schematically in Figures 2.8 and 2.9, respectively.

Referring to Figures 2.8 and 2.9, when the frame reaches its target drift, the shear forces and end moments in shear links at all levels are assumed to reach the maximum expected shear strength, V_u and maximum expected moments, M_C and M_B. The column at the lowermost level is also assumed to have reached its maximum capacity, M_{pc}. At this stage, the required

balancing lateral forces applied on this free body are assumed to maintain the distribution as used earlier and can be easily calculated by using moment equilibrium of the free body. The lateral forces should be updated based on the expected strength of shear links because they have significant influence on the internal forces of members outside the shear links.

For the interior column 2 shown in Figure 2.8a; if the lateral forces are acting to the right, the sum of those lateral forces, F_R, can be obtained by taking moment equilibrium at column base:

$$F_R = \frac{(L-e)\cdot\sum_{i=1}^{n}(V_u)_i + \sum_{i=1}^{n}(M_B)_i - \frac{(L-e)^2}{2}\sum_{i=1}^{n}w_{iu} + M_{pc}}{\sum_{i=1}^{n}\alpha_i h_i} \tag{2.23}$$

where M_B is the maximum expected link end moment at the brace side specified in Eq. 1.9; w_{iu} is the factored uniformly distributed gravity load, it is taken as $1.2DL + 0.5LL$ in this study; and:

$$\alpha_i = \frac{F_i}{\sum_{i=1}^{n}F_i} = \frac{(\beta_i - \beta_{i+1})}{\sum_{i=1}^{n}(\beta_i - \beta_{i+1})} \qquad \text{when } i = n,\ \beta_{n+1} = 0 \tag{2.24}$$

For the case when the lateral forces are directed to the left (Figure 2.8b), the sum of the applied lateral forces, F_L, can be obtained as:

$$F_L = \frac{(L-e)\cdot\sum_{i=1}^{n}(V_u)_i + \sum_{i=1}^{n}(M_B)_i + \frac{(L-e)^2}{2}\sum_{i=1}^{n}w_{iu} + M_{pc}}{\sum_{i=1}^{n}\alpha_i h_i} \tag{2.25}$$

For the case of interior column 1 shown in Figure 2.9, the design is governed by the lateral forces acting to the right (Because the downward link shears are applied to the columns as compression forces in addition to the compression forces result from gravity loading). The sum of lateral forces, F_R, can be calculated as:

$$F_R = \frac{\sum_{i=1}^{n}(V_u)_i \cdot \frac{(d_c)_i}{2} + \sum_{i=1}^{n}(M_C)_i + M_{pc}}{\sum_{i=1}^{n}\alpha_i h_i} \tag{2.26}$$

where M_C is the maximum expected link end moment at the brace side specified in Eq. 1.8; d_c is the depth of the column section and can be taken as constant in the preliminary design stage.

For configuration of EBFs other than the one shown in Figure 2.7, the corresponding column free bodies and forces as derived in Eqs. 2.23 to 2.26 can be easily obtained by following similar procedure.

After the lateral forces are calculated as described above, the required strength of elements (beam segments, braces, and columns) can be easily computed by using an elastic structural analysis program such as *RISA-3D* to model the column free bodies shown in Figures 2.8 and 2.9. Preliminary sections can be assumed at the beginning and revised later. $\alpha_i F_R$ ($\alpha_i F_L$), $(V_u)_i$, $(M_B)_i$, $(M_C)_i$, w_{iu}, and $(P_u)_i$ are applied as external loads. $(P_u)_i$ are axial forces in the columns resulting from tributary gravity loadings. Design of these elements is performed in

accordance with the AISC LRFD provisions through conventional elastic design procedures. For EBFs with hinged bases, the column free body models may be structurally unstable when loaded since they are basically determinate cantilever beams. Nevertheless, the hinge support can be replaced with fixed support for computing the element forces without altering the results because all the external forces are already balanced and moment at the column base will automatically be null (because of hinged supports).

Flowcharts are given in Figures 2.10 and 2.11 to illustrate the proposed design procedure.

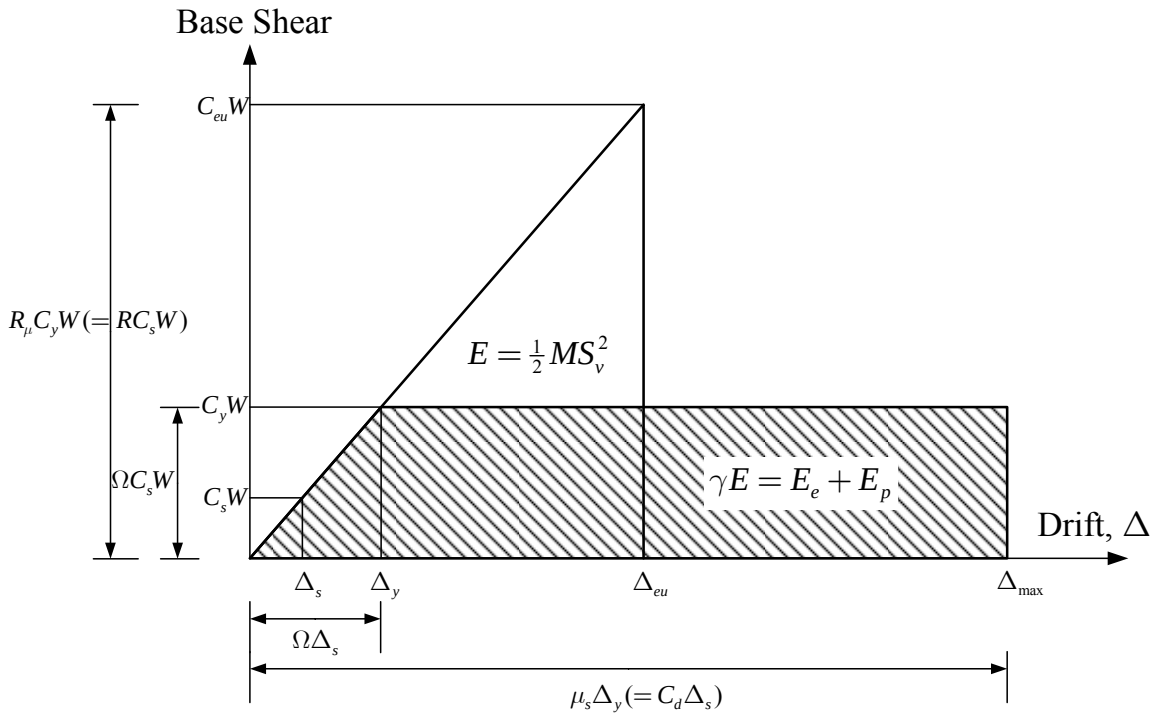

Figure 2.1 Structural idealized response and energy balance concept

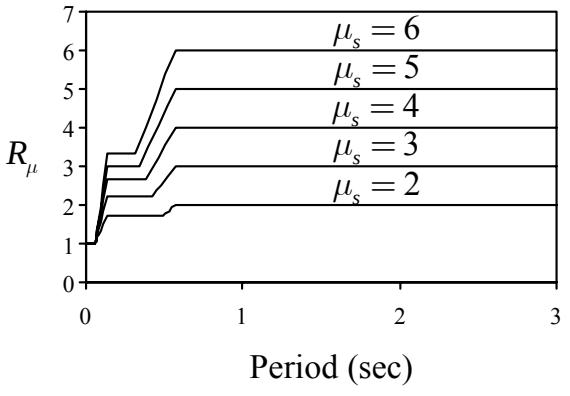

Figure 2.2 Ductility reduction factors proposed by Newmark and Hall (1982)

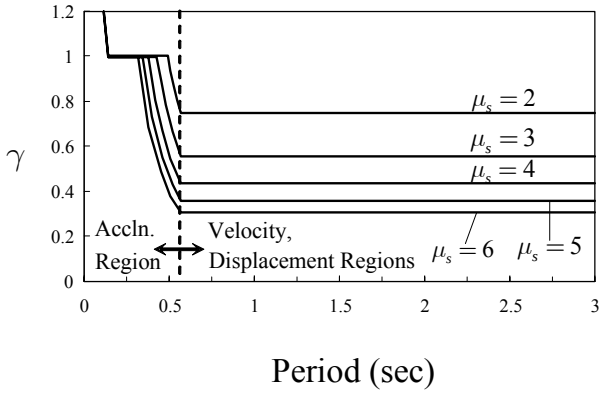

Figure 2.3 Modification factors for energy equation versus period

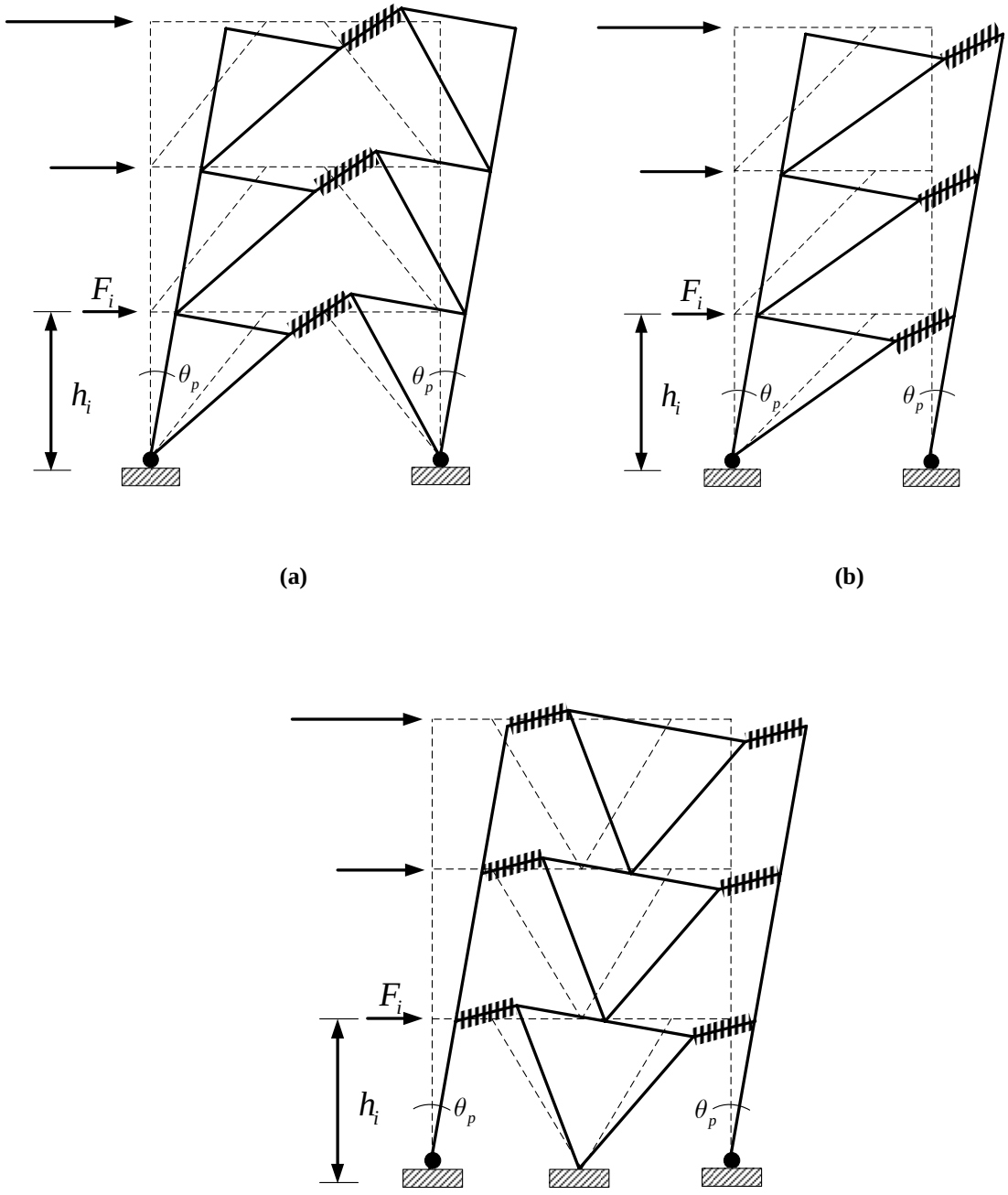

Figure 2.4 Pre-selected yield mechanism of EBFs with various geometries: (a) K-braced EBF; (b) D-braced EBF; (c) V-braced EBF

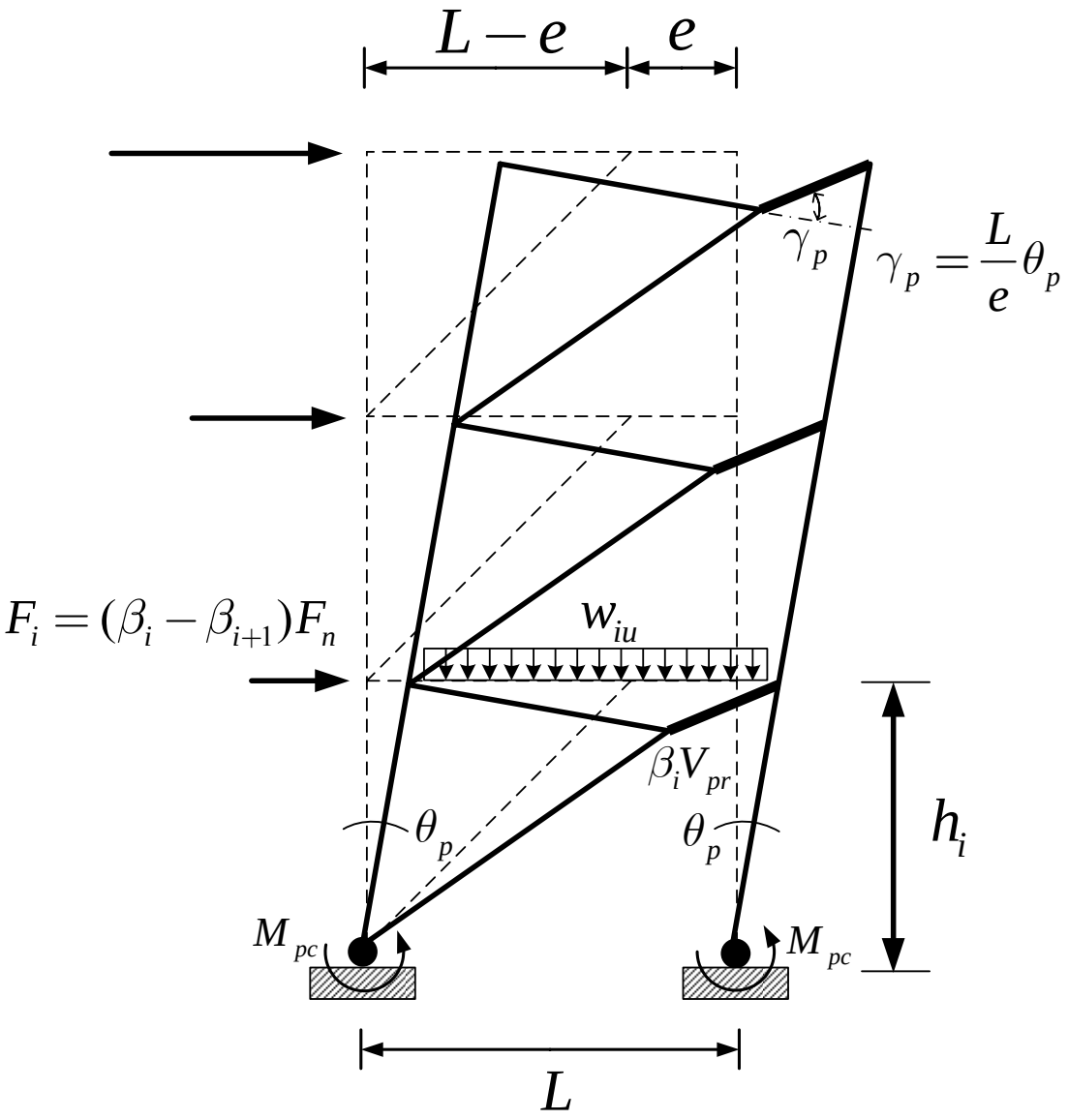

Figure 2.5 One-bay D-braced EBF with pre-selected yield mechanism for calculating required strength of shear links; note that the values of F_i and F_n are for one bay only

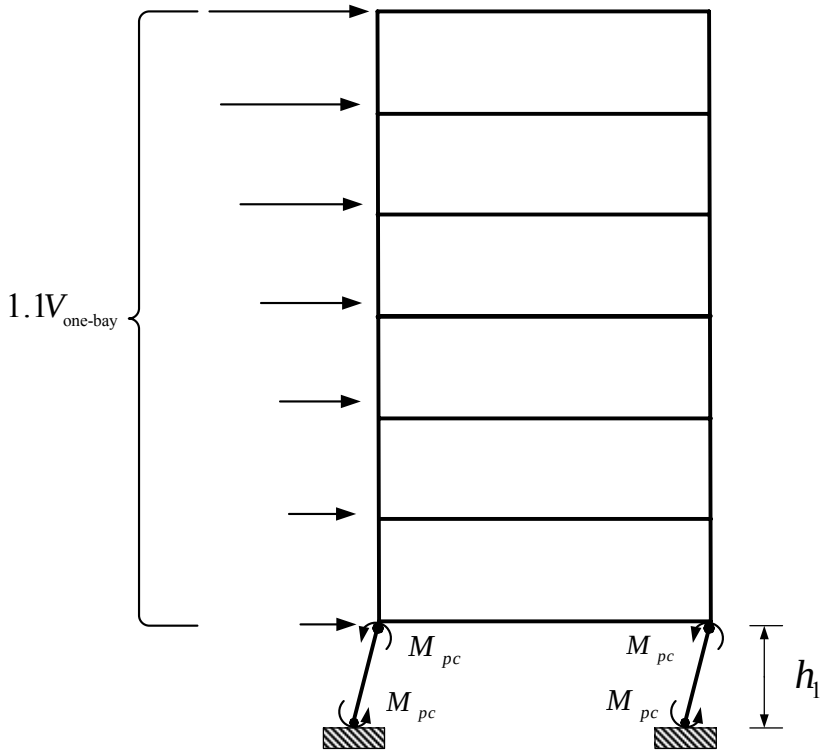

Figure 2.6 One-bay frame with soft-story mechanism (Leelataviwat et al., 1999)

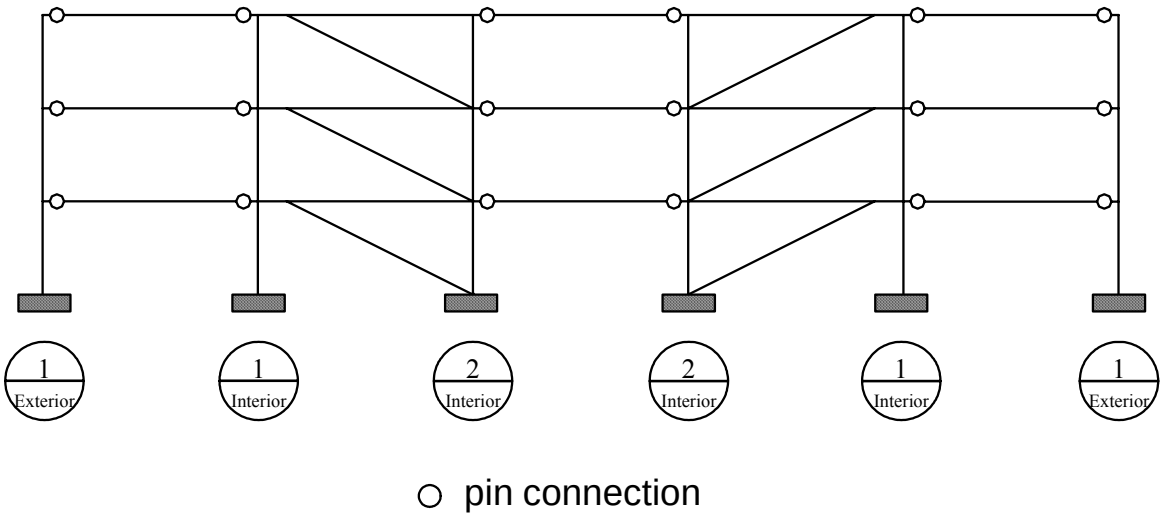

Figure 2.7 Example EBF used to explain the design procedure of members outside shear links

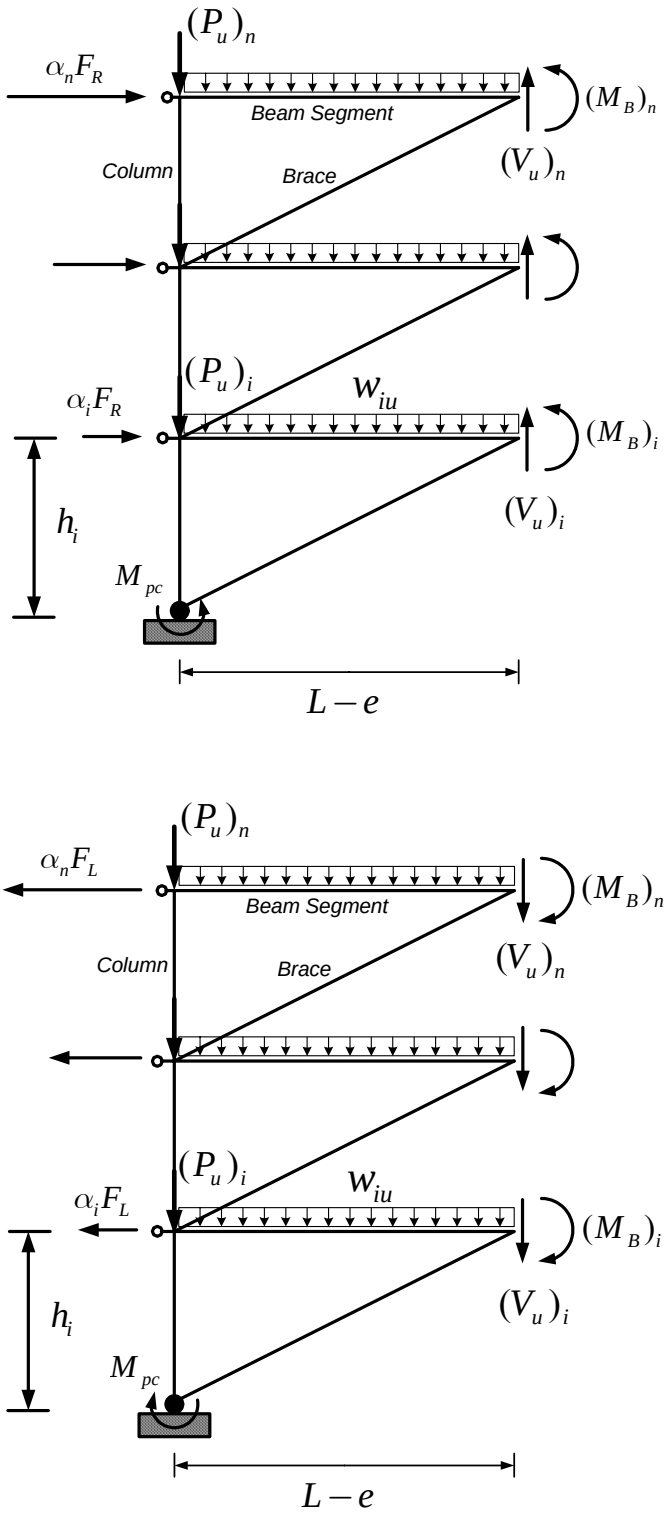

Figure 2.8 Free body diagram of interior column *2* and associated beam segments and braces: (a) lateral forces acting toward right; (b) lateral force acting toward left

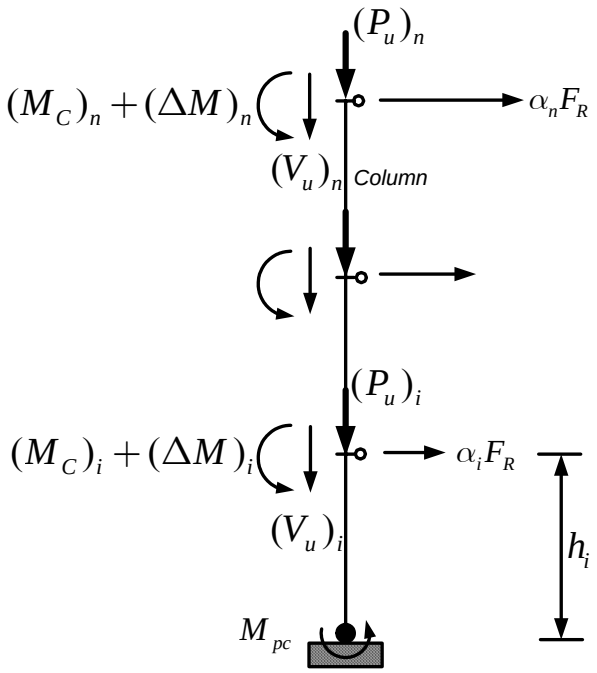

(a)

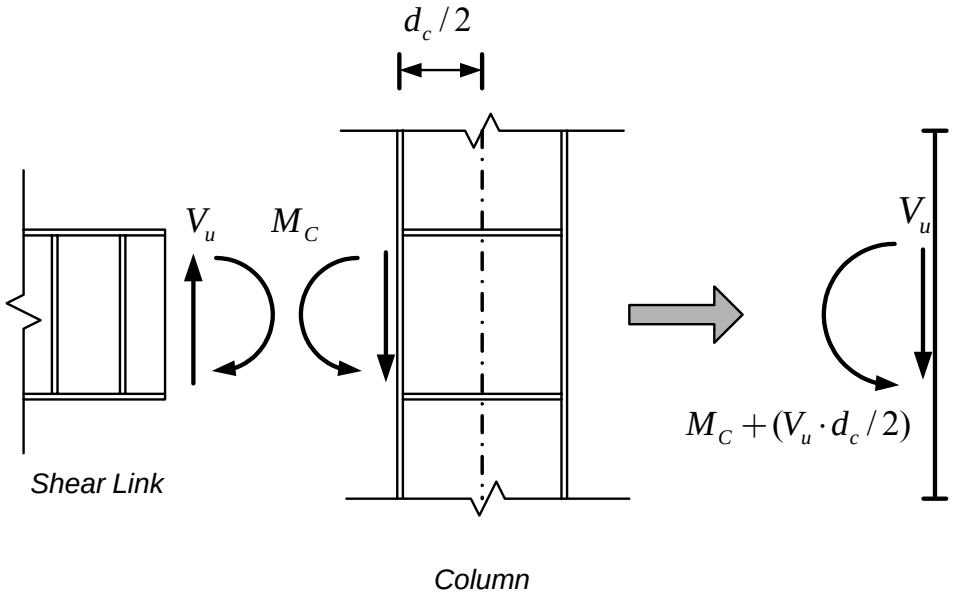

(b)

Figure 2.9 (a) Free body diagram of interior column *1* and associated beam segments and braces subjected to lateral forces toward right; (b) Illustration showing ΔM

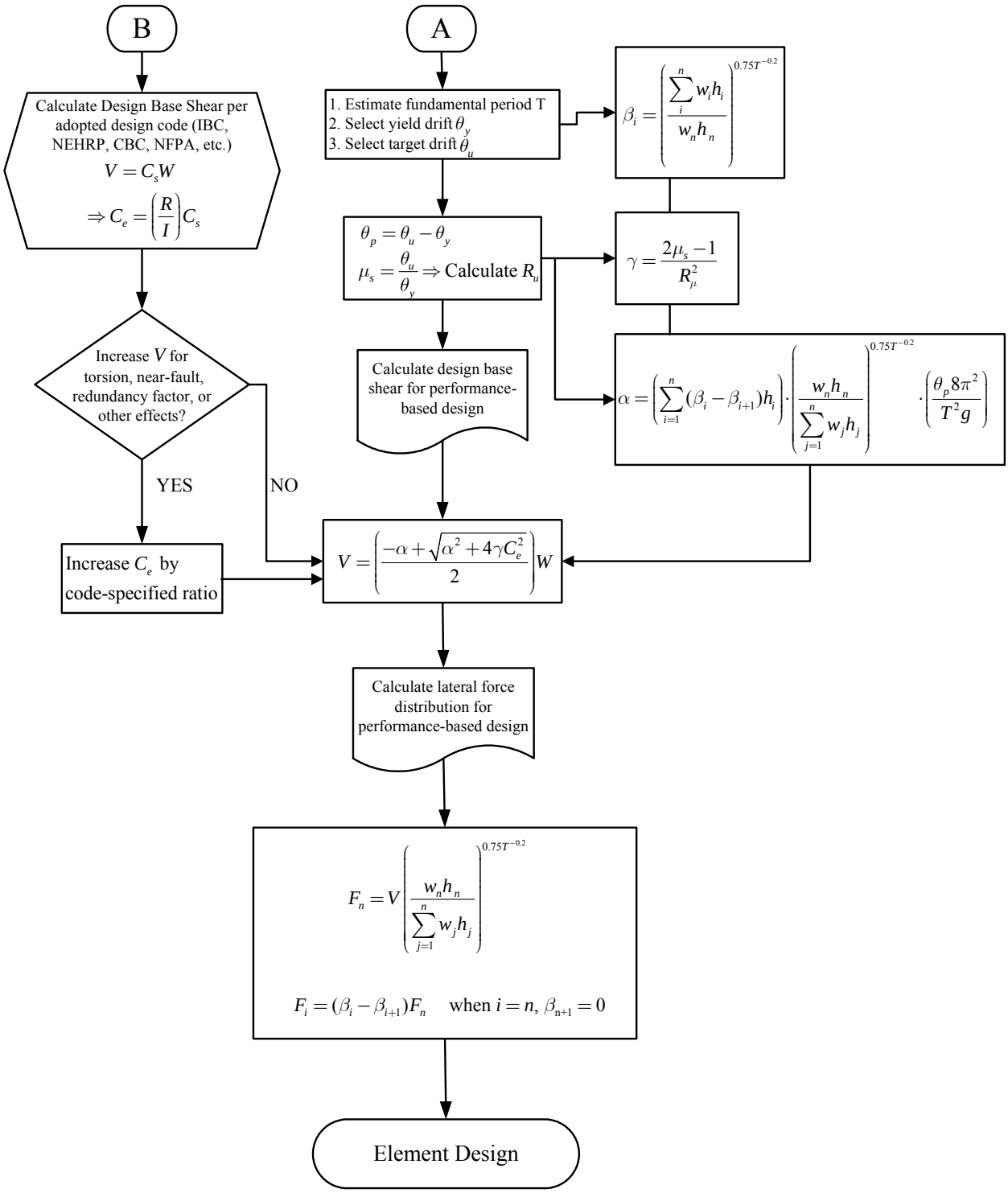

Figure 2.10 Performance-based plastic design flowchart: design base shear and lateral force distribution

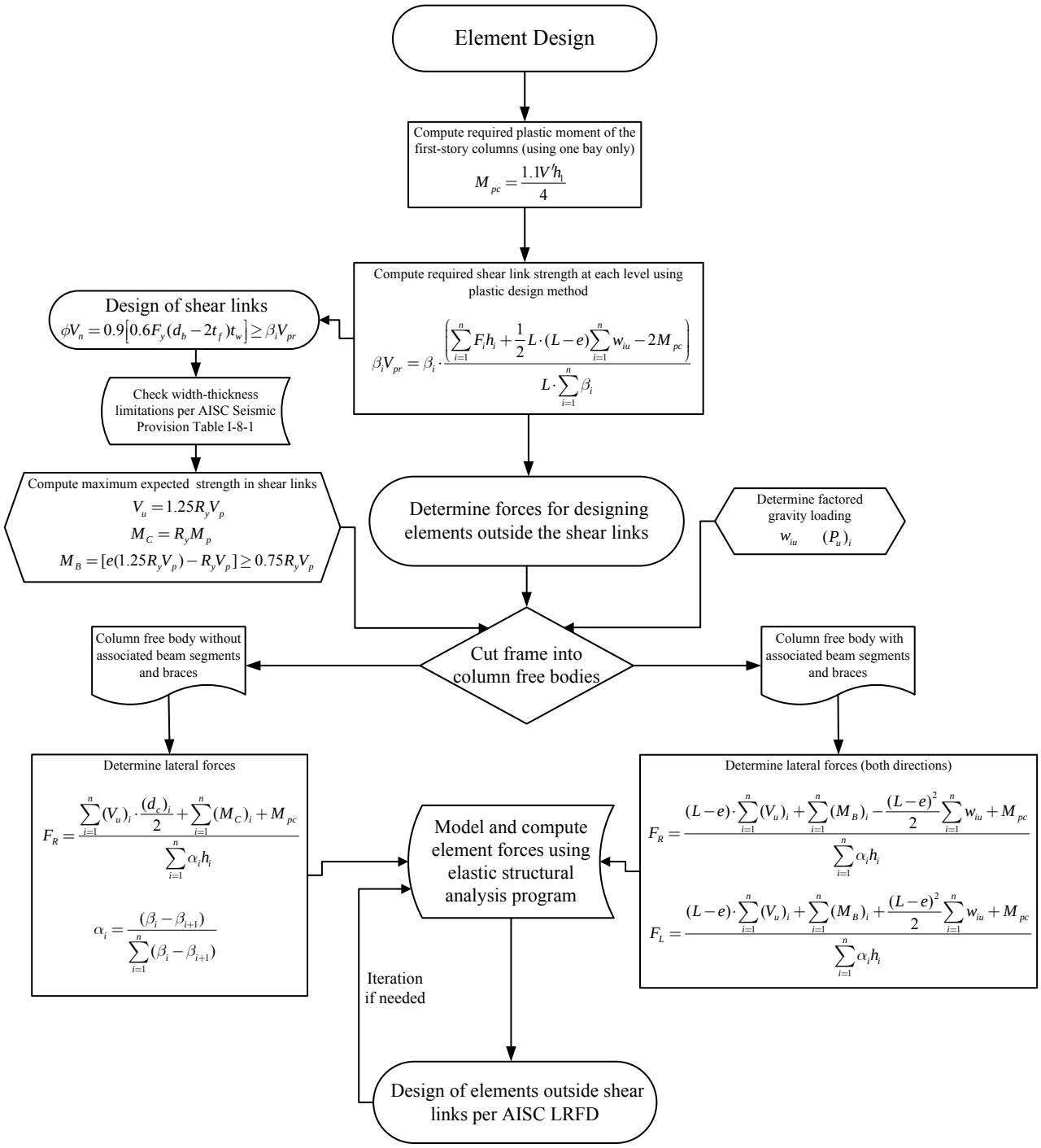

Figure 2.11 Performance-based plastic design flowchart for EBF: element design

CHAPTER 3
Design of Study EBFs

3.1 Description of study buildings

Two eccentrically braced frames were investigated, one with three stories and the other with ten stories. Both frames (called **IBC** frames in this study) were originally designed using conventional elastic design method in accordance with IBC 2000 criteria by AISC Steel Solution Center (Richards, 2004). The frame plan layouts are illustrated in Figure 3.1. With slightly different design parameters but with the same frame configurations, these two frames were redesigned using the proposed performance-based plastic design procedure as illustrated in Figures 2.10 and 2.11 (thus called **PPD** frames in this study). The floor loadings for the 3-story and 10-story IBC and PPD buildings are listed in Tables 3.1 and 3.2, respectively. The gravity loading applied on the PPD eccentrically braced frames were calculated based on corresponding tributary areas. The factored gravity loading ($1.2DL + 0.5LL$) is shown in Table 3.3 and Figure 3.2 for the 3-story and 10-story EBFs. For comparison purposes, this gravity loading was applied to both IBC and PPD frames when conducting nonlinear analysis, even though the IBC frames were designed for larger gravity loading.

3.2 Design of IBC Frames

The IBC frames were designed according to IBC 2000 (ICC, 2000) using conventional elastic method. The design base shears were obtained based on the 5% damped design spectral

response accelerations.

3.2.1 Background

The Maximum Considered Earthquake (MCE) is defined as the ground shaking for a 2%/50 year earthquake at a site (i.e. 2475 year mean recurrence interval). It is the largest earthquake that can be generated by known seismic sources. In the 1997 UBC or earlier NEHRP Provisions, the design ground motions are based on a 90 percent probability of not being exceeded in 50 years. However, it is recognized that larger ground motions are possible and they could occur at any time. ***The Design Earthquake*** in the IBC 2000 is taken as two-thirds of the MCE in order to have some "seismic margin". against larger, less probable ground motions.

3.2.2 Design base shear and lateral force distribution

The procedure for determining the design base shear in accordance with IBC 2000 is briefly described as follows:

(1) The maximum considered earthquake spectral response acceleration (used to construct the response spectra) at short periods, S_S, and at 1-second period, S_1, can be determined from IBC 2000 Figures 1615(1) through 1615(10) or directly from the USGS maps from their website by specifying the latitude and longitude of the site.

(2) Modifying S_S and S_1 for the soil conditions at the site:

$$S_{MS} = F_a S_S \tag{3.1}$$

$$S_{M1} = F_v S_1 \tag{3.2}$$

where F_a, F_v are site coefficients defined in IBC 2000 Table 1615.1.2 based on different site classes (IBC 2000 Table 1615.1.1).

(3) Design spectral response accelerations (two-thirds of MCE):

$$S_{DS} = \frac{2}{3} S_{MS} \tag{3.3}$$

$$S_{D1} = \frac{2}{3} S_{M1} \tag{3.4}$$

(4) Determine Seismic Use Group and Importance Factor (I) according to IBC 2000 Table 1604.5

(5) Determine Seismic Design Category (A~F) according to IBC 2000 Table 1616.3 (1) and (2).

(6) Determine building period T:

$$T_a = C_T h^{3/4} \tag{3.5}$$

where $C_T = 0.03$ for EBF. The calculated period

$$T \le C_U \times T_a \tag{3.6}$$

The coefficient C_U can be obtained from IBC 2000 Table 1617.4.2.

(7) Seismic design base shear:

$$V = C_s W \tag{3.7}$$

where $C_s = \frac{V}{W}$ is the seismic response coefficient which is determined by:

$$C_s = \frac{S_{DS}}{(R/I)} \le \frac{S_{D1}}{(R/I)T}$$

$$\ge 0.044 S_{DS} I \qquad (3.8)$$

$$\ge \frac{0.5 S_1}{(R/I)}$$

The last inequality applies to the Seismic Design Categories E and F, or where $S_1 \ge 0.6g$. R is the response modification factor (= 8.0 for EBF).

(8) Vertical distribution of seismic forces:

$$F_x = C_{vx} V \qquad (3.9)$$

$$C_{vx} = \frac{w_x h_x^k}{\sum_{i=1}^{n} w_i h_i^k} \qquad (3.10)$$

$T \le 0.5 \text{ sec} \Rightarrow k = 1$
$T \ge 2.5 \text{ sec} \Rightarrow k = 2$
$0.5 < T < 2.5 \Rightarrow$ linear interpolation of k

3.2.3 Design of the IBC frames

The design base shear for IBC frames, *V*, were calculated based on the preceding discussion;

however, a redundancy factor, $\rho = 1.47$, was used to amplify the design base shear V (Richards, 2004):

$$V' = \rho V = (\rho C_s) W = C_s' W \tag{3.11}$$

The corresponding design parameters for the 3-story and 10-story IBC EBFs are listed in Table 3.4. It is noted that the IBC frames have been optimized to have similar capacity to demand ratio as required in Eq. 1.13 to avoid concentration of large inelastic link deformation (Popov, Ricles, and Kasai, 1992). As a consequence, rather heavy link sections were used at the second level of the IBC 10-story frame due to the stiffness irregularity. Table 3.5 summarizes the link capacity to demand ratio for the 3-story and 10-story IBC frames. The member sections are shown in Figures 3.3 (a) and 3.4 (a) for 3-story and 10-story frames, respectively.

3.3 Design of PPD Frames

3.3.1 Design based on Lee-Goel lateral force distribution

The two PPD EBFs were designed based on the proposed performance plastic design methodology introduced in Chapter 2. However, instead of using Eq. 2.2, the lateral force distribution employed was according to the one originally proposed by Lee and Goel (2002):

$$F_n = V \left(\frac{w_n h_n}{\sum_{j=1}^{n} w_j h_j} \right)^{0.5T^{-0.2}} \tag{3.12}$$

From Eq. 2.4, the normalized design pseudo-acceleration, C_e, can be calculated by:

$$C_e = \left(\frac{R}{I}\right) C_s \tag{3.13}$$

Note C_s is first obtained from the applicable code under which the structure is designed. It is, in this case, calculated based on Eq. 3.8. It is noted, however, that according to the design flowchart shown in Figure. 2.10, C_s' in Eq. 3.11 can be used to calculate C_e, which will lead to heavier sections. Nevertheless, the redundancy factor was not accounted for in this study for PPD frames. The design parameters for both 3-story and 10-story frames are shown in Table 3.6. Compared with Table 3.4, it is seen that the design parameters are slightly different. Tables 3.7 and 3.8 list the floor weights and distributed lateral forces at all story levels for the PPD frames. The final design sections for all frames are shown in Figures 3.3 (b) and 3.4 (b). In general, the EBFs designed by the proposed performance-based plastic procedure have lighter beam/link sections and heavier column sections than the frames designed by IBC method. It is important to note that the 10-story EBF has a sudden change in stiffness due to larger height of the second story compared to the other stories. This stiffness irregularity would result in a concentration of deformation in the second level if no remedy is done. Nevertheless, for research purposes, no adjustment was made for the PPD frame in the preliminary design in order to investigate the influence of stiffness irregularity on the seismic behavior.

3.3.2 Initial results and modifications

Seven SAC Los Angeles region 10% in 50 years ground motion time histories (see Chapter 4

for detail) were used for the nonlinear dynamic analysis of the PPD frames. Several notable features were observed and associated corrections were proposed:

1) The first mode structural periods from dynamic analyses are much larger than the ones calculated based on IBC 2000. The first mode periods for the 3-story and 10-story PPD frames are 0.523 second and 1.784 seconds, respectively. However, the corresponding periods are 0.418 second and 1.418 seconds per IBC 2000. This discrepancy was also observed in the modal analysis study performed by Richards (2004), wherein the same IBC frames analyzed in this study were used. Therefore, a design period of 1.6 seconds was used for the final design of 10-story PPD frame, and 0.418 second for the 3-story PPD frame.

2) Hysteretic energy dissipated by shear links and maximum link plastic rotations was not uniformly distributed among all floors. Results from selected earthquake records are shown in Table 3.9 and Figures 3.5 and 3.6. In general, the shear links in top floors exhibited smaller link rotations and dissipated much less seismic energy. On the other hand, shear links in the lower floors tended to dissipated most of the input energy thus showed larger deformations, especially at the second level where the story stiffness has abrupt change.

3) One reason for the non-uniform distribution of link rotations and dissipated energy along the building height is that the lateral force distribution used for design did not represent realistic lateral force distribution during major earthquake events. Eq. 3.12 is primarily obtained from limited earthquake time histories, thus further calibration using more records is needed.

   As can be seen in Figure 3.7, the Lee-Goel distribution (2002) is generally on the left bound

of the distributions from nonlinear dynamic analyses, which resulted in concentrated deformation and dissipated energy in the lower floors. In contrast, the IBC 2000 distribution tends to be on the right bound, which will lead to larger deformation in the upper floors as will be further explained in Chapter 5. Based on this observation, a modification distribution was proposed as shown in Eq. 2.2 and Figures 3.7. This proposed distribution better represents the envelope of the realistic story shear distributions.

4) The stiffness irregularity resulting from the change of story height is responsible for the deformation and energy-dissipation concentration at the second floor. A design modification was proposed to remedy this problem as described next.

3.3.3 Remedy for the stiffness irregularity

The PPD frame was first redesigned using the proposed lateral force distribution (Eq. 2.2), as well as the revised fundamental period. The corresponding design parameters are listed in Table 3.10. Same earthquake time histories were employed and the results from LA 17 event are shown in Table 3.11. As compared with Table 3.9, it is seen that the deformation distribution is more uniform and upper floor links exhibited larger deformation because of using the proposed distribution. However, a relatively large link rotation still occurred in the shear links of second floor due to the stiffness irregularity.

It was shown in Figure 1.2 that, link rotation at a particular story is proportional to the lateral drift of this particular story. If weak story stiffness is inevitable, the link rotation can be controlled by adjusting the link strength (namely, the link section size) based on the ratio of

target story stiffness to the current story stiffness in order to offset the stiffness irregularity effect. That is:

$$V_p' = V_p \cdot \frac{K_t}{K_{story}} \tag{3.14}$$

where V_p is the design link shear strength obtained according to the proposed design method, without taking the stiffness irregularity into consideration; V_p' is the modified link shear strength; K_t is the target story stiffness which will be explained later; K_{story} is the elastic story stiffness for EBFs which is given by:

$$K_{story} = K_{column} + K_{brace} \tag{3.15}$$

If both column ends are fixed:

$$K_{story} = \sum_i \frac{12E_sI_i}{h^3} + \sum_i \frac{(\sin\theta)(\cos^2\theta)E_sA}{h} \tag{3.16}$$

If one column end is hinged (as column base with flexibility at first floor):

$$K_{story} = \sum_i \frac{3E_sI_i}{h^3} + \sum_i \frac{(\sin\theta)(\cos^2\theta)E_sA}{h} \tag{3.17}$$

where E_s is the elastic modulus; I_i is the moment of inertia for *i*th column in a particular story; h is the story height; θ is the angle of brace as shown in Figure 3.8; A is the cross sectional area of each brace. It is noted that, the elastic stiffness can be used since the columns and braces are generally expected to remain elastic during major earthquakes. The associated story stiffnesses were calculated for the 3-story and 10-story PPD frames (after lateral force distribution and period modifications) and presented in Table 3.12. As shown in Table 3.12 (a), the story stiffness difference between adjacent stories in the 3-story frame is generally small. As a consequence, no modification was made in the 3-story frame. However, the story stiffness of the second floor in the 10-story frame is significantly smaller than that of adjacent stories. This was remedied by the following treatment.

In general, story stiffness has maximum value at the bottom story and decreases gradually when story height increases. Therefore, the target story stiffness K_t for the second floor should be somewhat in between the story stiffnesses of the first and third floors. Accordingly:

$$K_t \approx \frac{5152+7008}{2} = 6080 \text{ kip/in} \tag{3.18}$$

Therefore, the strength of the second floor was increased as:

$$V_p' = V_p \cdot \frac{K_t}{K_{story}} = V_p \cdot \frac{6080}{3796} = 1.6V_p \tag{3.19}$$

which translates into the required web area (See Eq. 2.21)as:

$$A_w' = \left[\left(d_b - 2t_f\right)t_w\right]' = 5.91 \times 1.6 \approx 9.4 \text{ in}^2 \tag{3.20}$$

Hence the W18x97 shape was selected to replace the preliminary design W16x67 shape as shown in Table 3.13 (a). Table 3.13 (a) suggests that this remedy can effectively reduce the demand on the deformation. After modifying the link/beam section, columns and braces should also be modified based on the procedure described in Figure 2.11.

It is worth noting that the link rotation at first level remained small even the link section was considerably increased at the second floor. In practice, the design can stop after modifying columns and braces; however, for study and optimization purposes, the link size at the first level was reduced to W10x39 shape in this report. Two selected nonlinear dynamic analysis results given in Tables 3.13 (b) and 3.13 (c) suggested that uniform distributed link rotations throughout the frame height were achieved.

Based on the above modifications, the final design member sections for the 3-story and 10-story PPD frames are shown in Figures 3.9 and 3.10.

Table 3.1 (a) Roof loading for the design of IBC frames

Roofing	9 psf
Combined Mechanical, Electrical, Plumbing (CMEP)	5 psf
Deck and Concrete	47 psf
Partitions	5 psf
Framing	12 psf

Table 3.1 (b) Floor loading for the design of IBC frames

Combined Mechanical, Electrical, Plumbing (CMEP)	5 psf
Deck and Concrete	47 psf
Partitions	10 psf
Framing	12 psf
Curtain Wall	20 psf

Table 3.2 (a) Roof loading for the PPD frames

Roofing	9 psf
CMEP	5 psf
Deck and Concrete	47 psf
Partitions (below)	5 psf
Live Load	20 psf

Table 3.2 (b) Floor loading for the PPD frames

Deck and Concrete	47 psf
Partitions	10 psf
CMEP	5 psf
Live Load (reducible)	50 psf
Cladding	20 psf

Table 3.3 (a) Factored gravity loading for 3-story EBF

W_1	0.957 kips/ft
W_2	0.877 kips/ft
L_1	23.71 kips
L_2	17.84 kips
L_3	28.70 kips
L_4	26.31 kips

Table 3.3 (b) Factored gravity loading for 10-story EBF

W_1	0.957 kips/ft
W_2	0.877 kips/ft
L_1	17.97 kips
L_2	25.15 kips
L_3	16.53 kips
L_4	23.71 kips
L_5	11.26 kips
L_6	17.84 kips
L_7	18.33 kips
L_8	25.51 kips

Table 3.4 Design parameters for 3-story and 10-story IBC frames

Parameters	3-story	10-story
S_{DS}	1.13 g	1.13 g
S_{D1}	0.667 g	0.667 g
Seismic Use Group	I	I
Building Height	39 ft	134 ft
T_a	0.468	1.182
C_U	1.200	1.200
T	0.418	1.416
Importance Factor	1.00	1.00
Total Building Weight W	5072.5 kips	18604.7 kips
Design Base Shear V	714.3 kips	1088.4 kips
Redundancy Factor ρ	1.47	1.47
Amplified Design Base Shear $V' = \rho V$	1050 kips	1600 kips

Table 3.5 (a) Link capacity to demand ratio for 3-story IBC frame

Level	$\frac{\phi_v V_p}{V_u} = \lambda \geq 1.0$
3rd FLR	1.95
2nd FLR	2.02
1st FLR	1.97

Table 3.5 (b) Link capacity to demand ratio for 10-story IBC frame

Level	$\frac{\phi_v V_p}{V_u} = \lambda \geq 1.0$
10th FLR	3.63
9th FLR	2.21
8th FLR	1.85
7th FLR	1.85
6th FLR	1.76
5th FLR	1.78
4th FLR	1.69
3rd FLR	1.75
2nd FLR	1.70
1st FLR	1.82

Table 3.6 (a) Design parameters for 3-story and 10-story PPD frames

Parameters	3-story	10-story
S_S	2.380 g	2.380 g
S_1	0.840 g	0.840 g
F_a	1.000	1.000
F_v	1.500	1.500
S_{DS}	1.587 g	1.587 g
S_{D1}	0.840 g	0.840 g
Site Class	D	D
Seismic Use Group	I	I
Seismic Design Category	E	E
Building Height	39 ft	134 ft
T_a	0.468	1.182
C_U	1.200	1.200
T	0.418	1.418
Importance Factor	1.00	1.00
Total Building Weight W	4629.19 kips	15787.83 kips
Design Base Shear V	918.12 kips	1169.18 kips
$C_s = \frac{V}{W}$	0.198	0.074

Table 3.6(b) Design parameters for 3-story and 10-story PPD frames

Parameters	3-story	10-story
C_e	1.584	0.592
T	0.418	1.418
Yield Drift θ_y	0.5%	0.5%
Target Drift θ_u	2%	2%
$\mu_s = \frac{\theta_u}{\theta_y}$	4	4
R_μ	2.93	4
γ	0.814	0.4375
α	7.040	2.038
$\frac{V}{W}$	0.279	0.073
Design Base Shear V	1291.21 kips	1142.05 kips

Table 3.7 Design parameters for the 3-story PPD frame

Level	Floor Weight (kips)	Applied Story Forces (kips)
		PPD-Frame
3rd FLR	1600.0	868.47
2nd FLR	1515.0	293.70
1st FLR	1515.0	129.05

Table 3.8 Design parameters for 10-story PPD frame

Level	Floor Weight (kips)	Applied Story Forces (kips)
		PPD-Frame
10th FLR	1660.0	523.86
9th FLR	1560.0	173.78
8th FLR	1560.0	121.14
7th FLR	1560.0	91.70
6th FLR	1560.0	71.39
5th FLR	1560.0	55.77
4th FLR	1560.0	42.86
3rd FLR	1560.0	31.63
2nd FLR	1560.0	21.47
1st FLR	1560.0	8.46

Table 3.9(a) 3-story PPD Frame: Link section and corresponding link rotation when subjected to the LA 17 record

Level	Required $(d_b - 2t_f)t_w$*	Link Section	$(d_b - 2t_f)t_w$	Maximum Link Plastic Rotation (rad.)
3rd FLR	3.84	**W12x50**	4.04	0.01
2nd FLR	5.13	**W14x68**	5.21	0.06
1st FLR	5.70	**W16x67**	5.91	0.11

* See Eq. 2.21

Table 3.9(b) 10-story PPD Frame: Link section and corresponding link rotation when subjected to the LA 17 record

Level	Required $(d_b - 2t_f)t_w$*	Link Section	$(d_b - 2t_f)t_w$	Maximum Link Plastic Rotation (rad.)
10th FLR	2.28	**W10x39**	2.79	0.01
9th FLR	3.04	**W10x45**	3.10	0.05
8th FLR	3.56	**W12x45**	3.67	0.07
7th FLR	3.96	**W12x50**	4.04	0.08
6th FLR	4.27	**W14x48**	4.29	0.08
5th FLR	4.52	**W14x53**	4.65	0.08
4th FLR	4.70	**W14x61**	4.73	0.08
3rd FLR	4.84	**W14x68**	5.21	0.08
2nd FLR	4.93	**W14x68**	5.21	0.11
1st FLR	4.97	**W14x68**	5.21	0.04

* See Eq. 2.21

Table 3.10 Design Parameters for PPD Frames using the revised lateral force distribution

Parameters	3-story	10-story
C_e	1.584	0.559
T	0.418	1.600
Yield Drift θ_y	0.5%	0.5%
Target Drift θ_u	2%	2%
$\mu_s = \frac{\theta_u}{\theta_y}$	4	4
R_μ	2.93	4
γ	0.814	0.4375
α	6.583	1.491
$\frac{V}{W}$	0.297	0.086
Design Base Shear V	1374 kips	1358 kips

Table 3.11(a) 3-story PPD Frame with revised lateral force distribution: Link section and corresponding link rotation when subjected to the LA 17 record

Level	Required $(d_b - 2t_f)t_w$	Link Section	$(d_b - 2t_f)t_w$	Maximum Link Plastic Rotation (rad.)
3rd FLR	3.35	**W12x35**	3.44	0.04
2nd FLR	5.18	**W14x68**	5.21	0.07
1st FLR	6.07	**W16x77**	6.82	0.09

Table 3.11(b) 10-story PPD Frame with revised lateral force distribution: Link section and corresponding link rotation when subjected to the LA 17 record

Level	Required $(d_b - 2t_f)t_w$	Link Section	$(d_b - 2t_f)t_w$	Maximum Link Plastic Rotation (rad.)
10th FLR	1.88	**W8x31**	2.03	0.06
9th FLR	2.87	**W10x45**	3.10	0.08
8th FLR	3.62	**W12x50**	4.04	0.08
7th FLR	4.23	**W14x53**	4.65	0.07
6th FLR	4.73	**W14x68**	5.21	0.07
5th FLR	5.13	**W14x74**	5.68	0.07
4th FLR	5.44	**W14x74**	5.68	0.07
3rd FLR	5.67	**W16x67**	5.91	0.08
2nd FLR	5.83	**W16x67**	5.91	0.11
1st FLR	5.90	**W16x67**	5.91	0.04

Table 3.12(a) Elastic story stiffness of the 3-story PPD frame

Level	K_{column} (kip/in)	K_{brace} (kip/in)	K_{story} (kip/in)
3rd FLR	301	1390	1691
2nd FLR	379	2015	2395
1st FLR	120	2015	2135

Table 3.12(b) Elastic story stiffness of the 10-story PPD frame

Level	K_{column} (kip/in)	K_{brace} (kip/in)	K_{story} (kip/in)
10th FLR	357	3272	3629
9th FLR	467	3764	4231
8th FLR	629	3764	4393
7th FLR	752	3764	4516
6th FLR	1028	3764	4793
5th FLR	1107	3764	4871
4th FLR	1324	3764	5088
3rd FLR	1388	3764	5152
2nd FLR	872	2924	3796
1st FLR	3070	3938	7008

Table 3.13(a) 10-story PPD Frame with revised lateral force distribution—modification 1: Link section and corresponding link rotation when subjected to the LA 17 record

Level	Required $(d_b - 2t_f)t_w$	Link Section	$(d_b - 2t_f)t_w$	Maximum Link Plastic Rotation (rad.)
10th FLR	1.88	**W8x31**	2.03	0.07
9th FLR	2.87	**W10x45**	3.10	0.08
8th FLR	3.62	**W12x50**	4.04	0.08
7th FLR	4.23	**W14x53**	4.65	0.08
6th FLR	4.73	**W14x68**	5.21	0.07
5th FLR	5.13	**W14x74**	5.68	0.07
4th FLR	5.44	**W14x74**	5.68	0.07
3rd FLR	5.67	**W16x67**	5.91	0.07
2nd FLR	5.83	**W18x97**	9.02	0.06
1st FLR	5.90	**W16x67**	5.91	0.02

Table 3.13(b) 10-story PPD Frame with revised lateral force distribution—modification 2: Link section and corresponding link rotation when subjected to the LA 17 record

Level	Required $(d_b - 2t_f)t_w$	Link Section	$(d_b - 2t_f)t_w$	Maximum Link Plastic Rotation (rad.)
10th FLR	1.88	**W8x31**	2.03	0.06
9th FLR	2.87	**W10x45**	3.10	0.08
8th FLR	3.62	**W12x50**	4.04	0.08
7th FLR	4.23	**W14x53**	4.65	0.08
6th FLR	4.73	**W14x68**	5.21	0.07
5th FLR	5.13	**W14x74**	5.68	0.07
4th FLR	5.44	**W14x74**	5.68	0.08
3rd FLR	5.67	**W16x67**	5.91	0.07
2nd FLR	5.83	**W18x97**	9.02	0.07
1st FLR	5.90	**W10x39**	2.79	0.06

Table 3.13(c) 10-story PPD Frame with revised lateral force distribution—modification 2: Link section and corresponding link rotation when subjected to the LA 09 record

Level	Required $(d_b - 2t_f)t_w$	Link Section	$(d_b - 2t_f)t_w$	Maximum Link Plastic Rotation (rad.)
10th FLR	1.88	**W8x31**	2.03	0.06
9th FLR	2.87	**W10x45**	3.10	0.07
8th FLR	3.62	**W12x50**	4.04	0.07
7th FLR	4.23	**W14x53**	4.65	0.06
6th FLR	4.73	**W14x68**	5.21	0.05
5th FLR	5.13	**W14x74**	5.68	0.04
4th FLR	5.44	**W14x74**	5.68	0.06
3rd FLR	5.67	**W16x67**	5.91	0.06
2nd FLR	5.83	**W18x97**	9.02	0.07
1st FLR	5.90	**W10x39**	2.79	0.07

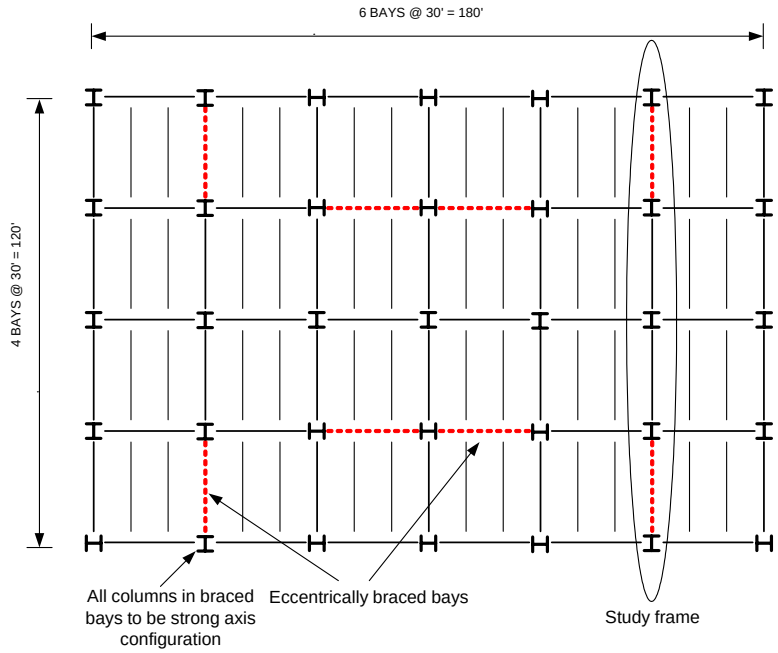

(a)

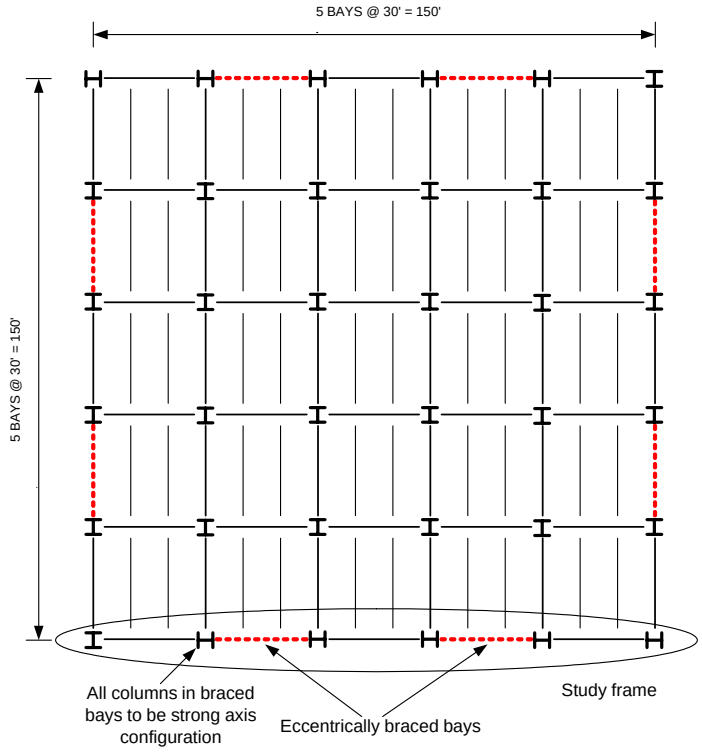

(b)

Figure 3.1 Study model building typical floor framing plan: (a) 3-story; (b) 10-story

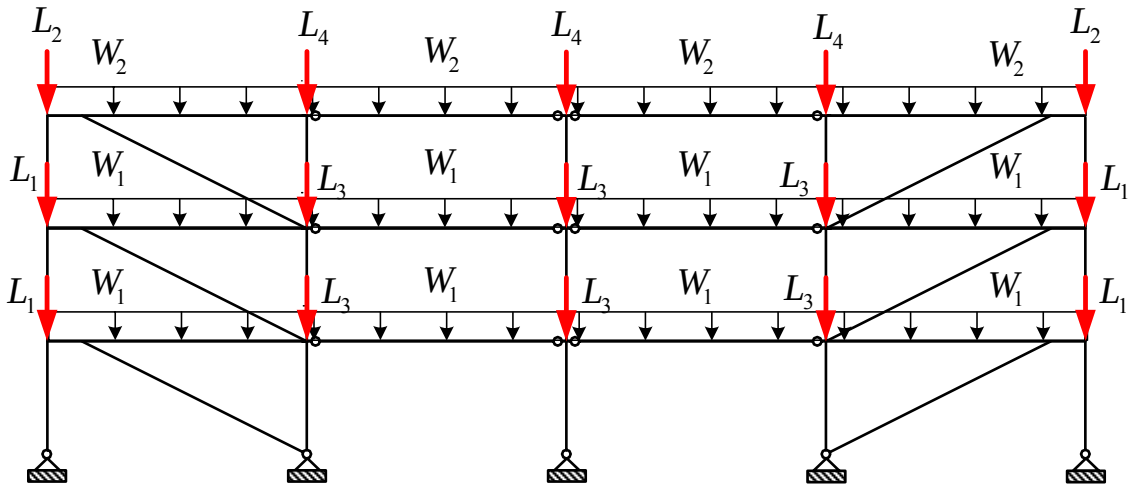

Figure 3.2 (a) Gravity loading definition for 3-story EBF

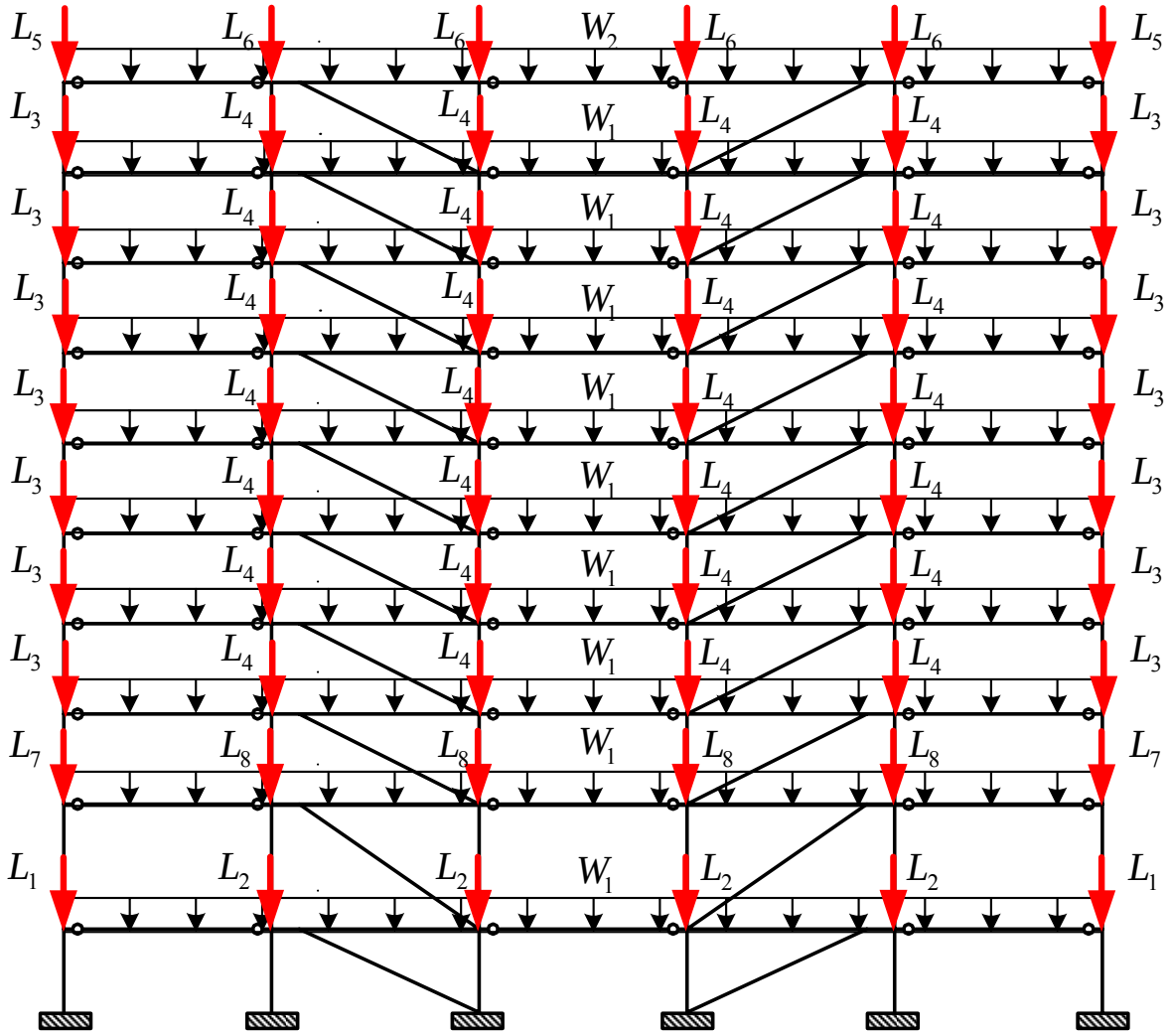

Figure 3.2 (b) Gravity loading definition for 10-story EBF

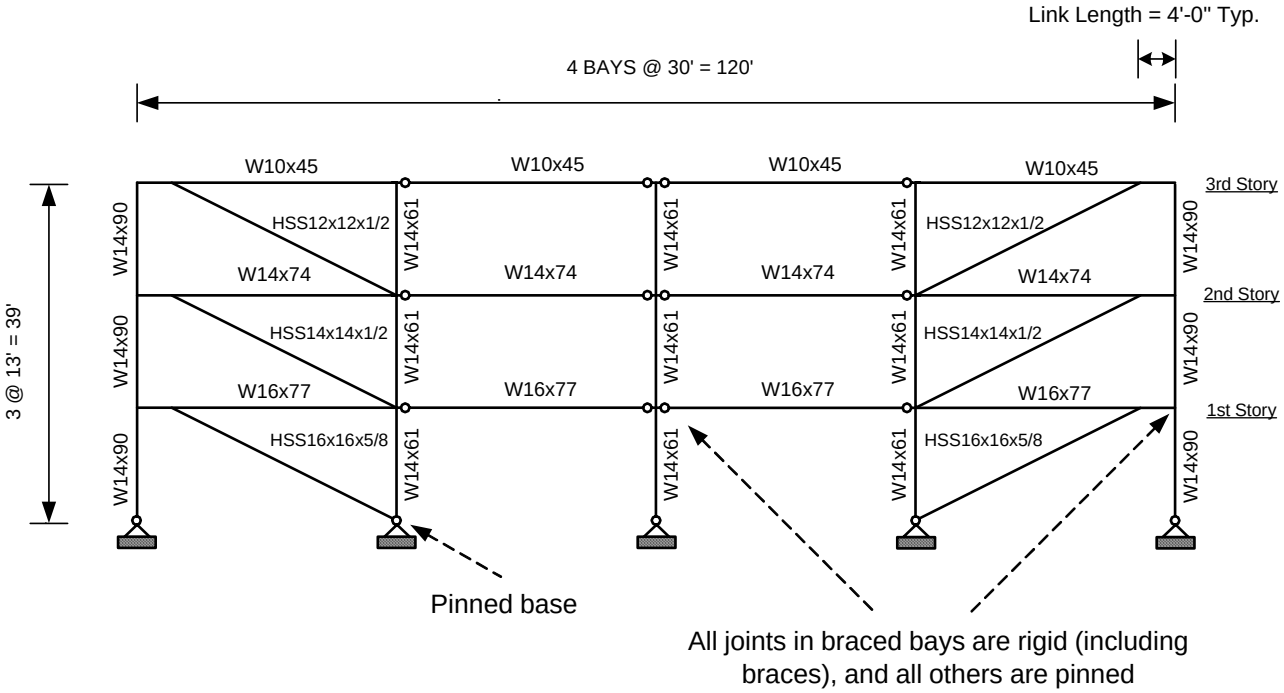

(a)

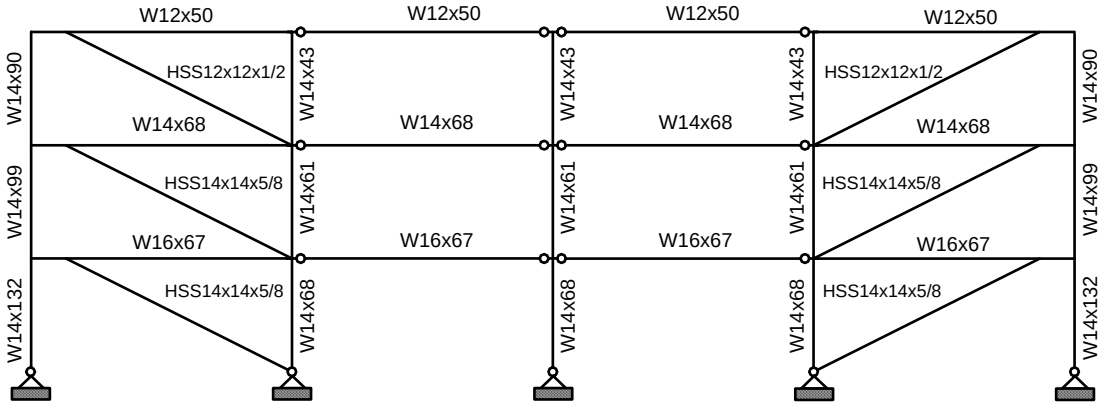

(b)

Figure 3.3 Member sections of 3-story EBF designed based on: (a) IBC 2000 approach; (b) proposed performance-based design approach (Preliminary design)

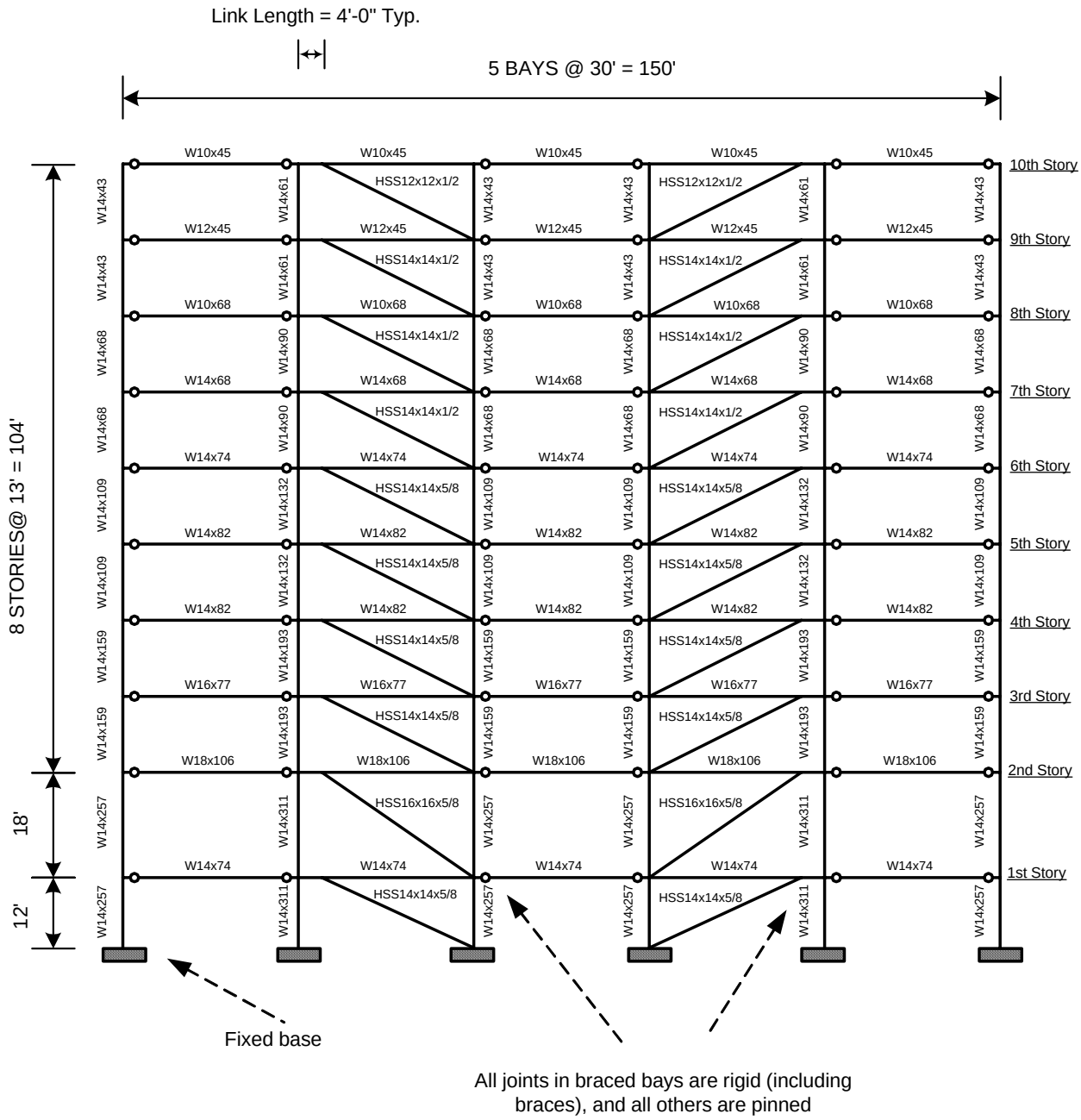

Figure 3.4 (a) Member sections of 10-story EBF designed based on IBC 2000 approach

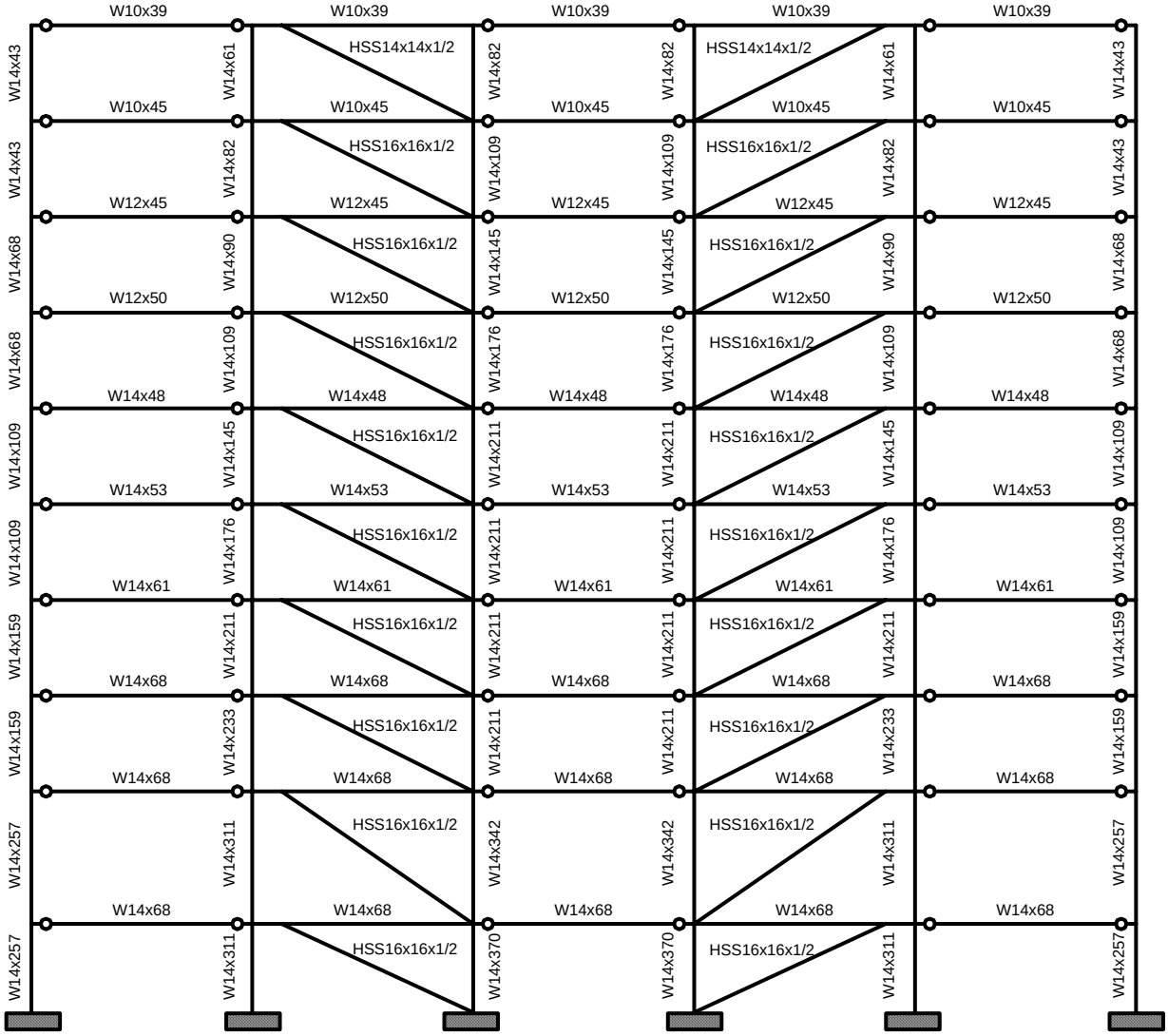

Figure 3.4 (b) Member sections of 10-story EBF designed based on proposed performance-based design approach (Preliminary design)

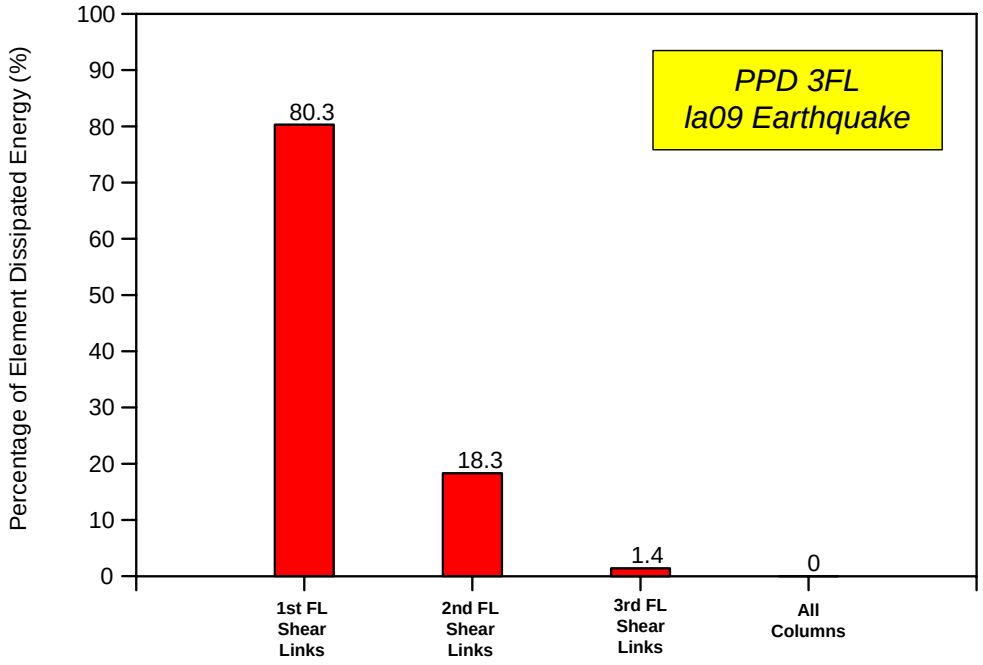

(a)

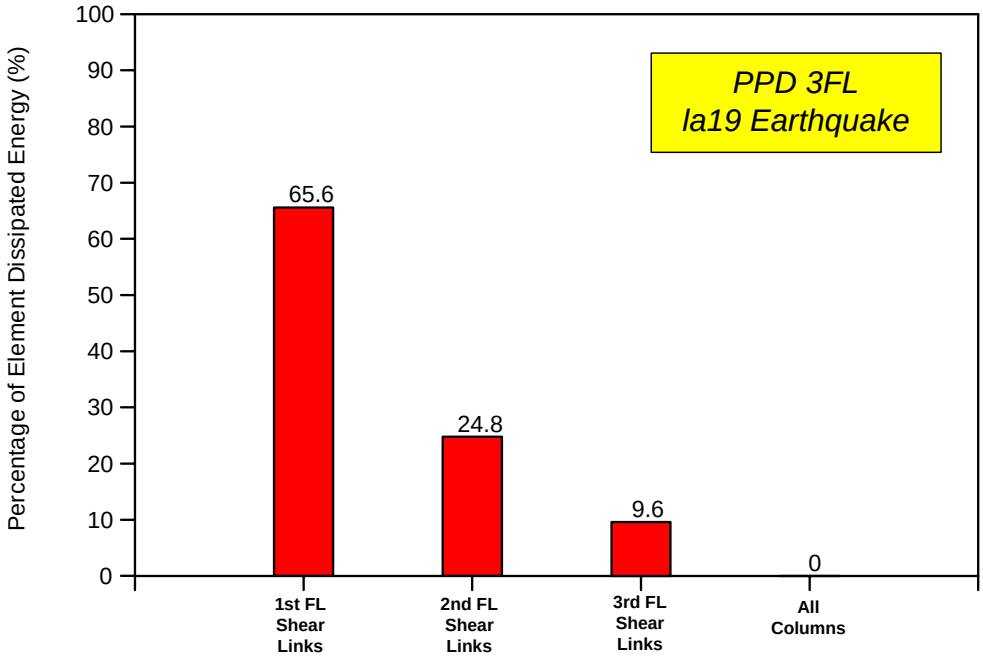

(b)

Figure 3.5 Dissipated hysteretic energy at each level of 3-story PPD frame: (a) LA 09 record; (b) LA 19 record

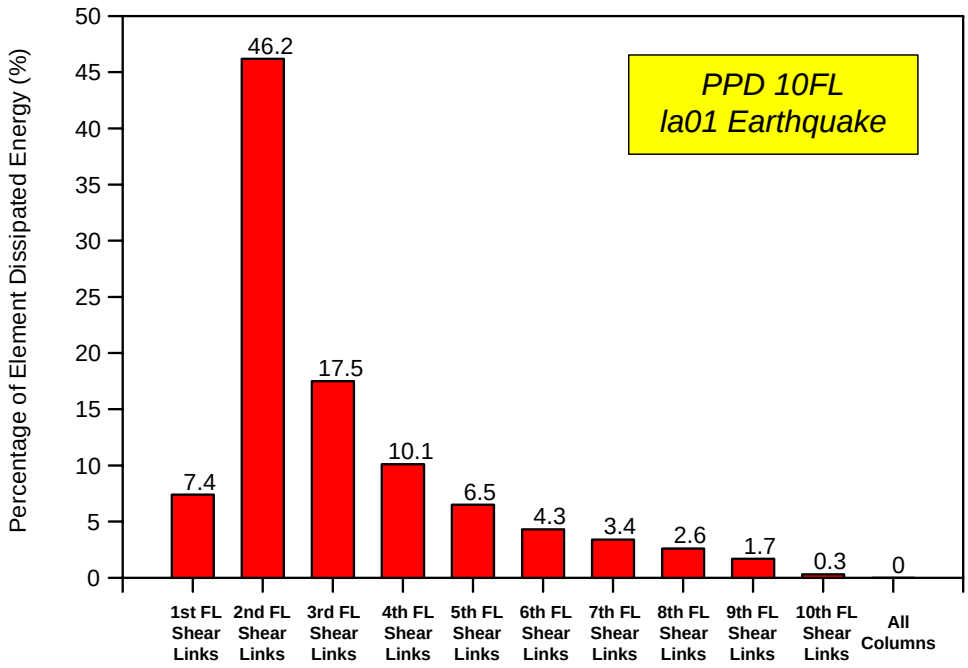

(a)

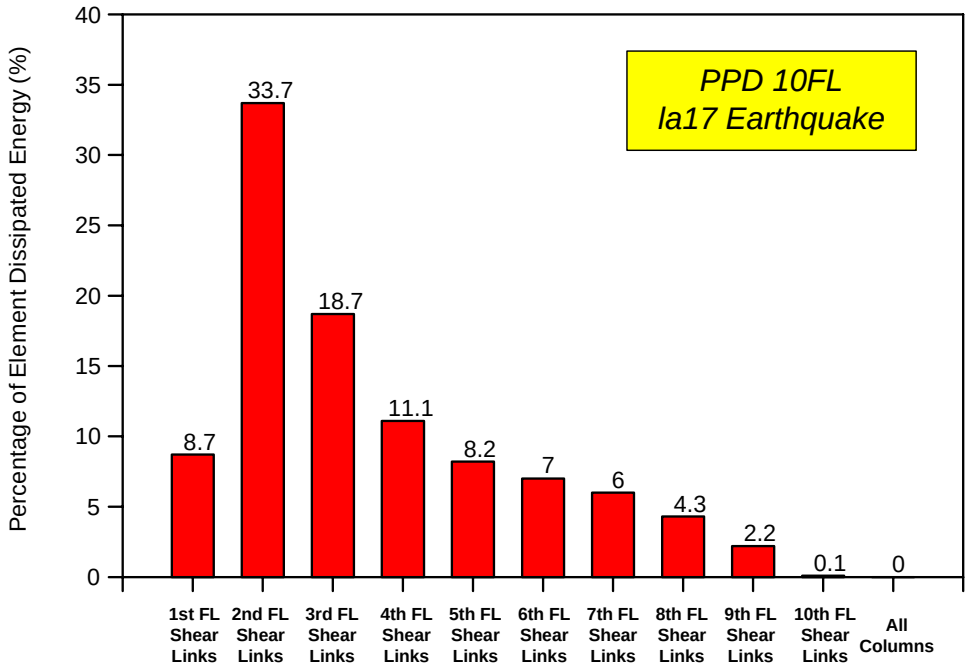

(b)

Figure 3.6 Dissipated hysteretic energy at each level of 10-story PPD frame: (a) LA 01 record; (b) LA 17 record

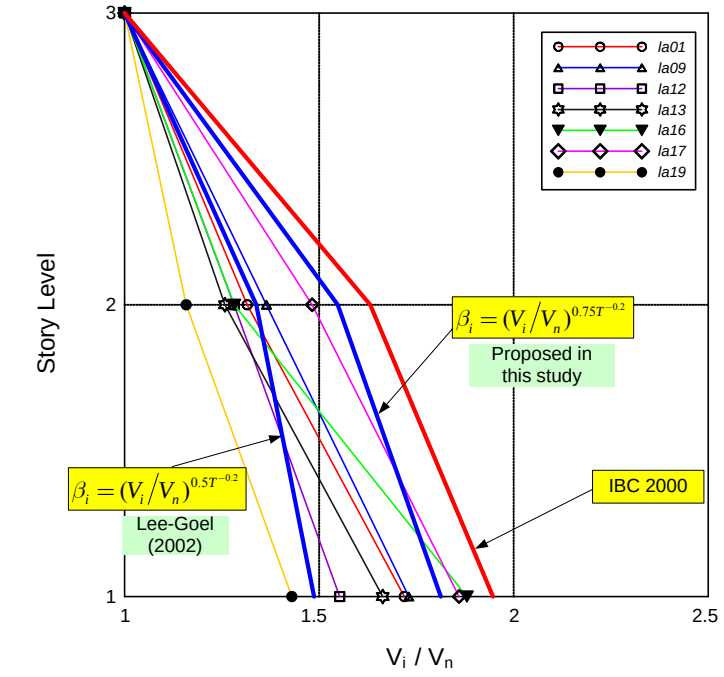

(a)

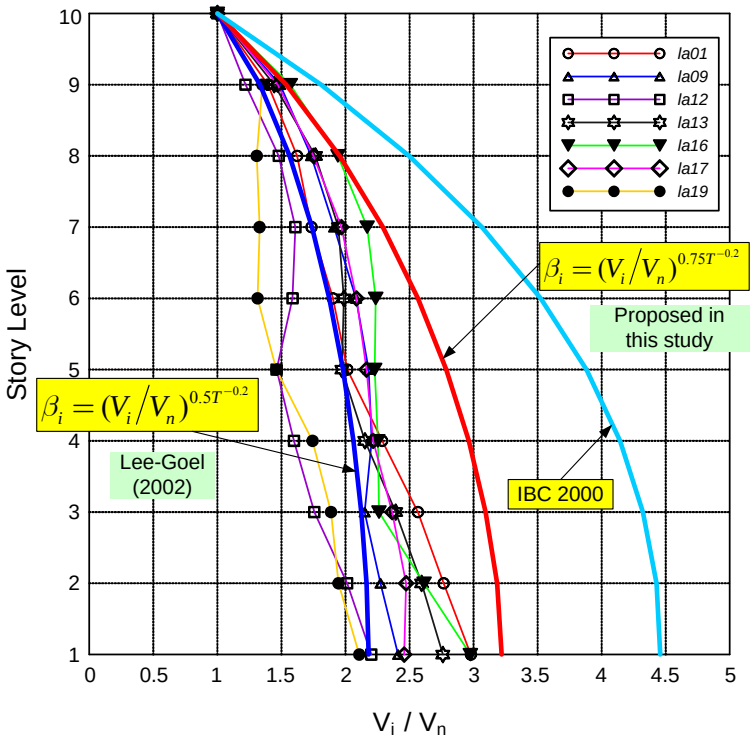

(b)

Figure 3.7 Relative story shear distributions in PPD frames from nonlinear dynamic analyses: (a) 3-story; (b) 10-story. The proposed and IBC 2000 distributions are also shown. Note: V_i is the story shear at *i*th level, and V_n is the story shear at top level

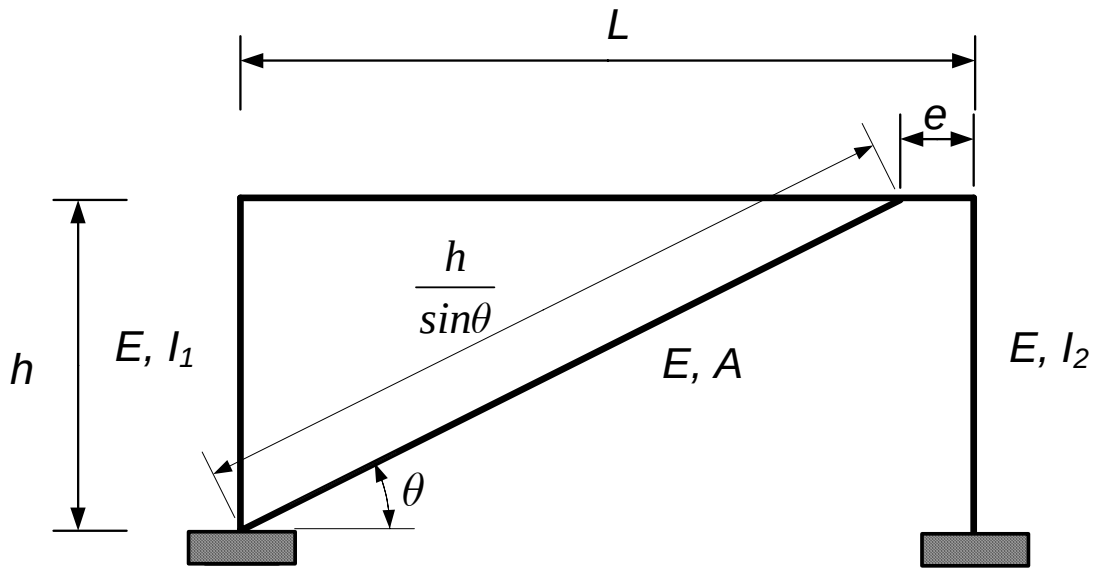

Figure 3.8 Story stiffness calculation in an EBF

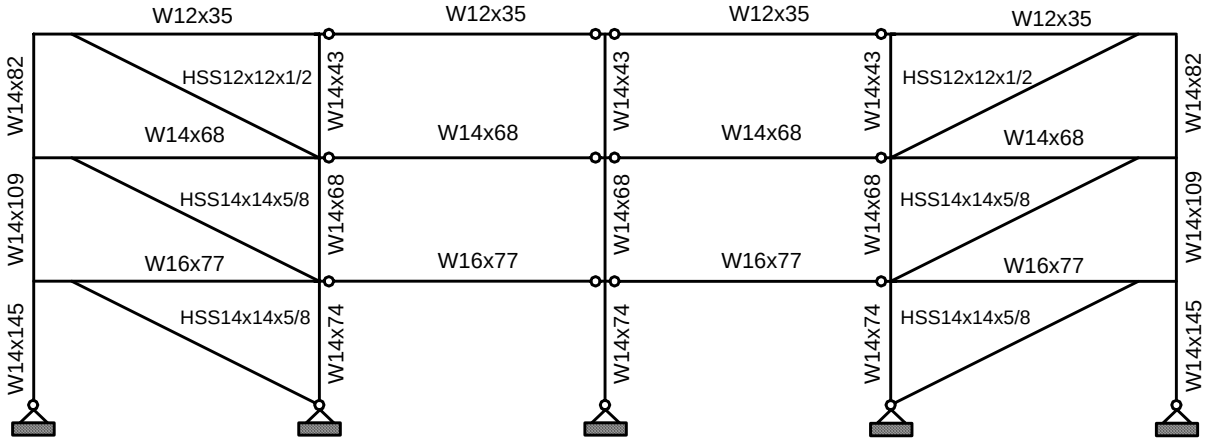

Figure 3.9 Final member sections of 3-story EBF designed based on proposed performance-based design approach

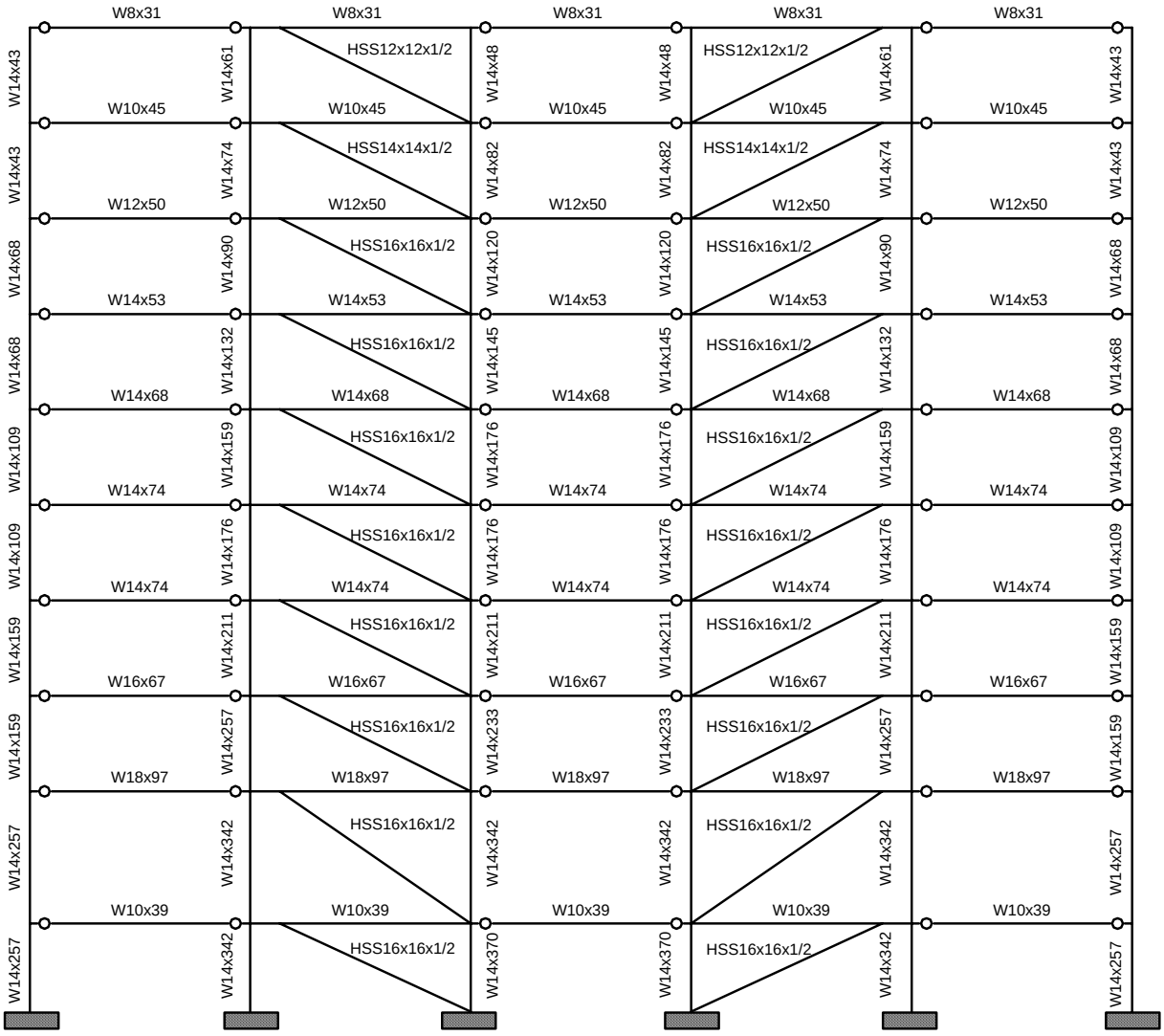

Figure 3.10 Final member sections of 10-story EBF designed based on proposed performance-based design approach

CHAPTER 4
Nonlinear Analysis Modeling and Earthquake Records

4.1 General

In order to investigate the behavior of the study buildings under major earthquakes, nonlinear analyses including both static push-over analysis and time-history dynamic analysis were conducted to compare the behavior of the IBC frames and the PPD frames. The analyses were performed using the Perform-3D (RAM, 2003) program which has a built-in shear link model. The SAC Los Angeles ground motions with 10 and 2 percent probability of exceedance in 50 years were selected as the input earthquake records.

4.2 Modeling of EBF Components

4.2.1 Force-deformation relations and component models

In general, inelastic deformation is intended to occur in the shear links only; however, it is still likely that plastic hinges could form at ends of beams and columns, or in the braces. In Perform-3D, the relation between moment and rotation of elements is modeled by a rigid-plastic moment hinge, which is closely analogous to a friction hinge that rotates only after enough moment has been applied to overcome the friction between the hinge pin and the casing. Figure 4.1 shows the hinge and corresponding moment-rotation relationship. The hinge is initially rigid, and begins to rotate at the yield moment (M_y). The moment can increase after yield moment is

reached if strain-hardening is taken into account. The maximum moment a rigid-plastic moment hinge can achieve is designated as M_u. Members outside the shear links were all modeled as beam-columns and the axial force-plastic moment surface is shown in Figure 4.2. The interaction between axial force and moment was represented using a straight line, which is slightly conservative than the one specified in AISC LRFD Manual. Although members outside the shear links are expected to remain elastic during a major earthquake, as indicated in Chapter 1, Schneider et al. (1993) had shown that members subjected to high axial loads exhibited rapid deterioration in strength and stiffness during cyclic deformation. Therefore strain-hardening was not included in the strength calculation of columns and braces. Assuming that the nominal axial (P_n) and bending (M_n) strengths for a column or brace are calculated in accordance with the AISC LRFD equations, the strengths used for the *P-M* interaction were given by:

$$P_y = R_y P_n \tag{4.1}$$

$$M_y = R_y M_n \tag{4.2}$$

where $R_y = 1.1$.

Figures 4.3 and 4.4 illustrate the column and diagonal brace models, which consist of an elastic segment, two rigid-plastic moment hinges with P-M interaction, and stiff end zones if needed. These models are “lumped plasticity” models, since the plastic deformations are concentrated in zero-length plastic hinges. The stiffness of the elastic segment is the initial stiffness of the member. The deformation of this elastic segment accounts for the elastic part of the total deformation. The rigid-plastic moment hinge then accounts for the plastic part of the total deformation (RAM, 2003).

Beams outside the shear links, as stated in Chapter 1, are generally strengthened by floor slab in resisting axial load and bending moment. Therefore, according to AISC Seismic Provisions, a strain hardening factor of 1.25 was used. The strengths of beam element for modeling were obtained by:

$$P_y = R_y P_n; \quad P_u = 1.25 \cdot R_y P_n \tag{4.3}$$

$$M_y = R_y M_n; \quad M_u = 1.25 \cdot R_y M_n \tag{4.4}$$

The beam members were also modeled as beam-column elements. Figure 4.5 shows the beam model, which has similar components as the column or brace model. For beams simply connected to the "gravity columns", moment releases were added at the ends to model the pinned connection.

Links in this study were primarily short shear yielding links, that is, shear yielding was the dominate mode. A rigid-plastic shear hinge similar to the moment hinge was used to model the shear yielding behavior as shown in Figure 4.6. Axial forces generally have small effect on short links in terms of load-carrying capacity, maximum link deformation, energy dissipation, and ductility (Ghobarah and Ramadan, 1990); therefore no axial force-shear interaction was considered in this study. In accordance with the AISC Seismic Provisions, strengths of the short links were calculated by:

$$V_y = R_y V_p; \quad V_u = 1.25 \cdot R_y V_p \tag{4.5}$$

Plastic link rotation at V_u was assumed to be 0.08rad. Figure 4.7 illustrates the shear link model in Perform-3D, which consists of:

(1) Two elastic segments that account for elastic axial, bending and shear deformations of the shear link.

(2) A shear hinge, which accounts for yielding in shear.

(3) A pair of moment strength sections, to present yielding in bending.

4.2.2 Gravity loads and seismic masses

The design gravity loads were described in Chapter 3 and a load combination of 1.2DL+0.5LL was applied to the structures during nonlinear static push-over and time-history dynamic analyses. Both $P-\Delta$ and $P-\delta$ effects were accounted for in the analysis. The seismic masses were lumped at frame joints as was done by Ricles and Popov (1987). Figures 4.8 and 4.9 show the lumped seismic masses for the 3- and 10-story EBFs, respectively.

4.2.3 Damping

In nonlinear dynamic analysis it is usual practice to use some viscous damping to account for the energy dissipation in addition to hysteretic energy. Perform-3D uses the "$\alpha M + \beta K$" (Rayleigh damping) model, which assumes that the structure has a constant damping matrix, [C], given by:

$$[C] = \alpha[M] + \beta[K] \tag{4.6}$$

where [*M*] is the structure mass matrix, [*K*] is the initial elastic stiffness matrix; α and β are multiplying factors. By combining αM and βK damping it is possible to have essentially constant damping over a significant range of periods, as indicated in Figure 4.10. As a structure yields it usually softens, its effective vibration period usually increases. By using this damping model, a constant elastic damping is maintained throughout the response. In this study, a 2% of critical viscous damping was assumed.

Ricles and Popov (1987, 1994) pointed out that viscous damping in shear link elements may result in unrealistically large brace and column axial forces due to large relative transverse velocity developed between link ends after yielding. They suggested using a nonproportional viscous damping (only αM damping, no βK damping) for shear link elements, while all the other elements (braces, column, beams) maintain traditional Rayleigh damping. This nonproportional viscous damping has been employed in the EBF dynamic analyses (Ricles and Popov, 1987; Richards and Uang, 2003). However, a pre-analysis conducted in this study indicated that, by using the proposed performance design approach, braces and columns remained elastic in most cases even the Rayleigh damping was used in all element including shear links. On the other hand, an unrealistically large link rotation and hence story drift resulted if nonproportional viscous damping was used for the shear links. Since a lower damping ratio of 2% was selected for the analysis, it is deemed that using nonproportional viscous damping in the links would be over conservative. As a consequence, the analyses performed in this study used Rayleigh damping for all elements.

4.3 Earthquake Records

Eight 10% in 50 years (return period 474 years) and Four 2% in 50 years (return period 2,475 years) SAC Los Angeles ground motions were selected for the nonlinear time history analysis as shown in Figures 4.11 and 4.12. In addition to the acceleration time histories, the companion velocity time histories shown in Figures 4.11 and 4.12 are good indication of near-fault type ground motion in which high velocity pulse is observed (Bolt, 2004). Figures 4.13 and 4.14 show the design spectrum from IBC 2000 (PPD frames only), as well as the response spectra of selected SAC earthquake records. Note that the SAC ground motions were already scaled (Somerville et al., 1997) hence no further scaling factor was used in this study.

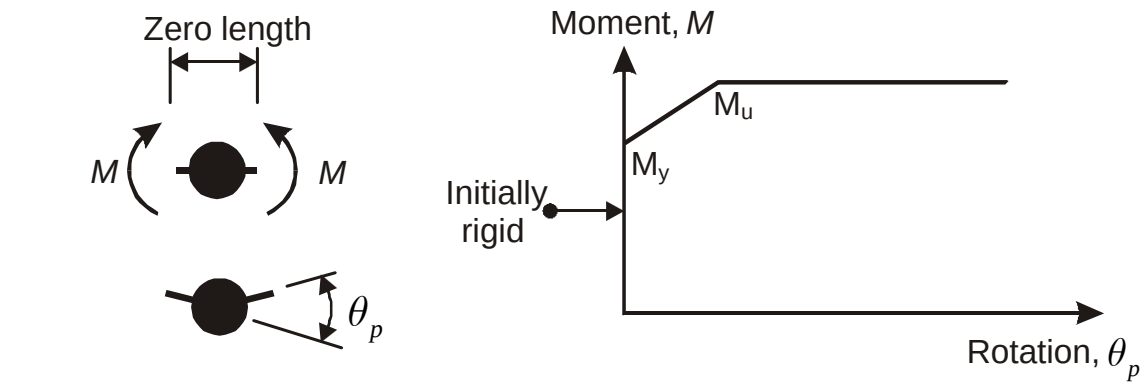

(a) Rigid-Plastic Moment Hinge (b) Moment-Hinge Rotation Relationship

Figure 4.1 Rigid-plastic hinge model and corresponding moment-rotation relationship

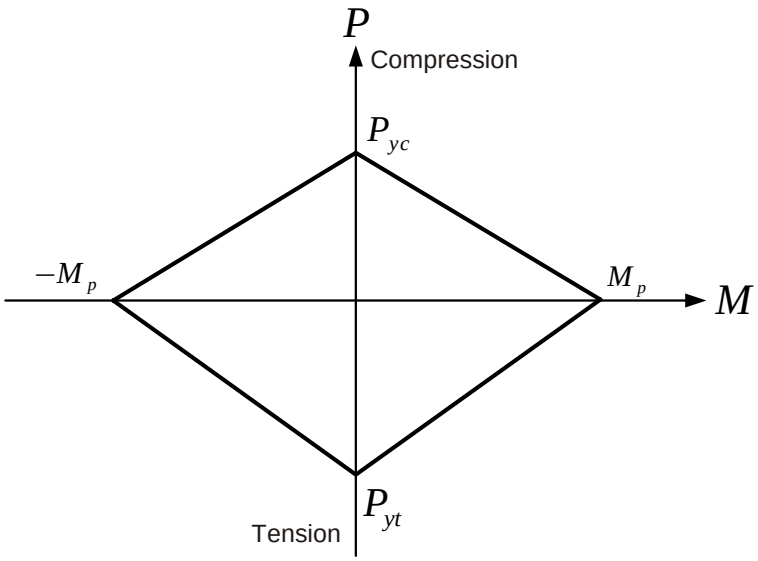

Figure 4.2 P-M interaction curve for Beam-Column elements

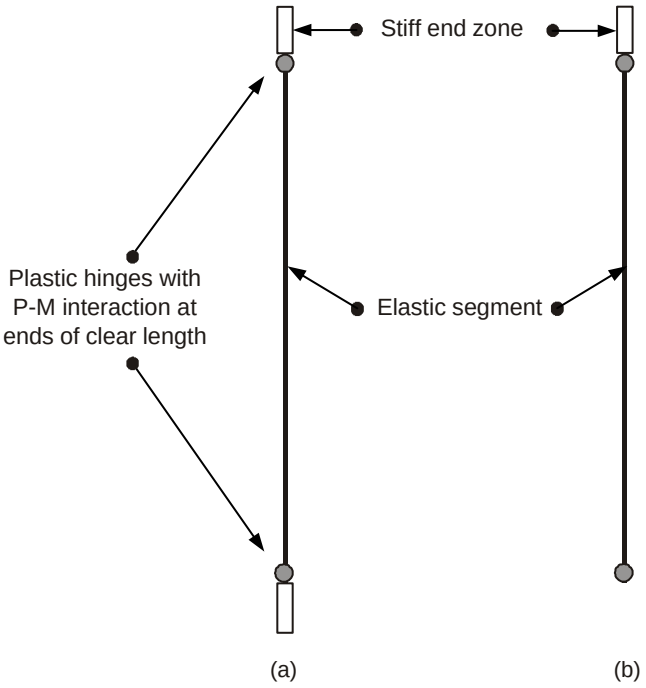

Figure 4.3 Column component model: (a) General floor columns; (b) First floor columns

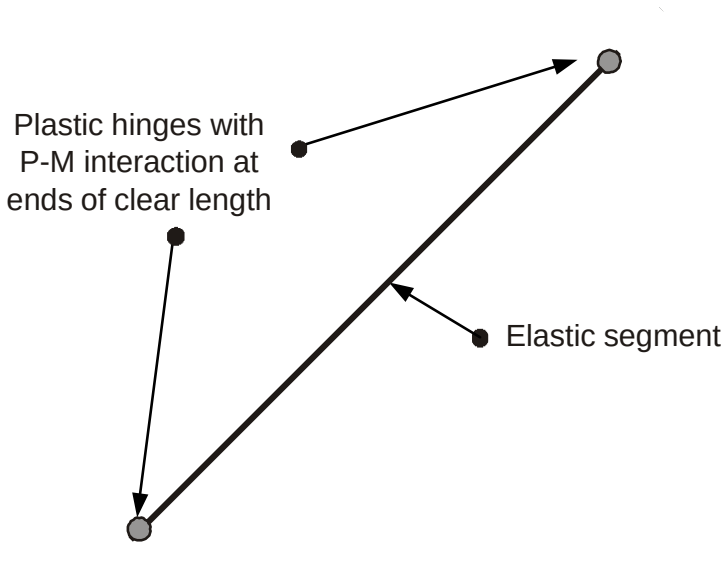

Figure 4.4 Diagonal brace component model

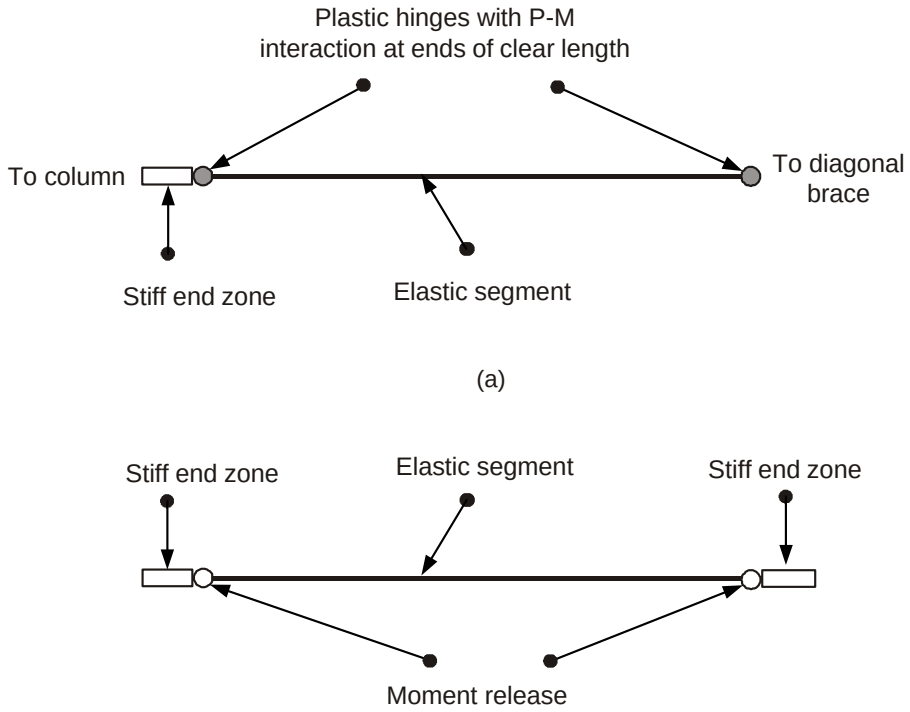

Figure 4.5 Beam component model: (a) Beams in braced bay; (b) Beams in gravity bay

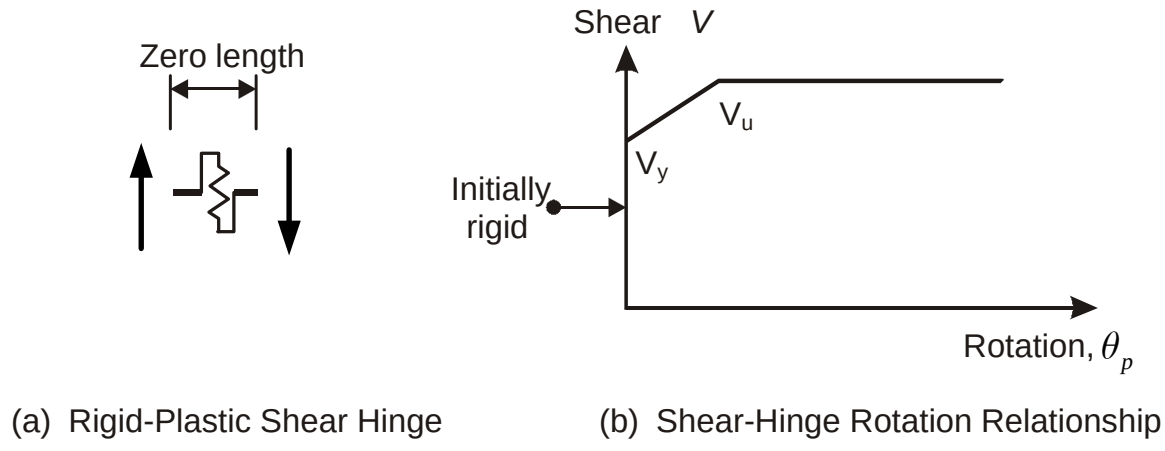

Figure 4.6 Rigid-plastic shear hinge model and corresponding shear-rotation relationship

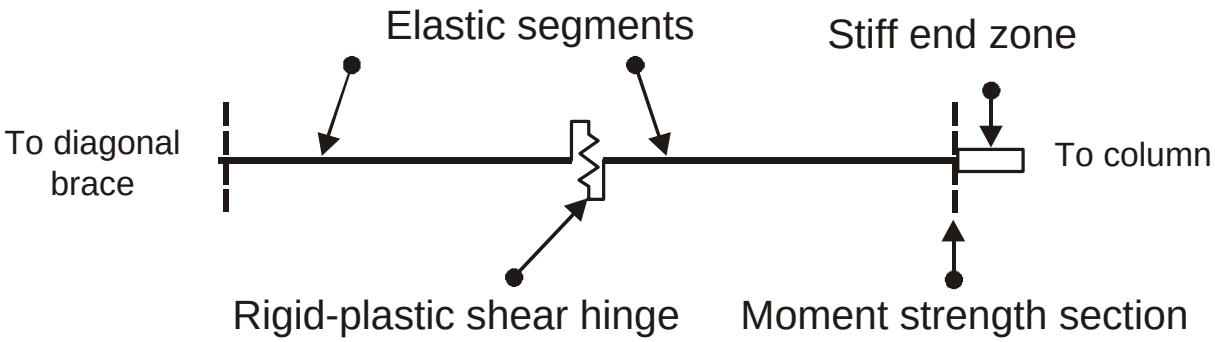

Figure 4.7 Shear link component model

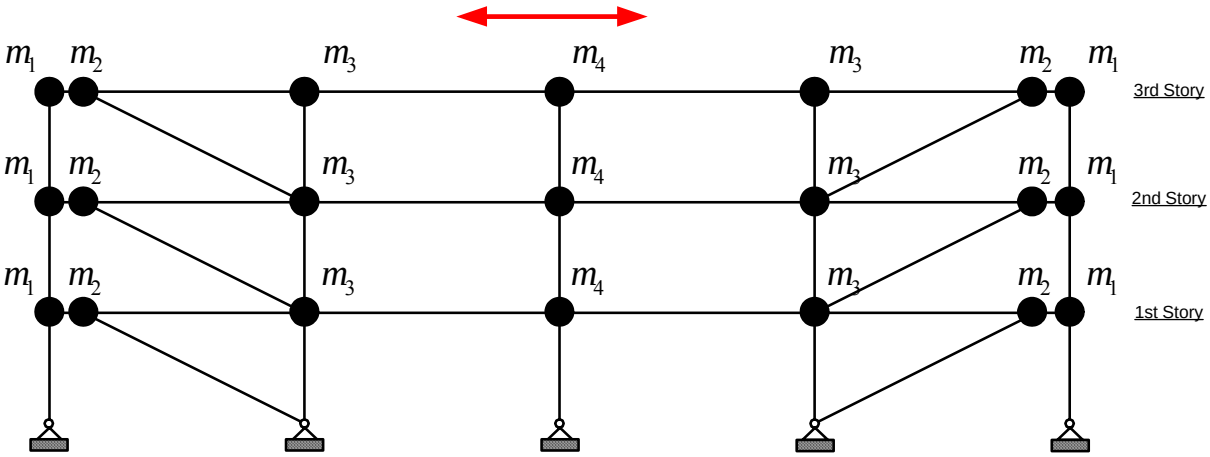

Story	m_1	m_2	m_3	m_4
3	0.0345	0.259	0.483	0.518
2	0.0327	0.245	0.457	0.490
1	0.0327	0.245	0.457	0.490

Seismic Mass: kips-sec^2/in (for one frame)

Figure 4.8 Lumped mass for 3-story EBF

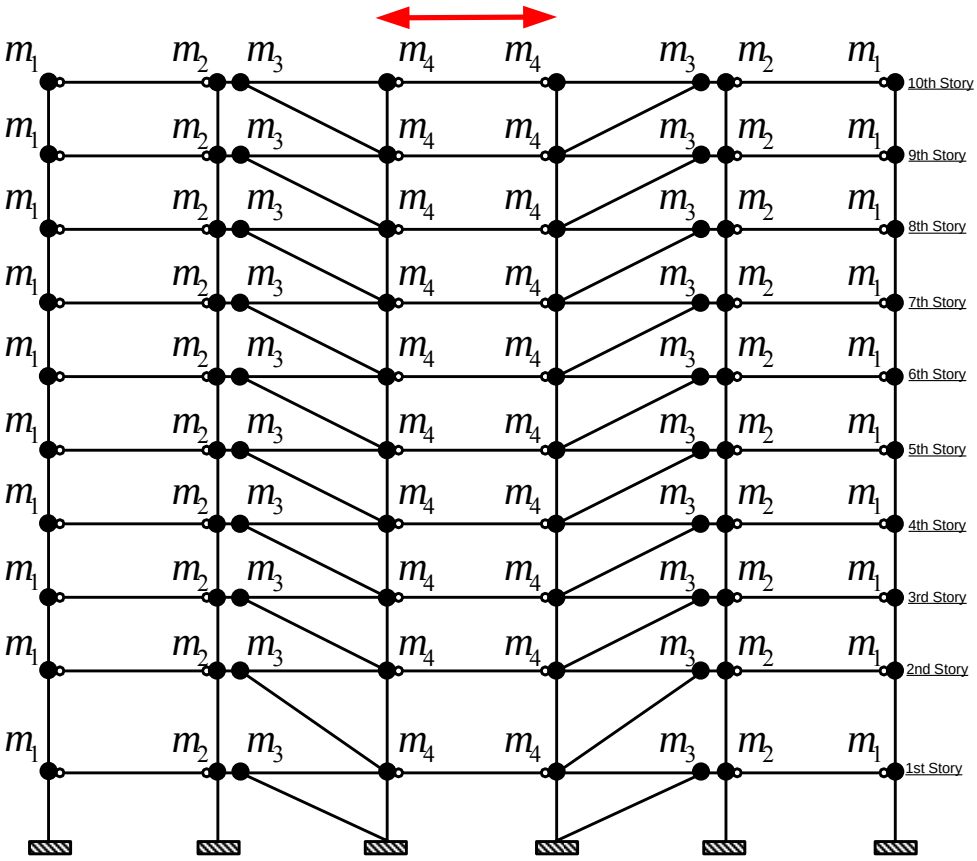

Story	m_1	m_2	m_3	m_4
10	0.215	0.243	0.215	0.401
9	0.202	0.229	0.202	0.377
8	0.202	0.229	0.202	0.377
7	0.202	0.229	0.202	0.377
6	0.202	0.229	0.202	0.377
5	0.202	0.229	0.202	0.377
4	0.202	0.229	0.202	0.377
3	0.202	0.229	0.202	0.377
2	0.202	0.229	0.202	0.377
1	0.202	0.229	0.202	0.377

Seismic Mass: kips-sec^2/in (for one frame)

Figure 4.9 Lumped mass for 10-story EBF

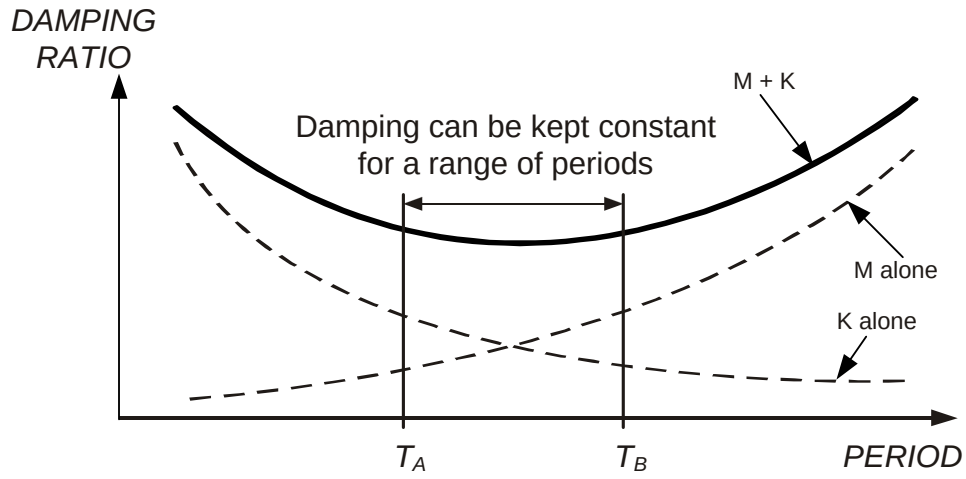

Figure 4.10 Variation of damping ratio with structural period

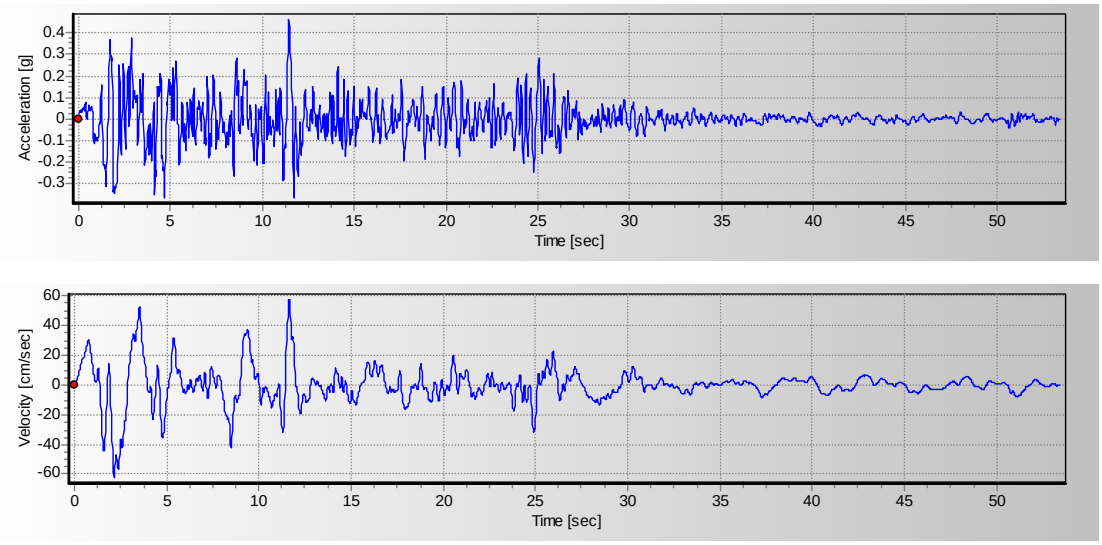

LA01 (Imperial Valley, 1940, El Centro)

Figure 4.11 Acceleration and velocity time histories of selected 10% in 50 years SAC records

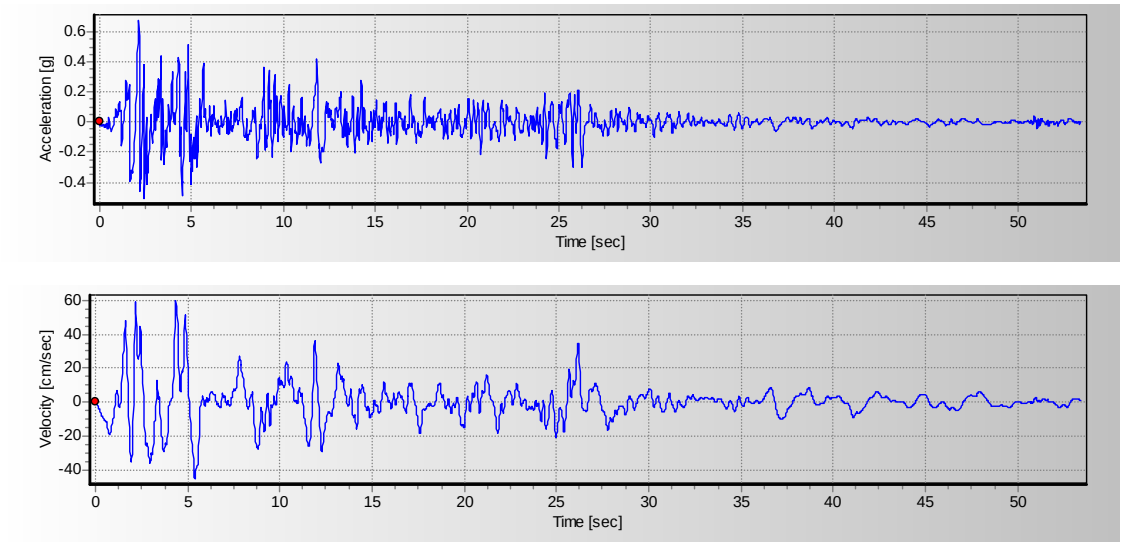

LA02 (Imperial Valley, 1940, El Centro)

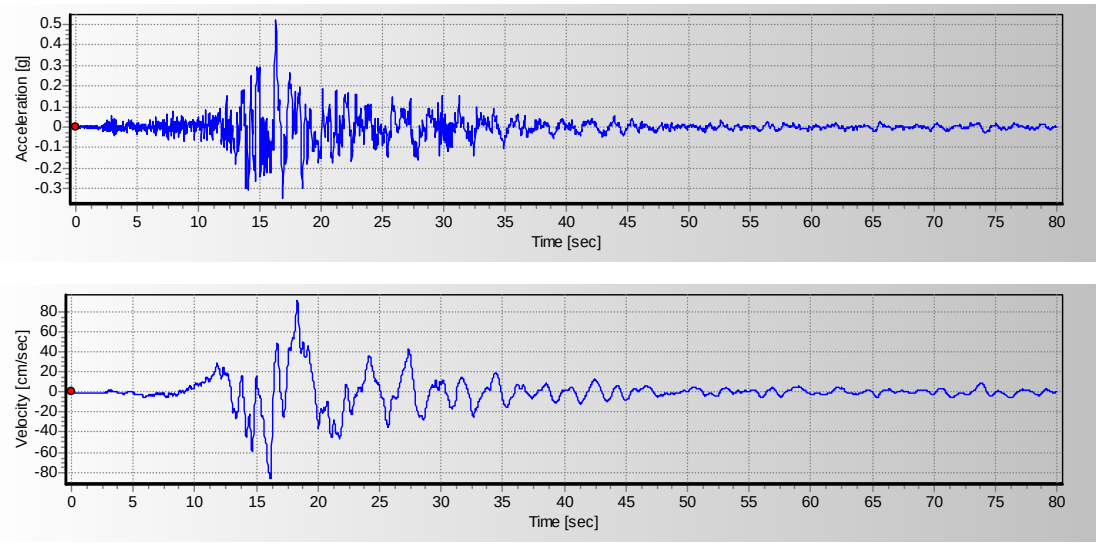

LA09 (Landers, 1992, Yermo)

Figure 4.11 Acceleration and velocity time histories of selected 10% in 50 years SAC records (con't)

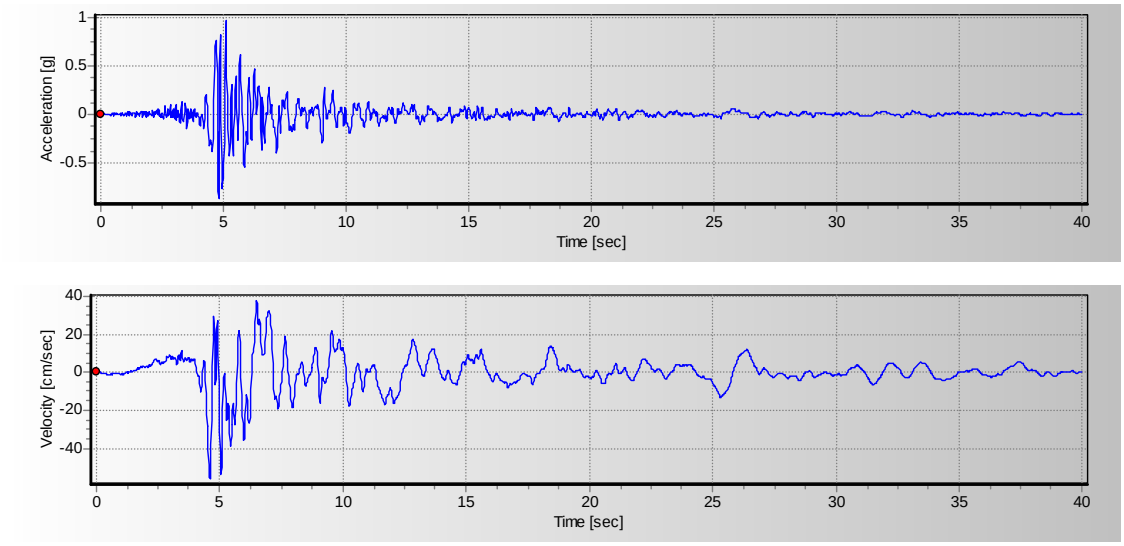

LA12 (Loma Prieta, 1989, Gilroy)

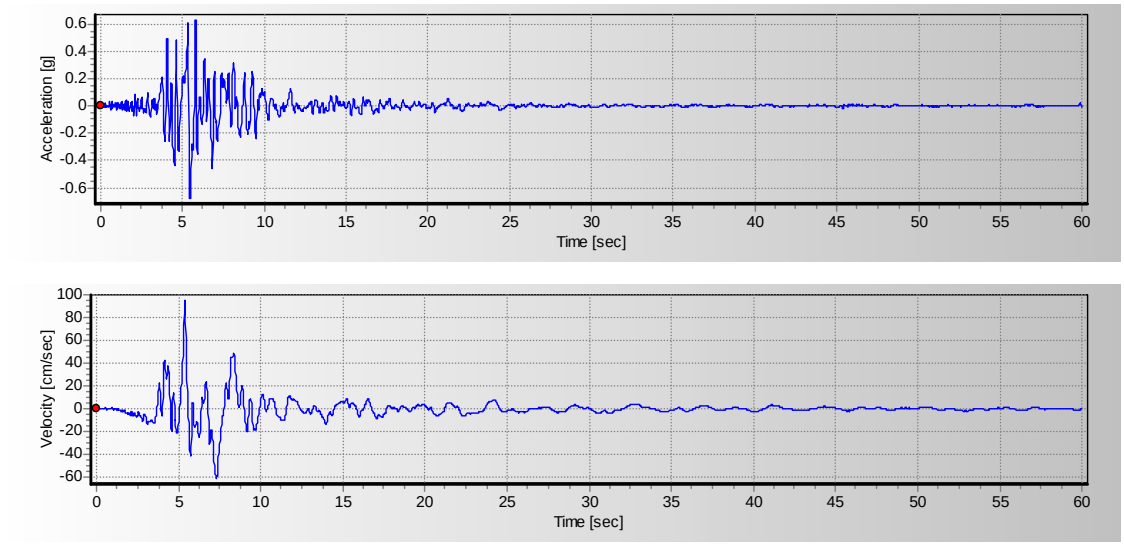

LA13 (Northridge, 1994, Newhall)

Figure 4.11 Acceleration and velocity time histories of selected 10% in 50 years SAC records (con't)

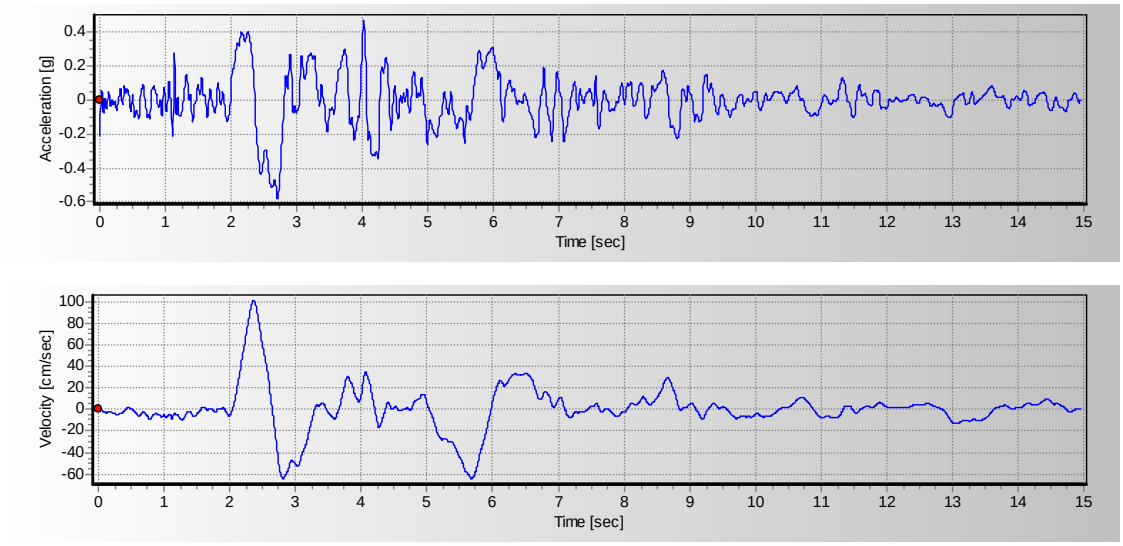

LA16 (Northridge, 1994, Rinaldi RS)

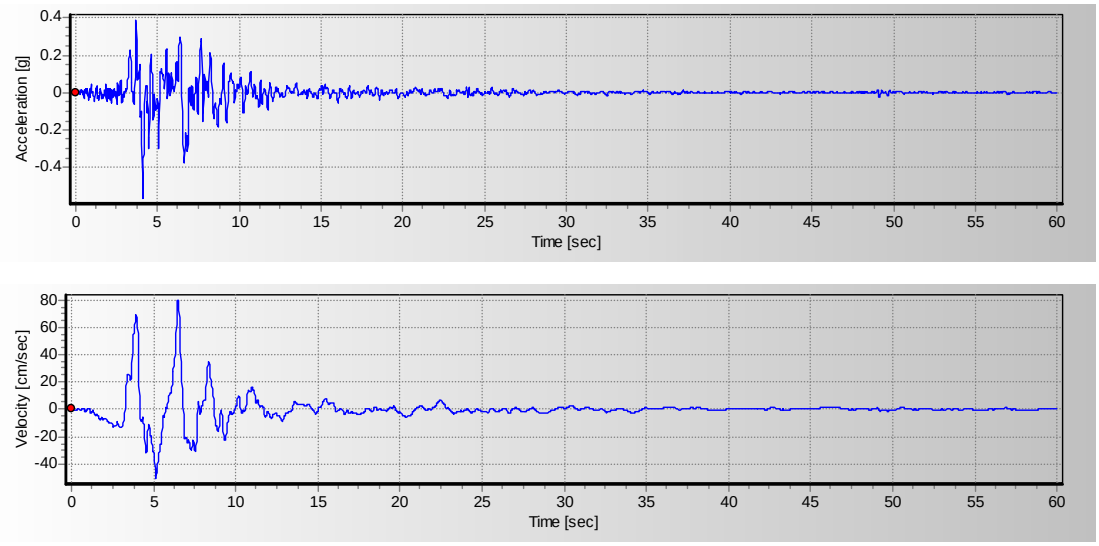

LA17 (Northridge, 1994, Sylmar)

Figure 4.11 Acceleration and velocity time histories of selected 10% in 50 years SAC records (con't)

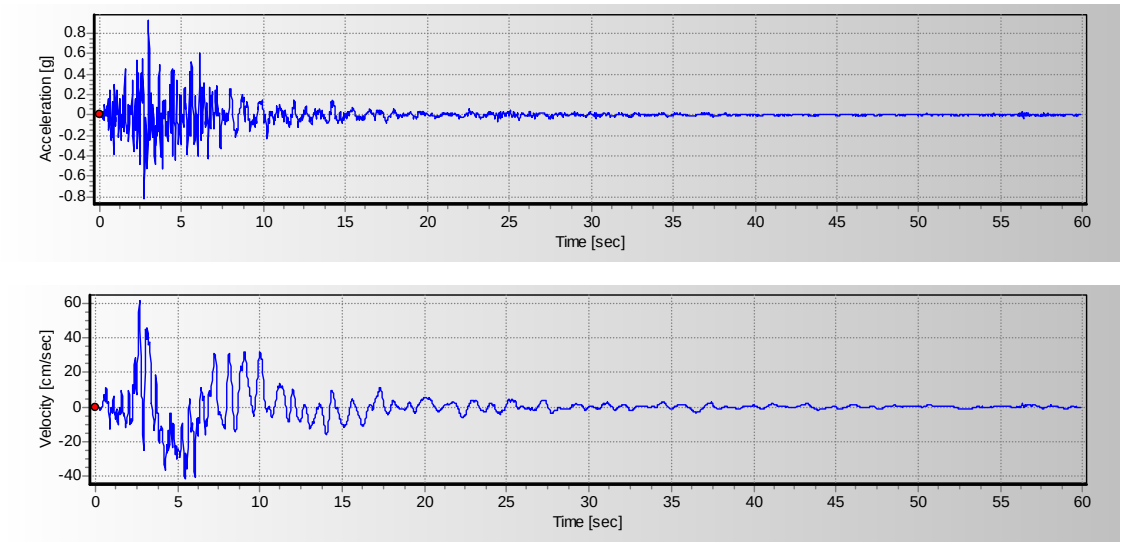

LA19 (North Palm Springs, 1986)

Figure 4.11 Acceleration and velocity time histories of selected 10% in 50 years SAC records (con't)

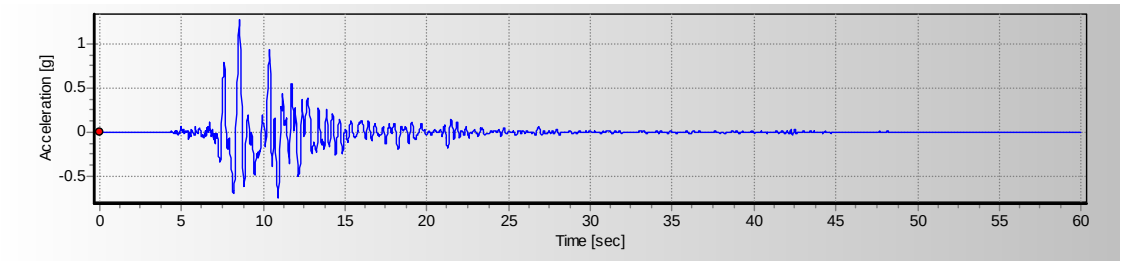

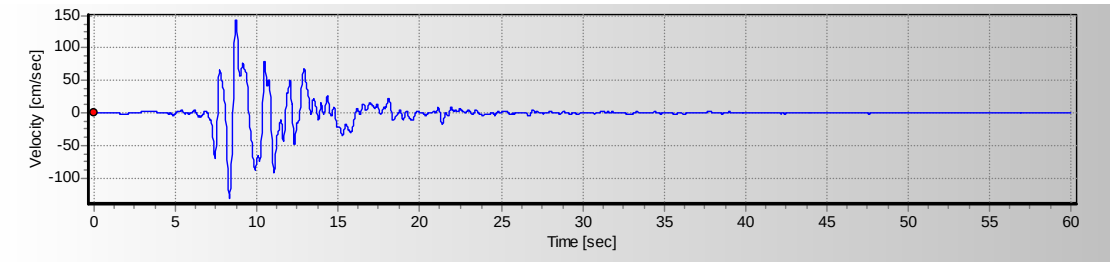

LA21 (Kobe 1995)

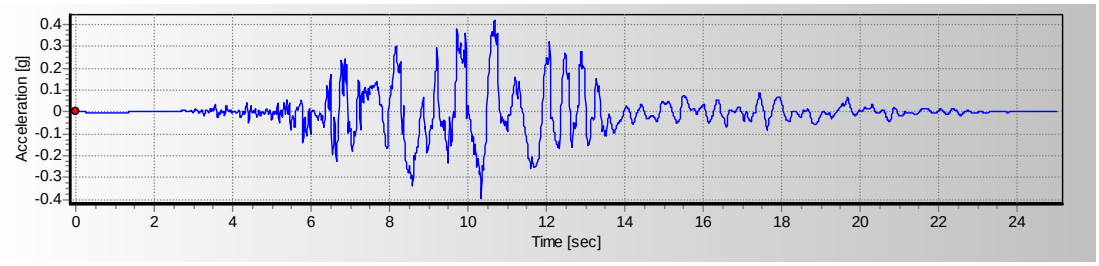

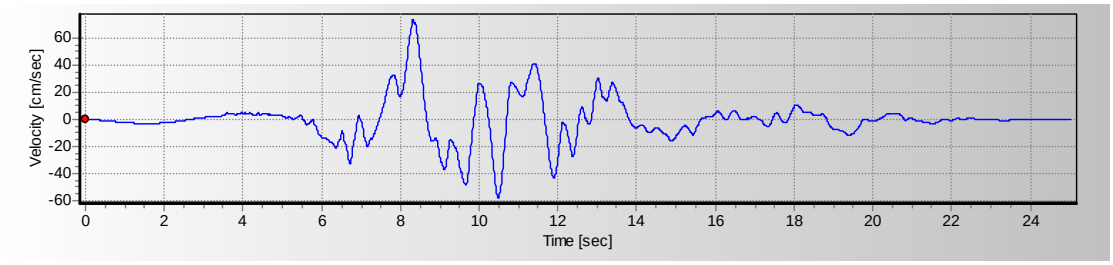

LA23 (Loma Prieta, 1989)

Figure 4.12 Acceleration and velocity time histories of selected 2% in 50 years SAC records

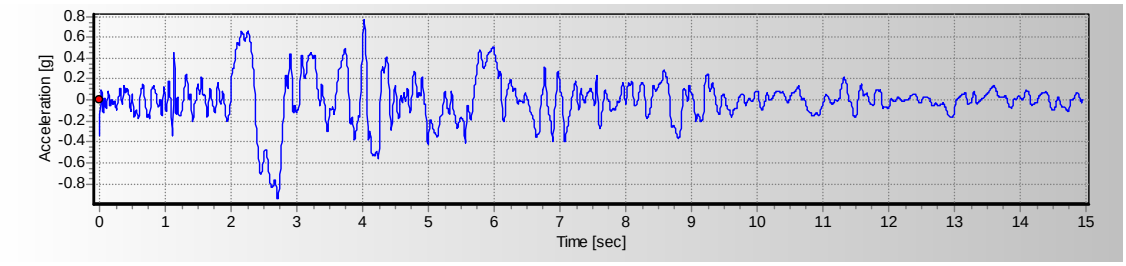

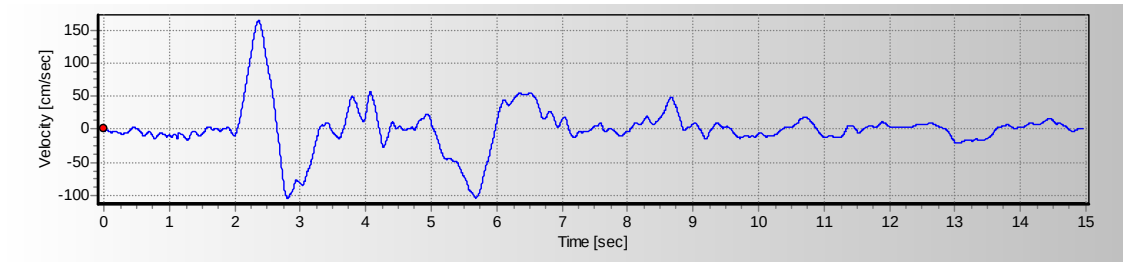

LA26 (Northridge, 1994)

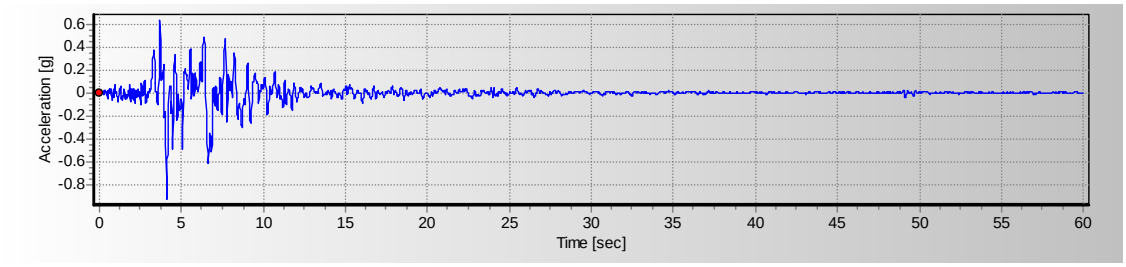

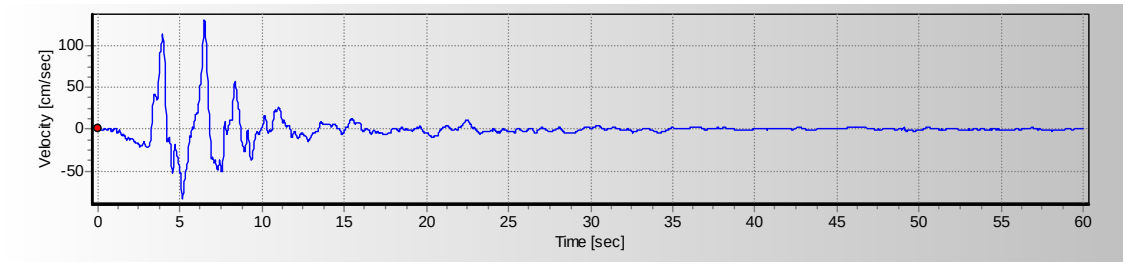

LA27 (Northridge, 1994)

Figure 4.12 Acceleration and velocity time histories of selected 2% in 50 years SAC records (con't)

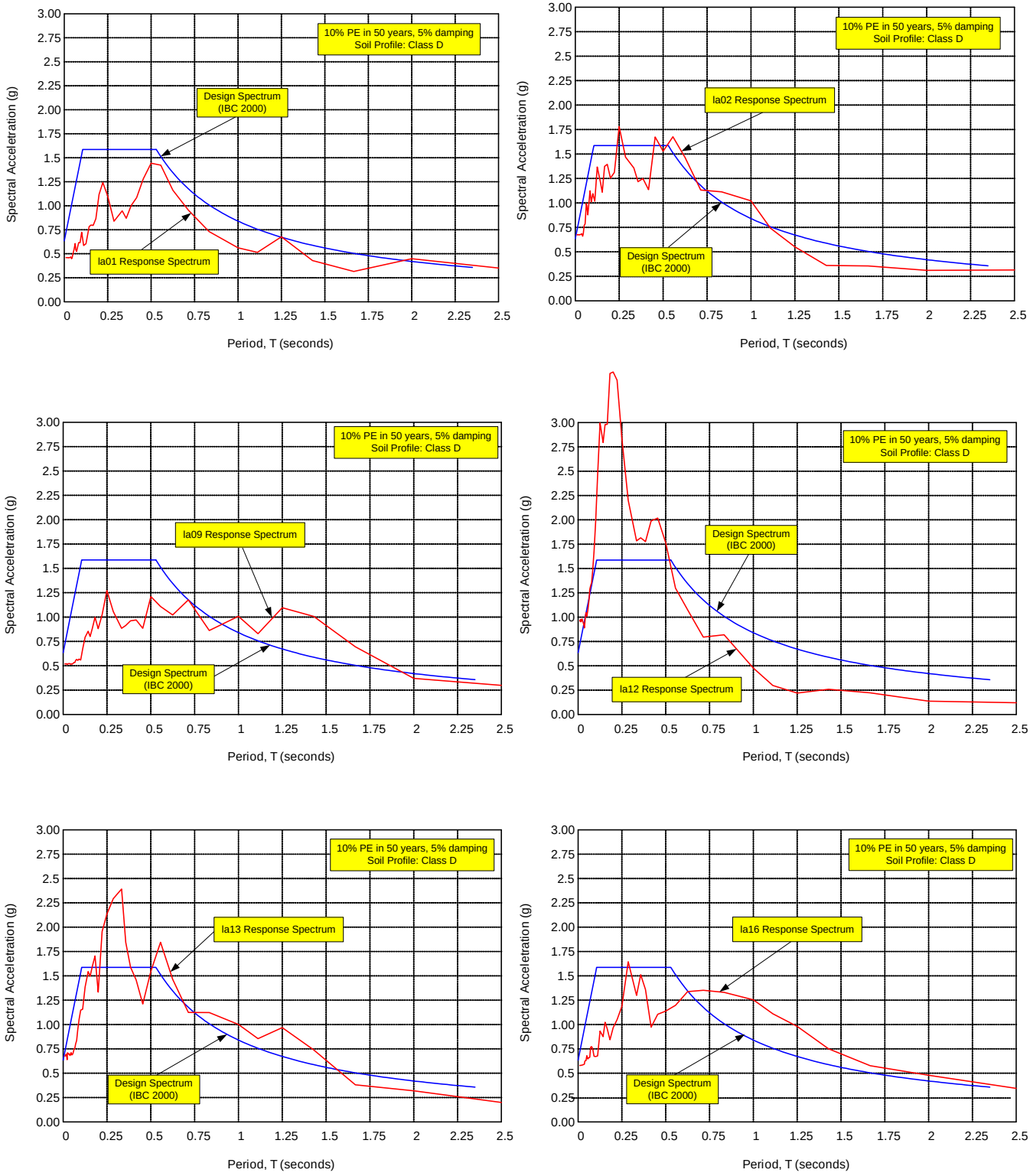

Figure 4.13 Design spectrum and response spectra of selected 10% in 50 years SAC earthquake records

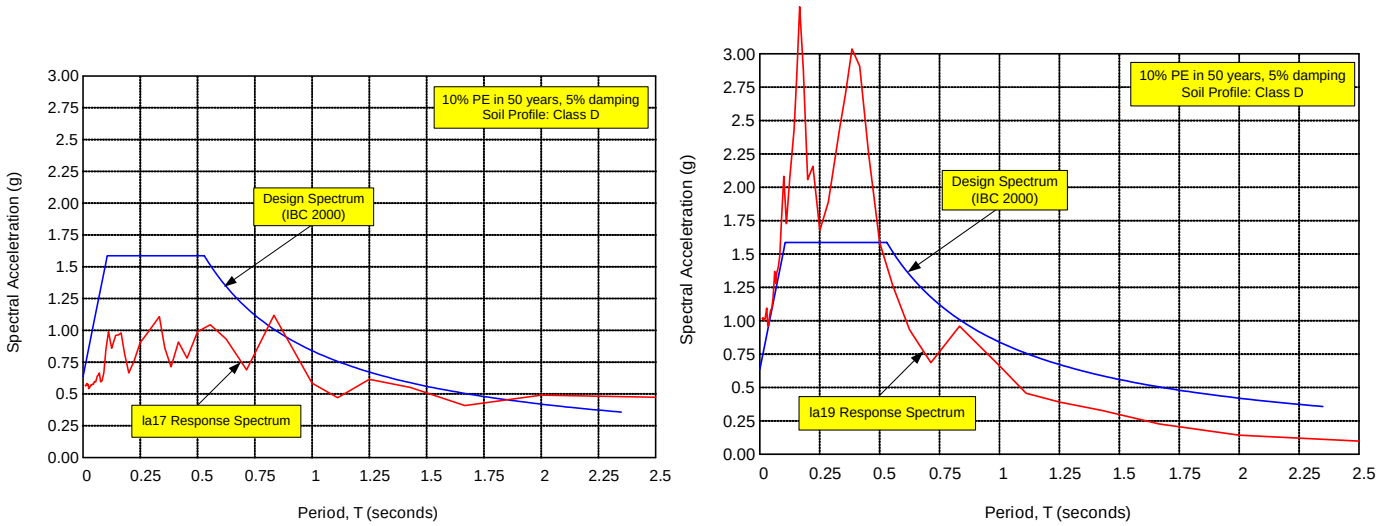

Figure 4.13 Design spectrum and response spectra of selected 10% in 50 years SAC earthquake records (con't)

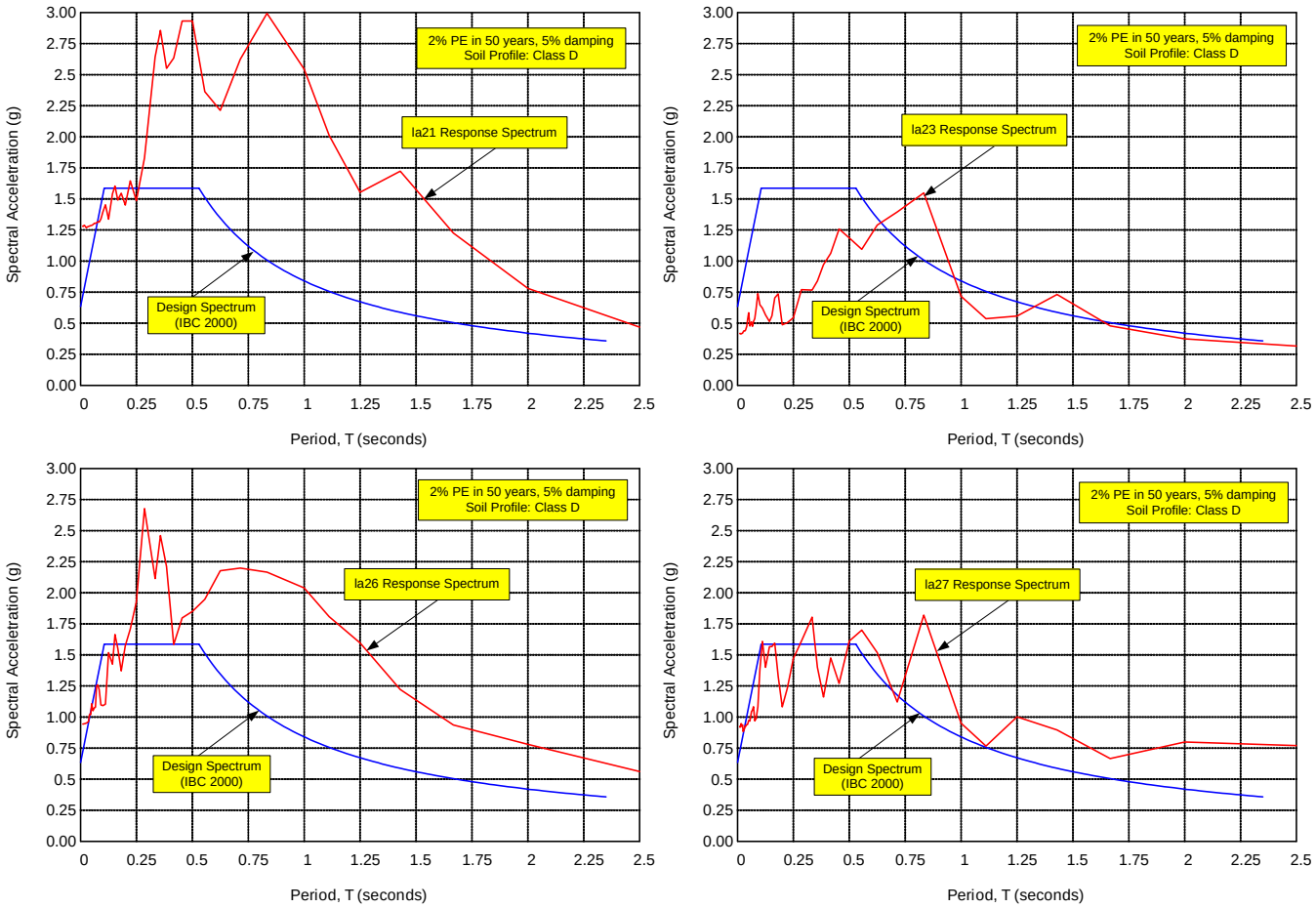

Figure 4.14 Design spectrum and response spectra of selected 2% in 50 years SAC earthquake records

CHAPTER 5
Performance Evaluation of Study EBFs

5.1 General

Serious efforts have been undertaken to develop the framework for performance-based earthquake engineering (PBEE) in the United States after 1994 Northridge Earthquake. Based on the requirement of PBEE, a structure should meet multiple performance objectives when subjected to earthquakes: for example, fully operational in the 72-year earthquake event (with 50% probability of exceedance in 50 years), and life safety in the 474-year event (10% in 50 years). This implies that the structural and nonstructural damage or performance needs to be accurately predictable in order for owners or users to make appropriate decisions on safety and risk. In current practice, the performance-based design is carried out in an indirect manner. In other word, it usually starts with an initial design according to conventional elastic design method based on modern design codes, and then an assessment analysis is performed. As a consequence, an iterative process between design and assessment is followed.

Two predominant methods, the Coefficient Method in FEMA 356 (ASCE, 2000) and Capacity-Spectrum Method in ATC-40 (ATC, 1996) are most often used in current practice. Both approaches use nonlinear static analysis (pushover analysis) to estimate the seismic demands. A target displacement, which is intended to represent the maximum displacement likely to be experienced during the design earthquake, is first calculated based on either coefficient method or capacity-spectrum method, then the structure is monotonically pushed by specified lateral

forces until the target displacement is exceeded. If the performance predicted by the pushover analysis, such as interstory drift, member rotational angle, and ductility demand, does not meet the required objectives, the design is revised and then the same process is repeated until performance targets are met.

These performance-based design approaches, while practical, may have several problems:

1) A poor initial design may be improved eventually through many iterations, but it most likely will never become a good or optimal design (Krawinkler and Miranda, 2004).
2) Since a nonlinear static analysis is required, engineers need to deal with mathematical models which directly incorporate the nonlinear load-deformation characteristics of individual components and elements of a structure. Together with the iterative design process, the entire design is more time-consuming than the conventional ones.
3) The performance evaluations focus primarily on the demands and capacities of individual components, rather than the global structural behavior. Consequently, the overall structural performance will depend on the weakest or least ductile elements which may have little influence on the overall structure behavior (Hamburger et al, 2004).
4) The nonlinear static procedures may not be reliable in predicting some demands as pointed out by FEMA 440 (ATC, 2004), such as maximum drifts at each level, story shear forces. A direct nonlinear dynamic analysis, in many cases, gives better indications.

While future improvement is needed in the current performance-based design practice, this study proposes a direct design method which basically requires no assessment after initial design. As illustrated in Chapter 2, the proposed performance-based plastic design approach has the

following advantages and features:

1) The seismic input energy is calculated based on the design spectra given by the design codes. Then the design base shear is obtained by the proposed energy balance criterion.
2) As shown in Chapter 2, the design proceeds with a pre-selected yield mechanism for the structure. The shear links at all levels are designed at the same time, as well as the elements outside the shear links. Thus, the designer is able to envision the targeted structural behavior during a major earthquake.
3) It is a direct performance-based design method which basically requires no nonlinear static or dynamic assessment after initial design. This is the result of using pre-selected yield mechanism, pre-selected target drift, plastic design and capacity design approaches, and more rational story shear distribution.
4) The design procedure is easy to follow and can be computerized. In case where structural irregularities are present, the proposed design method will provide a good initial design, which reduces the amount of iteration.

In order to validate the proposed performance-based design approach, extensive nonlinear dynamic analyses were carried out in this study.

The seismic performance of the study EBFs was evaluated through nonlinear static and dynamic analyses using Perform-3D program. Eight 10% in 50 years and four 2% in 50 years SAC LA region ground motion time histories were employed for the nonlinear dynamic analyses. The study parameters included: location of yielding, maximum link plastic rotation, maximum relative story shear distribution, maximum interstory drift, and peak floor acceleration. As noted

in Chapter 3, the design parameters are slightly different between IBC and PPD frames. For comparison purposes, the seismic weights utilized for nonlinear dynamic analyses in all frames were based on the design for PPD frames, even though the weights of IBC frames were heavier. Therefore, some response parameters in the IBC frames, such as maximum interstory drift and link plastic rotation, could be underestimated.

It has been seen in past earthquakes that seismic performance of nonstructural components has significant influence on the overall performance of a building. It is estimated that approximately 70% to 80% of the cost of a building goes into nonstructural components. This suggests that majority of the damage and potential economic losses are due to the damage to nonstructural components (Villaverde, 2004). Generally, nonstructural components can be categorized into two types based on FEMA 356 (ASCE, 2000): acceleration-sensitive components (such as mechanical equipments, piping systems, and storage vessels), and deformation-sensitive components (such as cladding, partitions, interior veneers, and glazing systems). The seismic performance of the former type is directly related to absolute floor accelerations, and interstory drifts have appreciable influence on the latter type. The maximum interstory drift is pre-selected in the beginning of the proposed design method, thus the performance of deformation-sensitive components can be assured. The seismic performance of acceleration-sensitive components can be assured by limiting the floor accelerations within certain the specified limits. A trapezoidal distribution of allowable floor accelerations is used in the IBC 2000:

$$(A_F)_i = 0.4 S_{DS} \left(1 + 2\frac{z}{h}\right) \tag{5.1}$$

where z is the height of the point of attachment of the component in the structure; h is the average roof height of the structure from the grade level. Assuming that the point of attachment is the floor, the design floor accelerations vary linearly from $0.4S_{DS}$ to $1.2S_{DS}$.

5.2 Nonlinear Static Analysis Results

The nonlinear static analysis (pushover analysis) was conducted by monotonically increasing the lateral forces until the 2% roof drift was reached. It should be noted that the IBC 2000 and the proposed lateral force distributions are different. The IBC frames were loaded by the IBC lateral force distribution and the PPD frames used the proposed distribution. Figures 5.1 (a) and 5.1 (b) show the pushover curves for the 3-story and 10-story EBFs, respectively. It is observed that the yield drift for low-rise EBFs is in the range of 0.375%, while the yield drift for the 10-story EBFs is approximately 0.5%, which is the assumed yield drift used in the proposed design as given in Tables 3.6 and 3.10. Therefore, a 0.5% yield drift for EBFs is generally reasonable, while a higher value may be used for high-rise EBFs. In any case, a higher but reasonable yield drift is suggested for conservatism since it results in higher design base shear.

5.3 Nonlinear Dynamic Analysis Results

5.3.1 Location of yield activity

In order to achieve the goal of damage control in PBEE, a predictable and known location of damage is essential. In the proposed design method, the yield mechanism, that is the location of yielding, is pre-selected. In an EBF, the inelastic activity is expected to occur at first level column bases and in shear links only. As shown in Figures 5.2 through 5.17, all the inelastic activity was limited in shear links and first floor column bases in PPD frames. On the other hand, the inelastic activity in the IBC frames was scattered, which also varied with different earthquake events. Such seismic behavior was also observed in analyses carried out by Richards and Uang (2003) on the same IBC frames. The maximum plastic column hinging rotation is 0.014 radian, which may be underestimated as explained earlier.

5.3.2 Maximum plastic rotation and dissipated hysteretic energy in shear links

Approximately, link rotation angle for the study EBFs can be estimated by (See Figure 1.2):

$$\begin{aligned}\gamma_p &= \frac{L}{e}\theta_p = \frac{30}{4}\theta_p = 7.5\theta_p \\ &= 7.5\left(\theta_u - \theta_y\right) \\ &= 7.5\left(\theta_u - 0.005\right)\end{aligned} \tag{5.2}$$

where θ_u is the target drift and θ_y is the yield drift which is 0.005 radian used in this study. The target drifts and corresponding link plastic rotations calculated according to Eq. 5.2 are listed in Table 5.1. As suggested by this table, if a maximum expected story target drift is 2%, the shear link should have a link plastic rotation capacity of 0.11 radian for the study EBFs. It is noted that the maximum allowable link plastic rotation specified in AISC Seismic Provisions is 0.08 radian; however, based on the tests performed by Okazaki et al (2004) at the University of Texas, Austin,

shear links subjected to the new AISC Loading Protocol (Richards and Uang, 2003) can easily reach 0.11 radian plastic rotation without stiffness and strength deterioration. Therefore, it can be expected that the shear links would not fail as long as maximum interstory drift is less than 2%, which is the design target drift used for the PPD frames.

As indicated in Figures 5.18 and 5.19, the maximum link plastic rotations in PPD frames are generally within the AISC limitation, 0.08 radian, and well below the maximum rotation observed in UTA tests. It is also noticed that, especially for the 10-story EBF, the PPD frame showed more uniformly distributed plastic rotation at all floors. This can be attributed to the proposed lateral force distribution used for the design as described in Chapter 3. In contrast, as shown in Figure 5.19 (a), the link plastic rotation angles are not evenly distributed among floors in the IBC frame. Although most maximum link plastic rotation angles at each floor are well below the AISC limitation, the plastic rotation at upper floors tended to increase suddenly and exceeded the 0.08 radian limitation in some time-histories. The top floor links exhibited only minor yielding which means the top floor links were not fully utilized to dissipate energy. Higher plastic rotation in the upper floor (except for top floor) shear links in EBFs designed according to elastic method and code specified lateral forces has also been observed in past studies (Popov et al, 1992).

The dissipated hysteretic energy in shear links for selected earthquake events is schematically shown in Figures 5.20 to 5.23. As can be seen, the energy can be uniformly dissipated in the PPD frames. It is evident that the proposed lateral force distribution leads to a uniform energy dissipation when contrasting Figure 3.5 with Figures 5.20 and 5.21. In comparison with Figure 3.6, Figures 5.22 and 5.23 indicate that the stiffness irregularity

adjustment proposed in Chapter 3 can effectively reduce the adverse impact on the seismic behavior resulting from the sudden change of story height in the second level of the 10-story EBF. The uniformly distributed link rotations can also be beneficial to the loss or damage estimation in the PBEE.

It has been observed that after 1994 Northridge Earthquake and 1995 Kobe Earthquake, a near-fault impulse type ground motion can be very damaging to structures if the structure cannot dissipate the sudden burst of energy. Most buildings designed by current design codes may not have enough time for cyclic vibration to efficiently utilize structural damping. Study performed by Naeim (1995) showed that damping has little effect in dissipating the energy when a moment frame was struck by a near-fault ground motion, and the large portion of the energy has to be dissipated through hysteretic energy. Furthermore, the seismic pulse tends to concentrate the inelastic behavior in the lower floors of buildings because the upper floors do not have sufficient time to respond. It is seen, however, that the seismic behavior of PPD frames was not affected by differences in far-field and near-filed ground motions.

5.3.3 Maximum interstory drifts

Figures 5.24 through 5.31 show the maximum interstory drifts resulting from eight 10% in 50 years ground motions for the 3-story and 10-story EBFs. It is seen that all the maximum interstory drifts of the PPD frames were within the 2% pre-selected target drift, signifying that the seismic performance of the deformation-sensitive components can be controlled by the proposed design procedure. It is also indicated in these figures that, the PPD frames generally exhibited more uniform interstory drifts than those in IBC frames.

5.3.4 Maximum absolute floor accelerations

As suggested in Figures 5.32 and 5.33, the maximum absolute floor accelerations are generally below the code-specified floor design acceleration, indicating that the seismic performance of the acceleration-sensitive components can also be satisfactory. It is also evident that the acceleration-sensitive components in a low-rise EBF are more vulnerable than in a high-rise EBF.

5.3.5 Maximum relative story shear distributions

The maximum relative story shear distributions (namely, the story shear in any story divided by the story shear in the top story) obtained from nonlinear dynamic analyses for the 3-story and 10-story PPD EBFs are shown in Figure 5.34. It can be seen that the proposed design story shear distribution well represents the envelope story shear distribution of the structure due to the ground motion records used in this study. It is also seen that, while the IBC2000 and proposed distributions have minor difference in the 3-story EBFs, the difference becomes more significant in the 10-story EBFs.

Further investigation was conducted by examining the story shear distributions under linear-elastic and nonlinear dynamic analyses. This was done to verify the code-specified distribution, which is generally based on the first mode elastic story shear distribution. Figure 5.35 (a) indicates that, when subjected to LA09 ground motion, the nonlinear story shear distributions are closer to the proposed distribution, while the elastic story shear distributions are closer to the IBC2000 distribution. However, as shown in Figure 5.35 (b), both elastic and

nonlinear distributions approach the proposed distribution due to the LA01 earthquake event. This observation implies that, the code-specified distribution, although includes the higher mode effect, cannot represent the realistic maximum story shear distribution during a major earthquake. Even in the elastic range, an EBF can have considerably different story shear distributions depending on specific ground motions. On the contrary, when an EBF yields, the maximum story shear distributions tend to shift towards the proposed distribution, which is more capable of representing the inelastic seismic behavior. It is also noted that, base on the observation from all nonlinear analyses performed in this study, the maximum story shear at each level generally occurred at approximately the same time.

The relative story shear distributions for IBC2000 and the proposed one, when translated into vertical distribution of seismic forces, are presented in Figure 5.36.

5.4 Multilevel Seismic Design

It was mentioned earlier that, performance objectives in PBEE typically include multiple goals. This multilevel design can be easily carried out by the proposed performance-based approach and is demonstrated in the following using the 10-story PPD frame.

In this study, the first performance level was: under 10% in 50 years hazard (2/3 MCE), the maximum interstory drift should be within 2%. For illustration purposes, a second performance level was assumed: under 2% in 50 years hazard (MCE), the maximum interstory drift should be within 3%. It is noted that, based on Table 5.1, before the study EBF reaches 3% drift, the shear

links may fail. However, this example is used for demonstration only, and no link failure was considered in the modeling.

The seismic response coefficient, C_s, calculated according to Eq. 3.8 and the normalized design pseudo-acceleration, C_e, obtained from Eq. 3.13, are then amplified 1.5 times to represent the MCE design base shear coefficient. The corresponding design parameters for the two level hazards are summarized in Table 5.2. It is seen that the first level governed the design since its design base shear is higher. Accordingly, 10-story PPD EBF should automatically satisfy the second level requirement, that is, interstory drift remains within 3% when subjected MCE level hazard. This was verified by performing nonlinear dynamic analyses using four 2% in 50 year SAC ground motions as shown in Figure 4.12. Results presented in Figure 5.37 confirm that the interstory drifts indeed remained within 3% for the ground motions used.

5.5 Material Weight Comparison

Tables 5.3 and 5.4 compare the material weight used in the IBC frames and PPD frames. Although the design base shears are different for the IBC and PPD frames, these tables give a general idea how the material difference exists in the two frames. As revealed in the two tables, while the IBC frames have heavier total beam weight and lighter total column weight, the PPD frames are just the opposite. The total material weights of the two frames are almost same. This shows that eccentrically braced frame, without changing the total material weight, can be optimized by virtue of the performance plastic design methodology proposed in this study, which generally results in superior dynamic behavior when experiencing severe earthquakes.

Table 5.1 Approximate relation between story drift and link plastic rotation for the study EBFs

Story Drift θ_u (%)	Link Plastic Rotation γ_p (rad.)
0.50	0.00
0.75	0.02
1.00	0.04
1.25	0.06
1.50	0.08
1.75	0.09
2.00	0.11
2.25	0.13
2.50	0.15
2.75	0.17
3.00	0.19

Table 5.2 Design parameters for the 10-story PPD frame in two level hazards

Parameters	10% in 50 year Hazard	2% in 50 year Hazard
C_e	0.559	0.8385
T	1.600	1.600
Yield Drift θ_y	0.5%	0.5%
Target Drift θ_u	2.0%	3.0%
Inelastic Drift θ_p	1.5%	2.5%
$\mu_s = \frac{\theta_u}{\theta_y}$	4	6
R_μ	4	6
γ	0.4375	0.306
α	1.491	2.486
$\frac{V}{W}$	0.086	0.084
Design Base Shear V	1358 kips	1313 kips

Table 5.3 Comparison of the material weight between two 3-story frames

	IBC	PPD	PPD/IBC
Beam Weight (lb)	23,520	21,600	0.92
Column Weight (lb)	14,157	15,951	1.13
Brace Weight (lb)	17,005	17,202	1.01
Total Weight (lb)	54,682	54,753	1.00

Table 5.4 Comparison of the material weight between two 10-story frames

	IBC	PPD	PPD/IBC
Beam Weight (lb)	108,150	89,700	0.83
Column Weight (lb)	113,668	137,966	1.21
Brace Weight (lb)	59,951	57,963	0.97
Total Weight (lb)	281,769	285,629	1.01

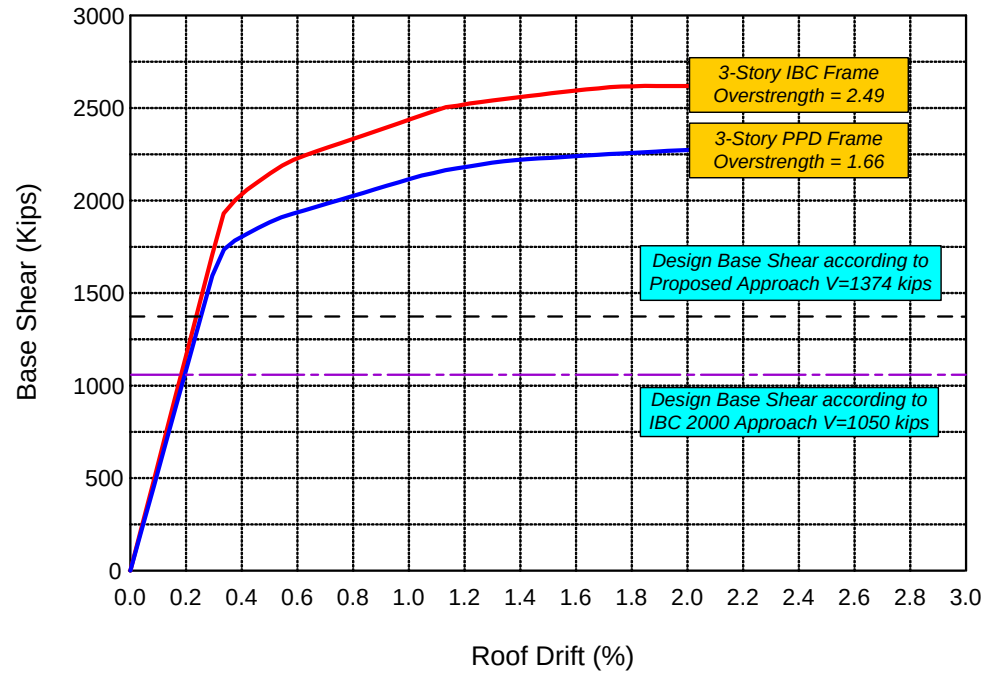

(a)

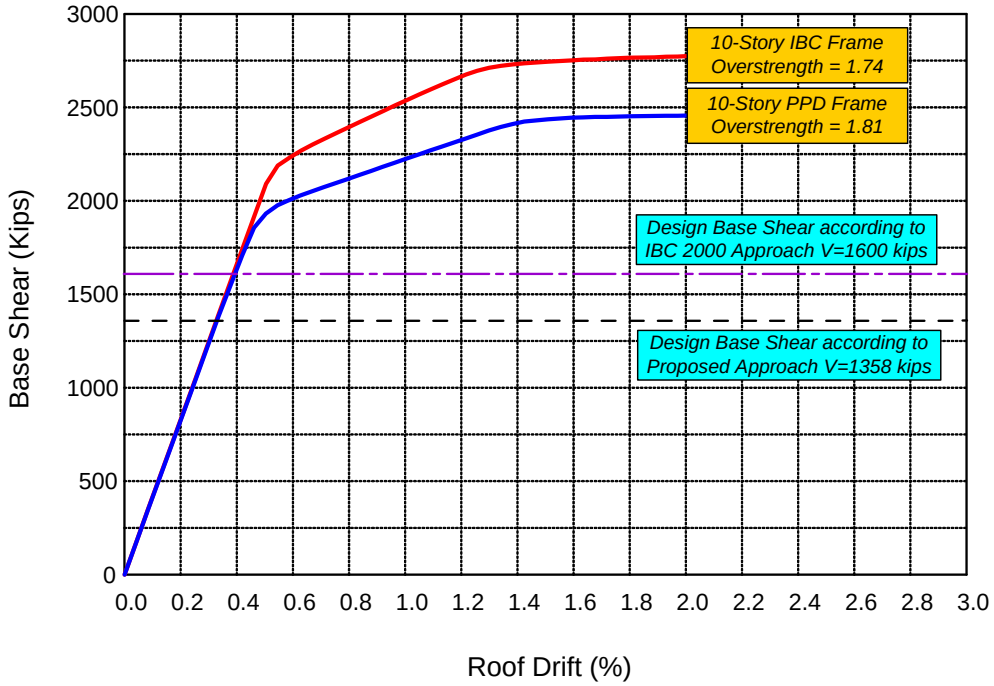

(b)

Figure 5.1 Nonlinear static pushover responses of study EBFs: (a) 3-story EBFs; (b) 10-story EBFs

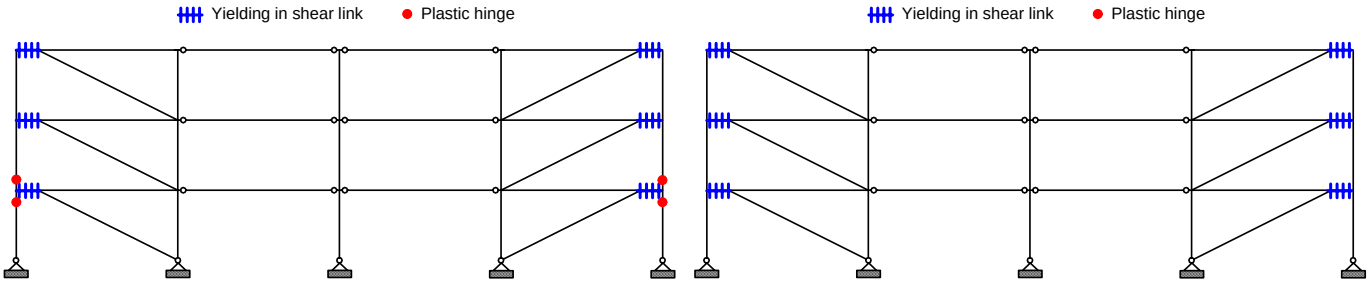

(a) (b)

Figure 5.2 Inelastic activities in 3-story (a) IBC EBF and (b) PPD EBF during LA01 event (Imperial Valley, 1940, El Centro)

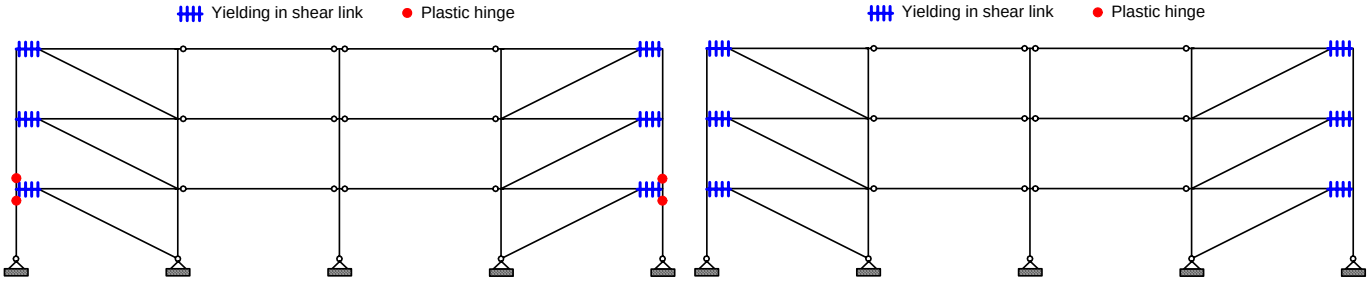

(a) (b)

Figure 5.3 Inelastic activities in 3-story (a) IBC EBF and (b) PPD EBF during LA02 event (Imperial Valley, 1940, El Centro)

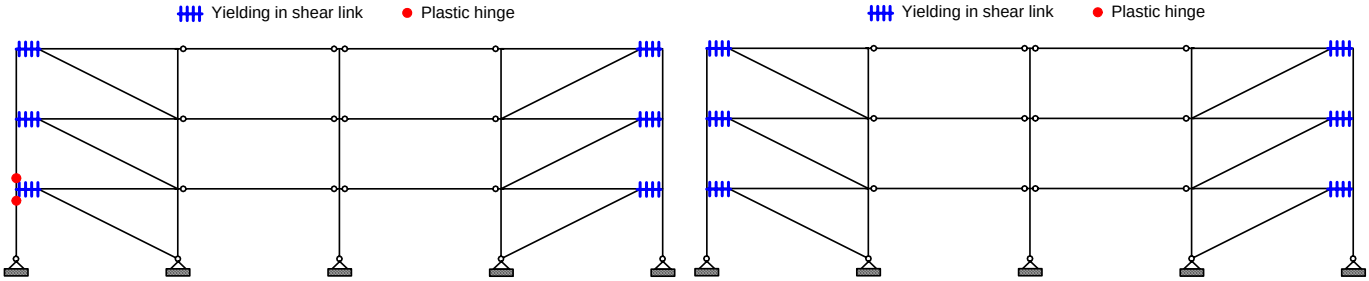

(a) (b)

Figure 5.4 Inelastic activities in 3-story (a) IBC EBF and (b) PPD EBF during LA09 event (Landers, 1992, Yermo)

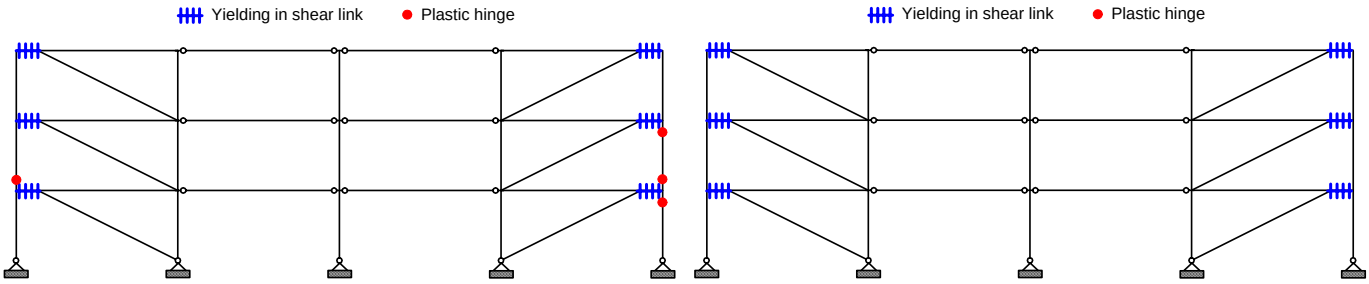

Figure 5.5 Inelastic activities in 3-story (a) IBC EBF and (b) PPD EBF during LA12 event (Loma Prieta, 1989, Gilroy)

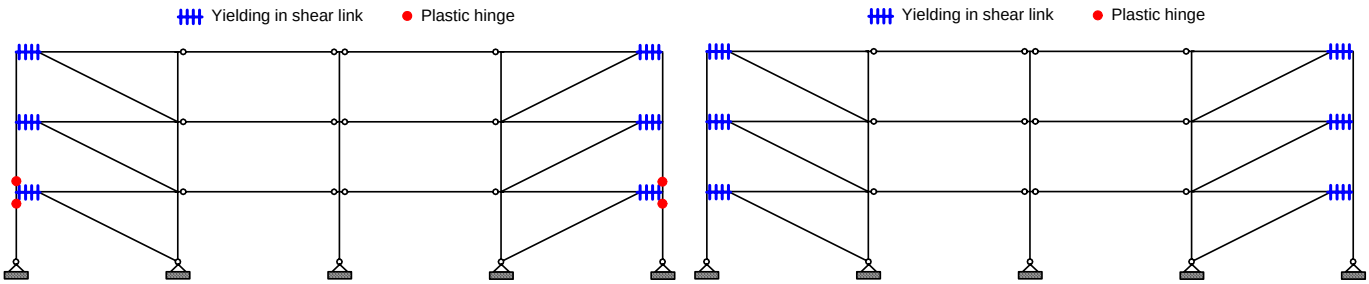

Figure 5.6 Inelastic activities in 3-story (a) IBC EBF and (b) PPD EBF during LA13 event (Northridge, 1994, Newhall)

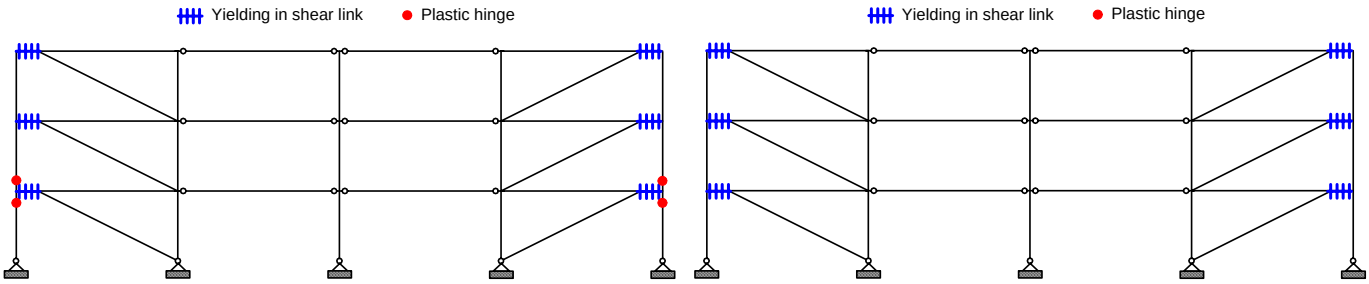

Figure 5.7 Inelastic activities in 3-story (a) IBC EBF and (b) PPD EBF during LA16 event (Northridge, 1994, Rinaldi RS)

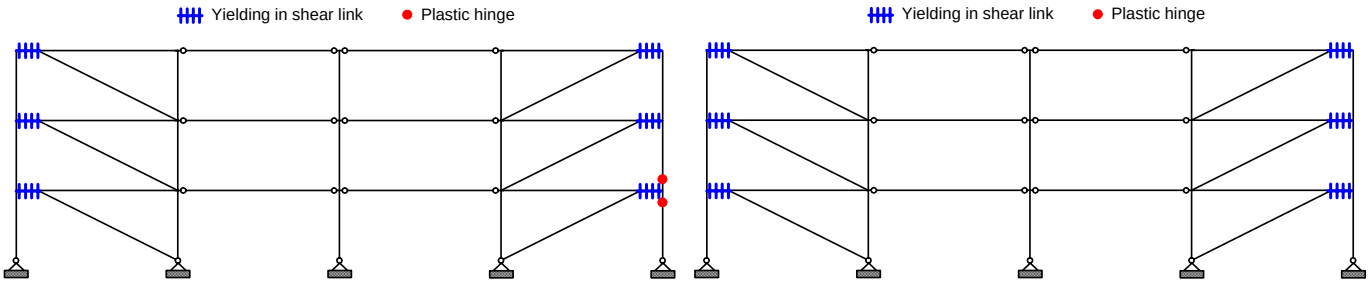

Figure 5.8 Inelastic activities in 3-story (a) IBC EBF and (b) PPD EBF during LA17 event (Northridge, 1994, Sylmar)

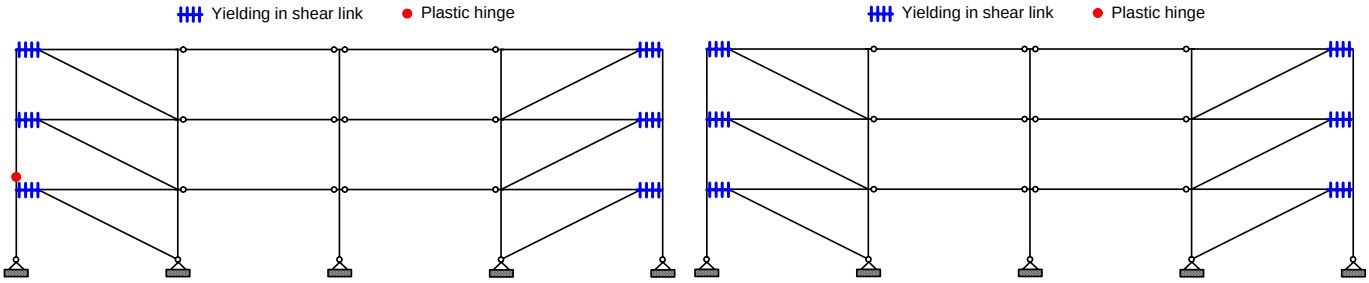

Figure 5.9 Inelastic activities in 3-story (a) IBC EBF and (b) PPD EBF during LA19 event (North Palm Springs, 1986)

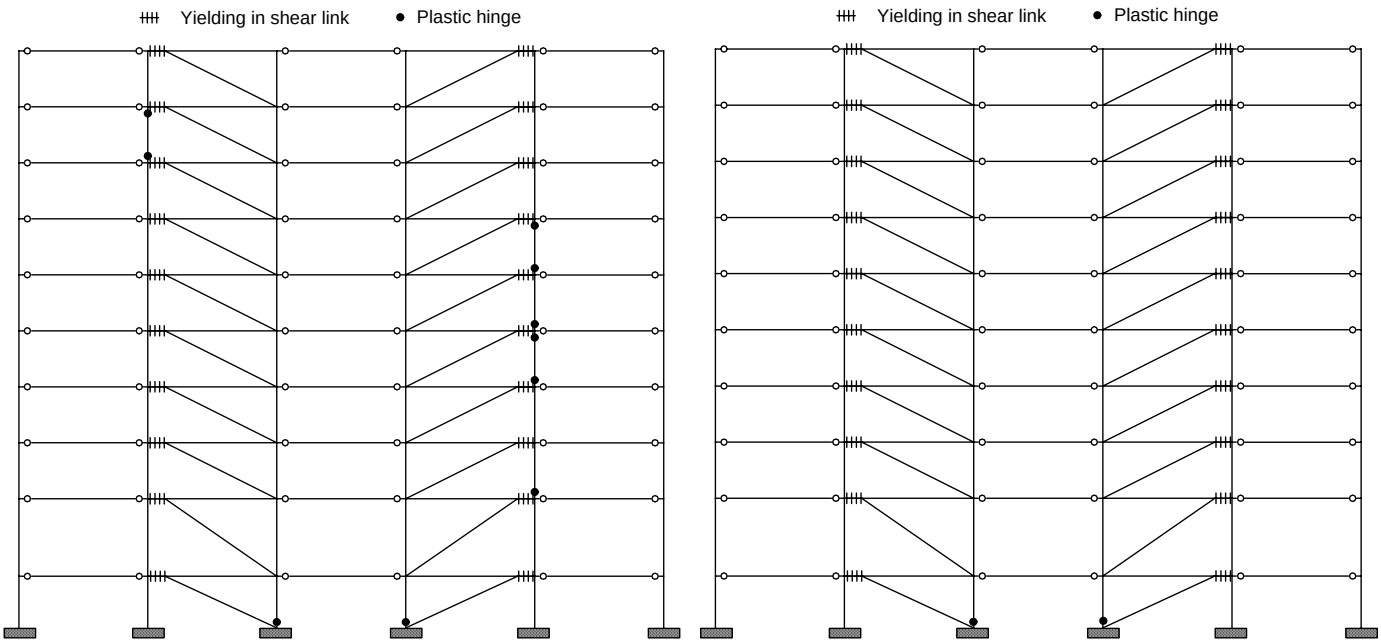

Figure 5.10 Inelastic activities in 10-story (a) IBC EBF and (b) PPD EBF during LA01 event (Imperial Valley, 1940, El Centro)

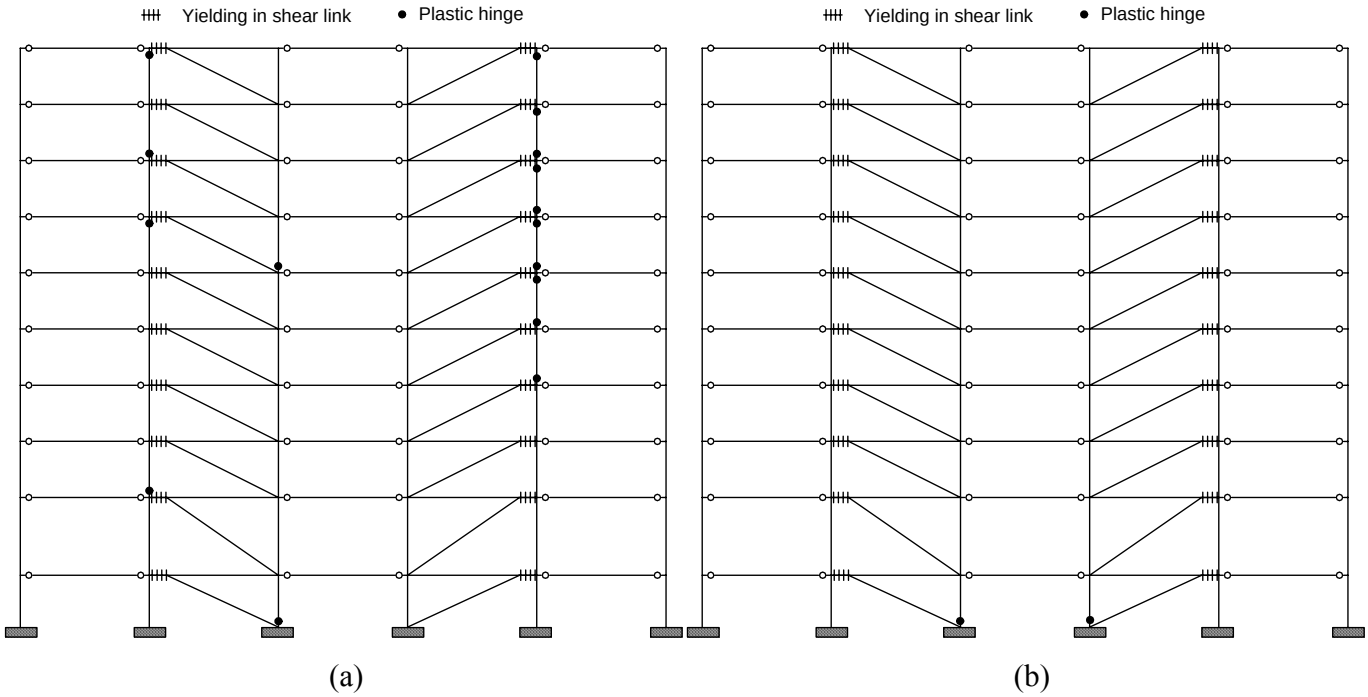

Figure 5.11 Inelastic activities in 10-story (a) IBC EBF and (b) PPD EBF during LA02 event (Imperial Valley, 1940, El Centro)

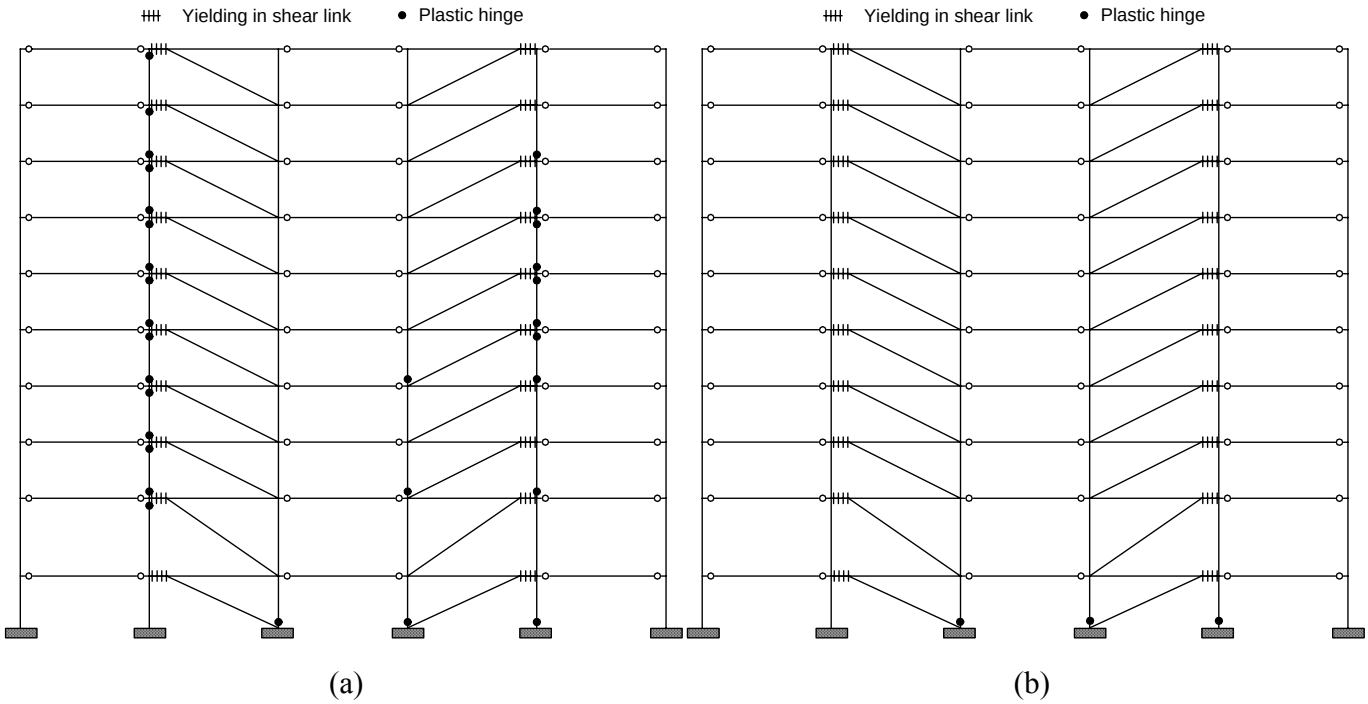

Figure 5.12 Inelastic activities in 10-story (a) IBC EBF and (b) PPD EBF during LA09 event (Landers, 1992, Yermo)

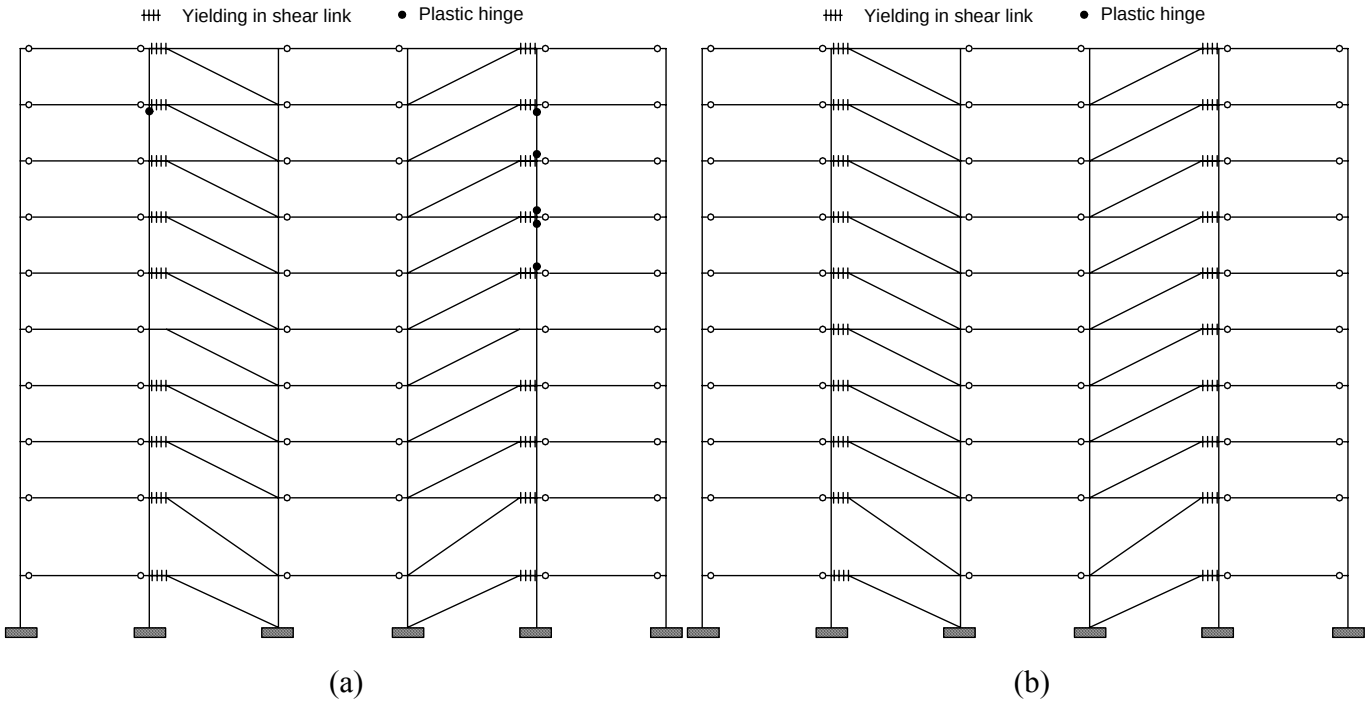

Figure 5.13 Inelastic activities in 10-story (a) IBC EBF and (b) PPD EBF during LA12 event (Loma Prieta, 1989, Gilroy)

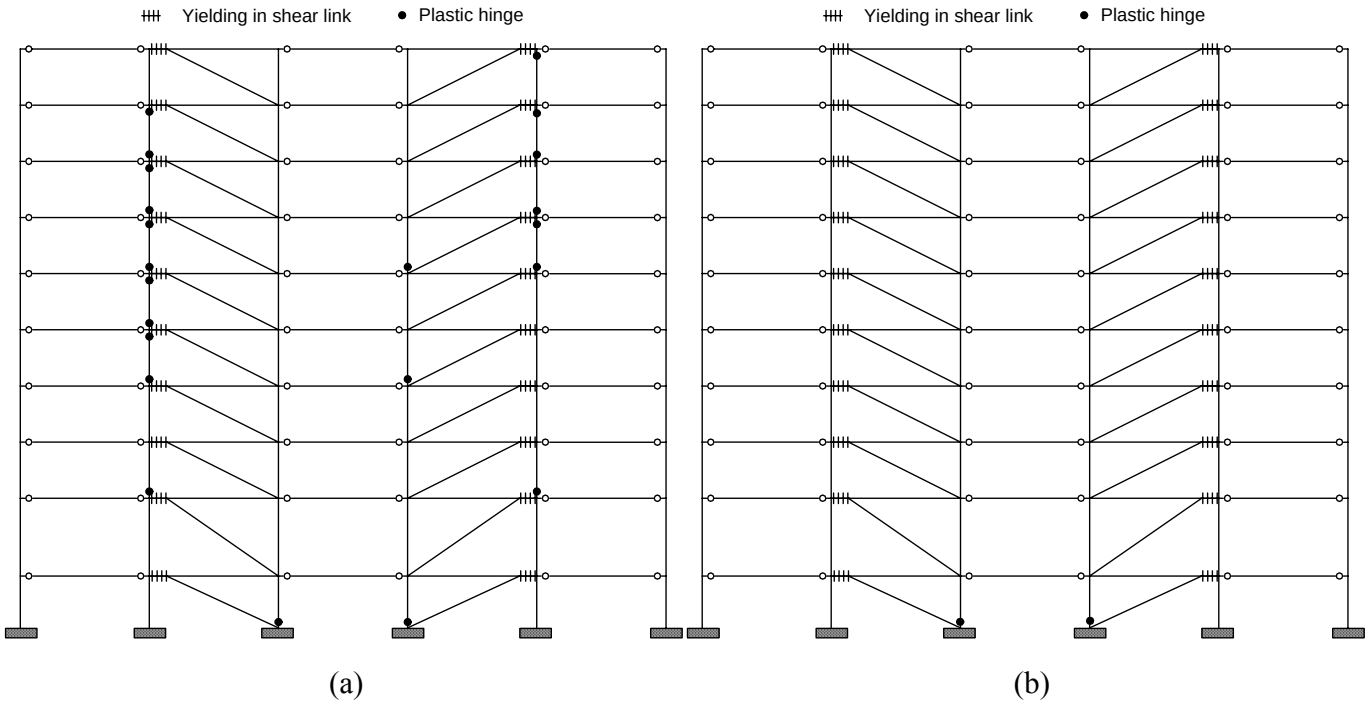

Figure 5.14 Inelastic activities in 10-story (a) IBC EBF and (b) PPD EBF during LA13 event (Northridge, 1994, Newhall)

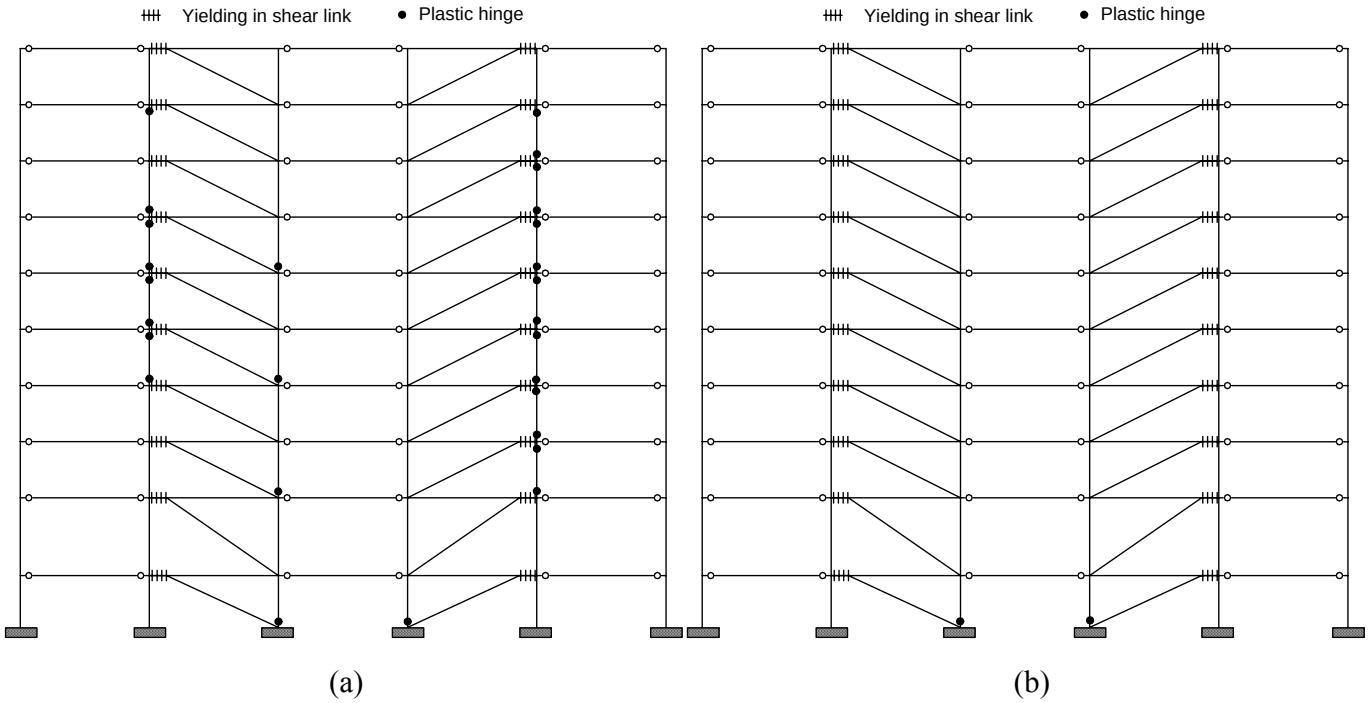

Figure 5.15 Inelastic activities in 10-story (a) IBC EBF and (b) PPD EBF during LA16 event (Northridge, 1994, Rinaldi RS)

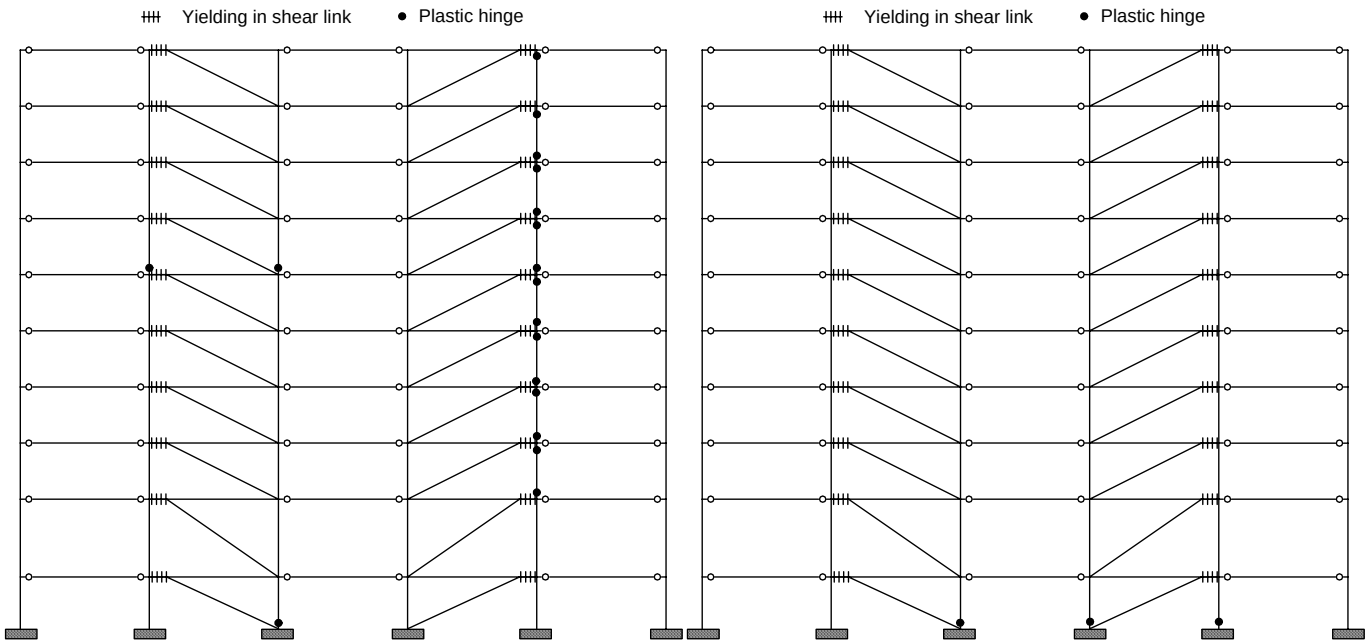

Figure 5.16 Inelastic activities in 10-story (a) IBC EBF and (b) PPD EBF during LA17 event (Northridge, 1994, Sylmar)

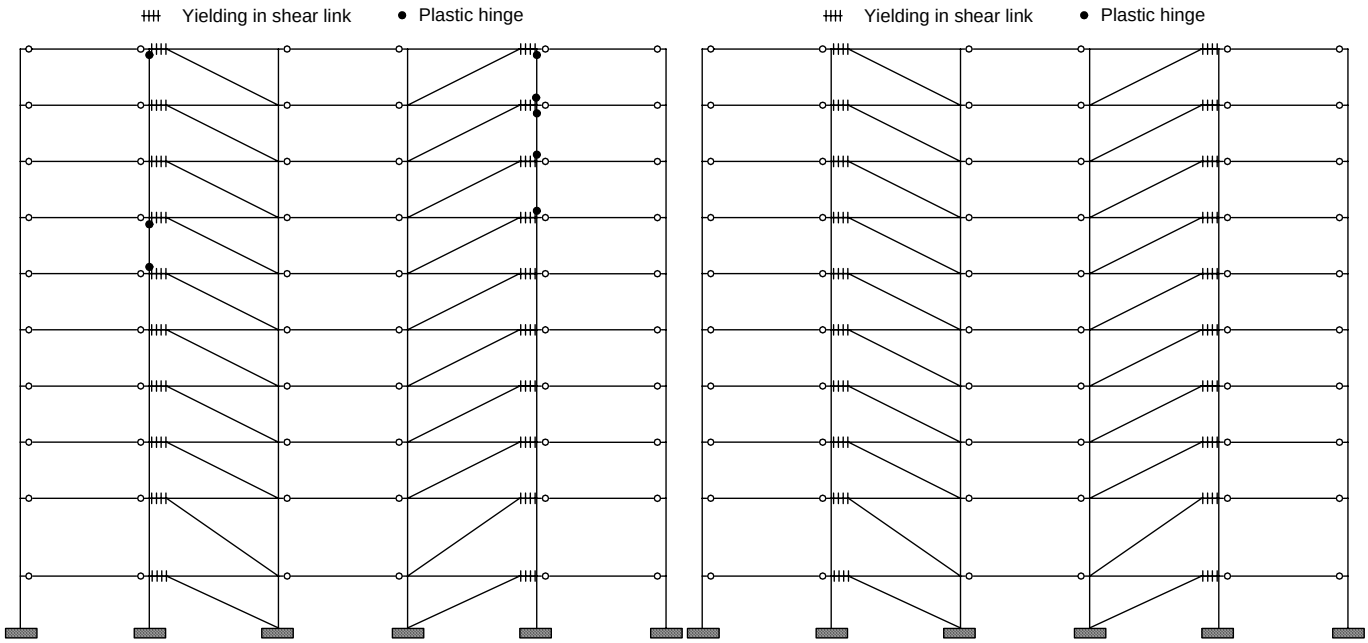

Figure 5.17 Inelastic activities in 10-story (a) IBC EBF and (b) PPD EBF during LA19 event (North Palm Springs, 1986)

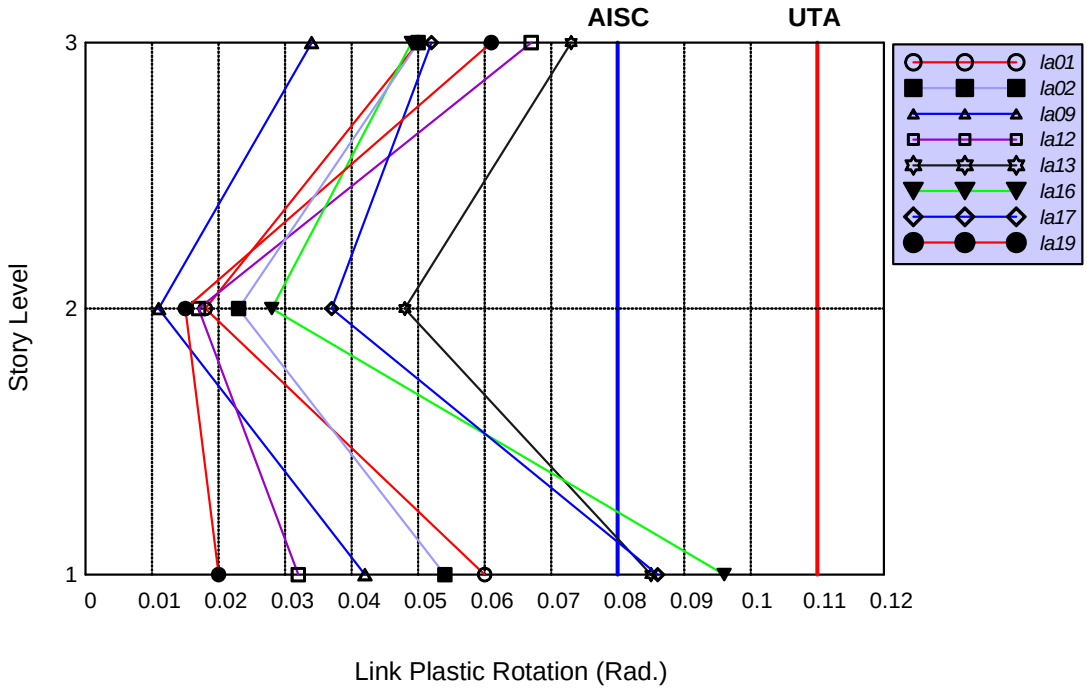

(a) IBC Frame

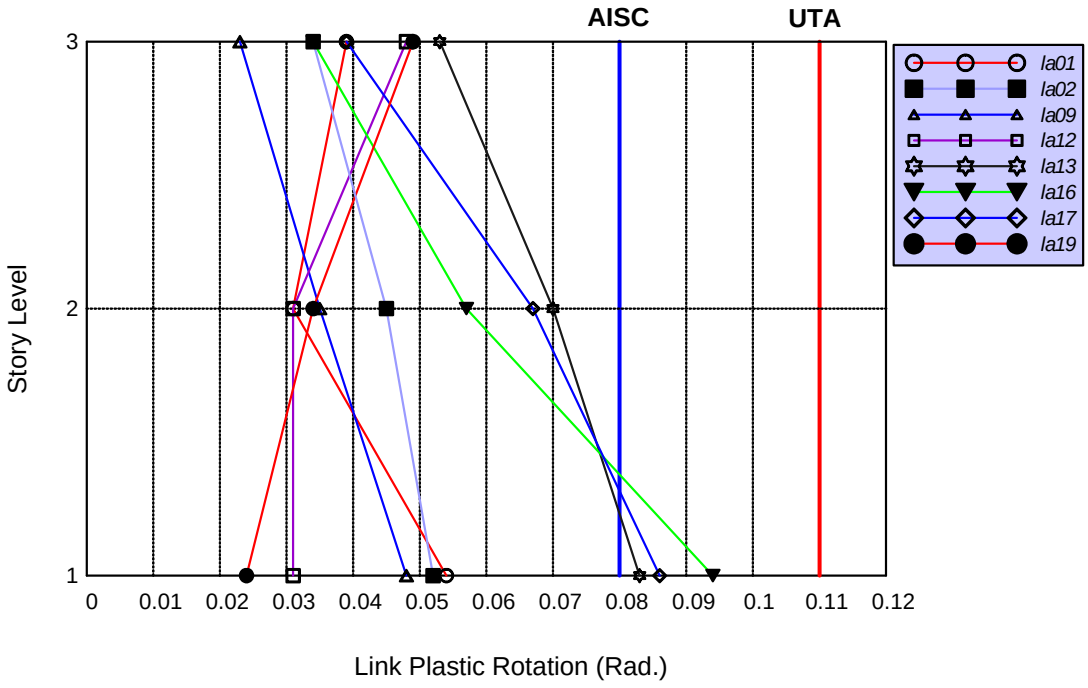

(b) PPD Frame

Figure 5.18 Maximum link plastic rotations in 3-story (a) IBC EBF and (b) PPD EBF

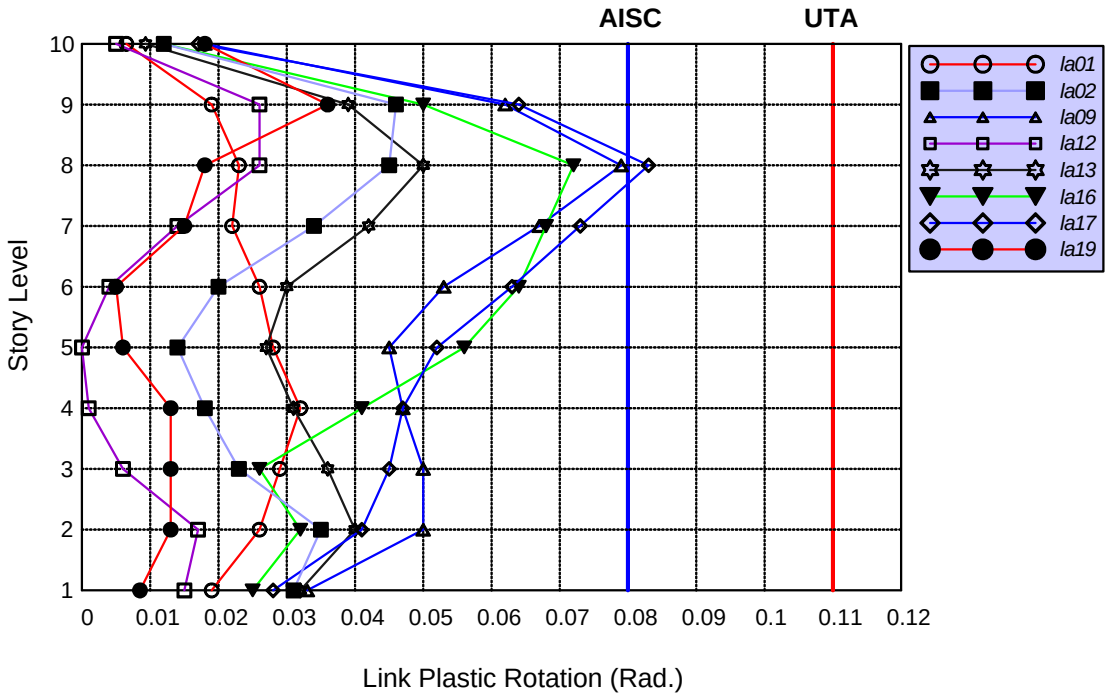

(a) IBC Frame

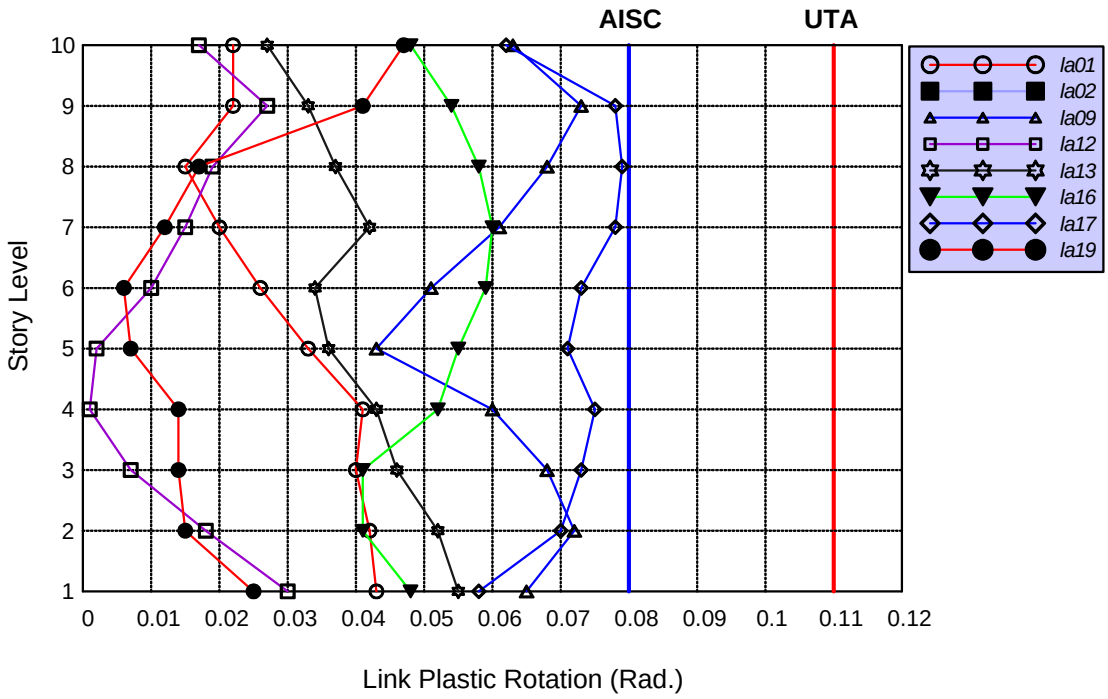

(b) PPD Frame

Figure 5.19 Maximum link plastic rotations in 10-story (a) IBC EBF and (b) PPD EBF

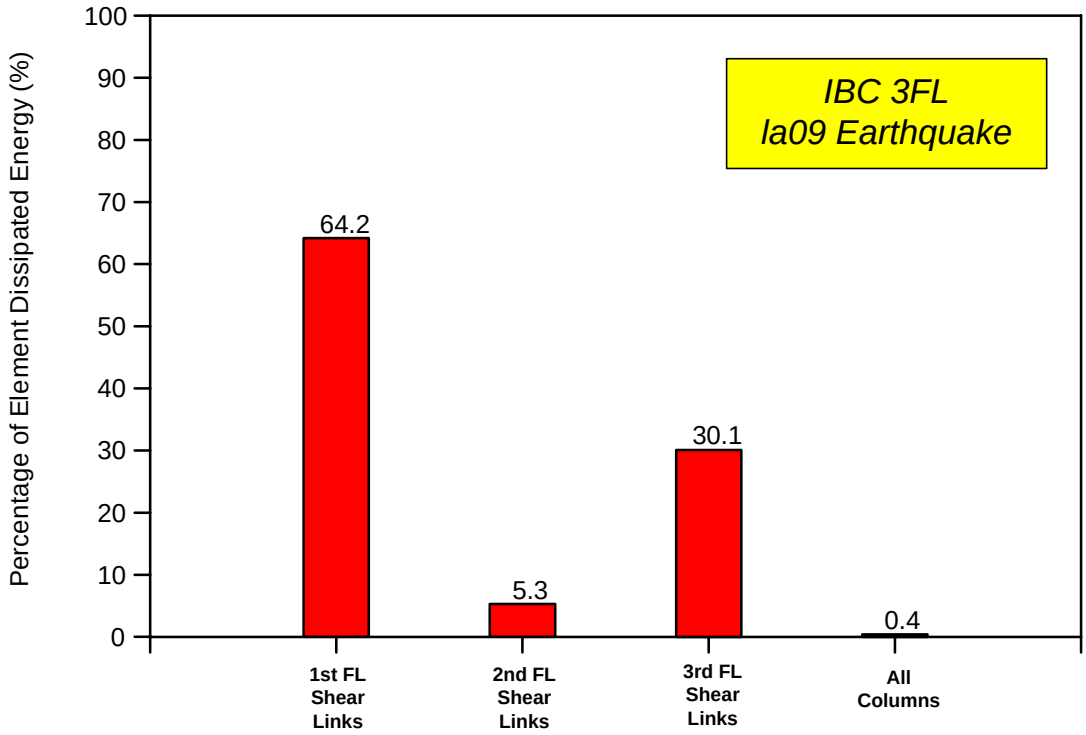

(a)

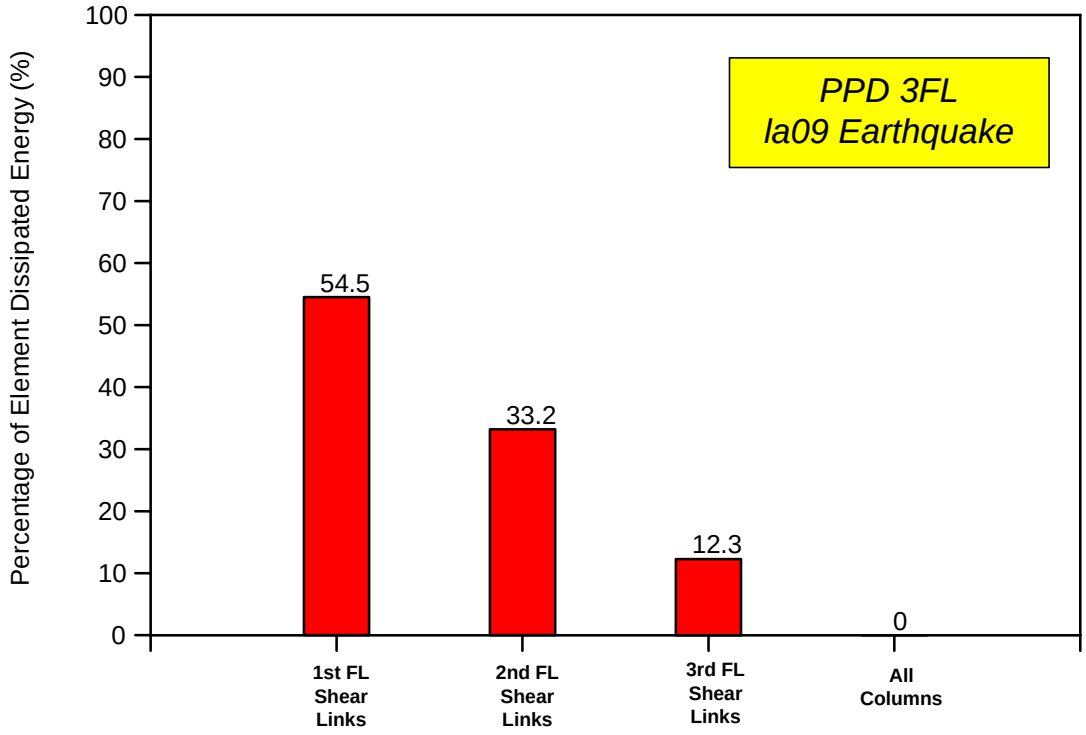

(b)

Figure 5.20 Dissipated hysteretic energy in 3-story (a) IBC EBF and (b) PPD EBF subjected LA 09 event

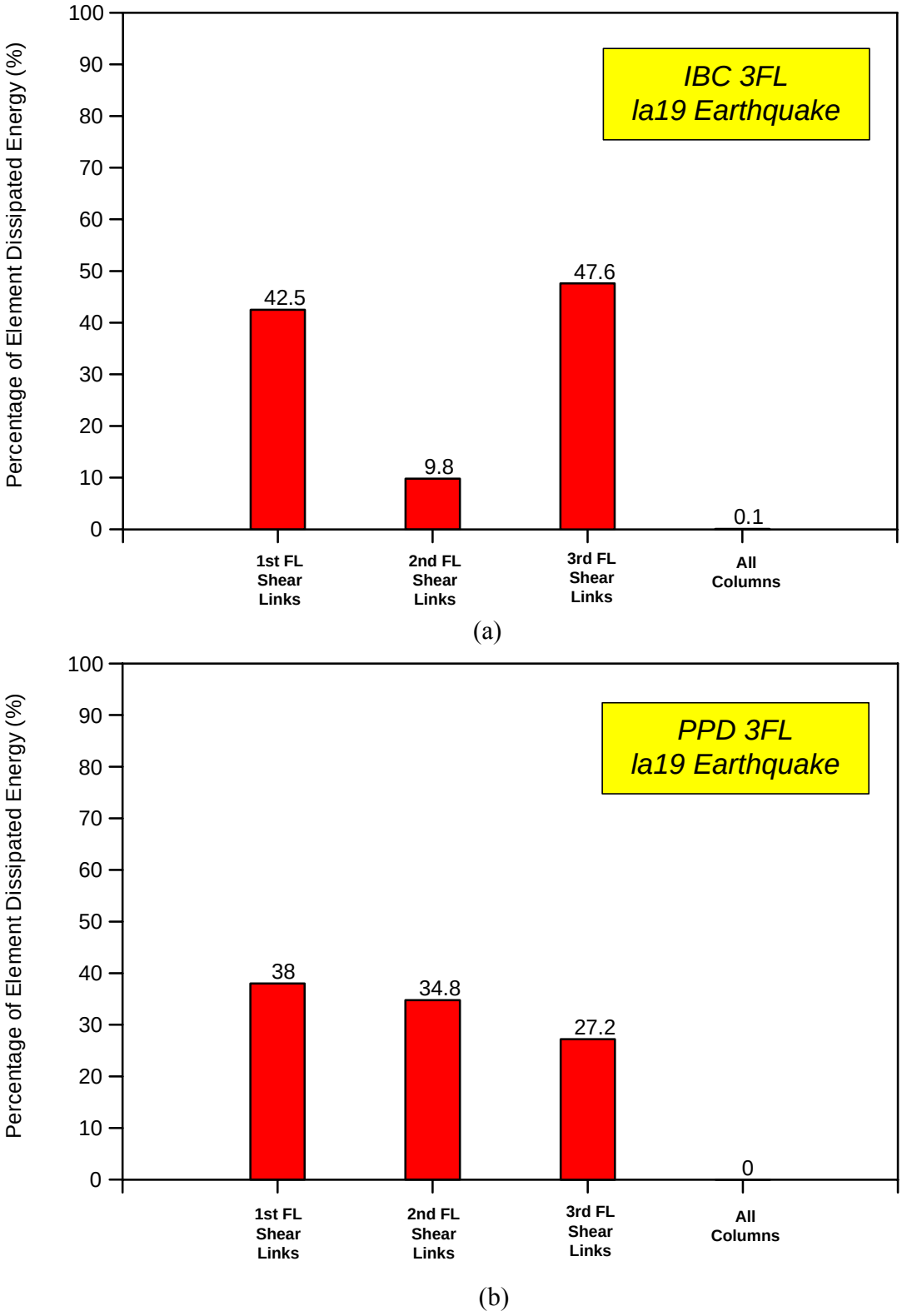

Figure 5.21 Dissipated hysteretic energy in 3-story (a) IBC EBF and (b) PPD EBF subjected LA 19 event

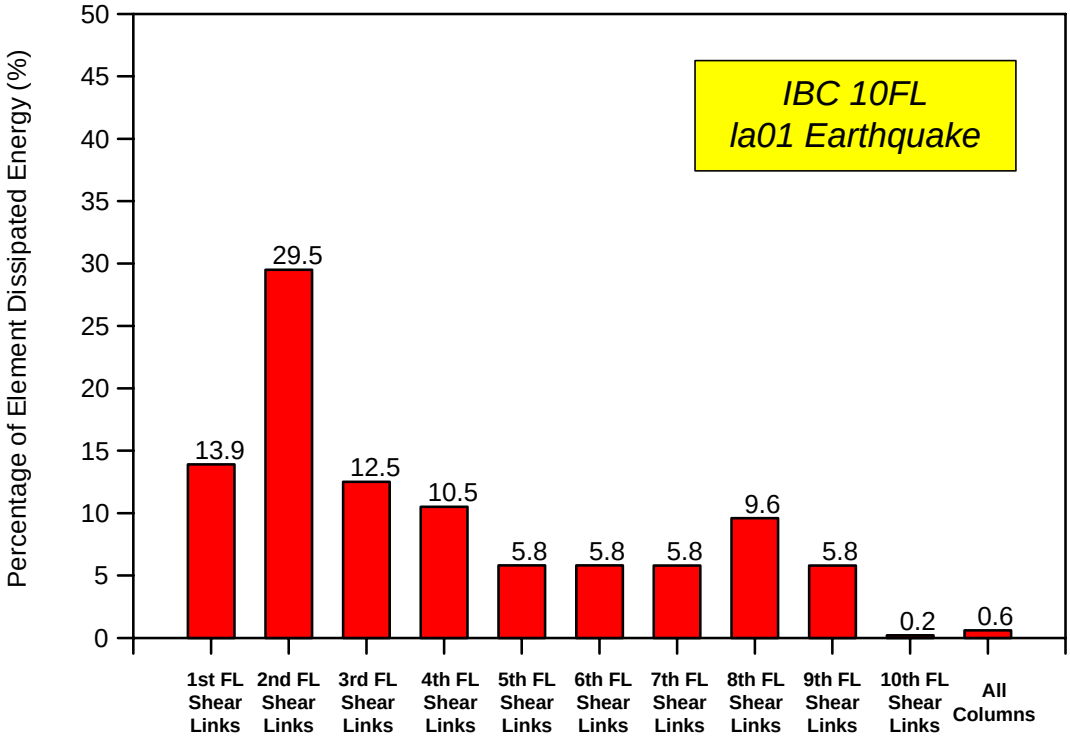

(a)

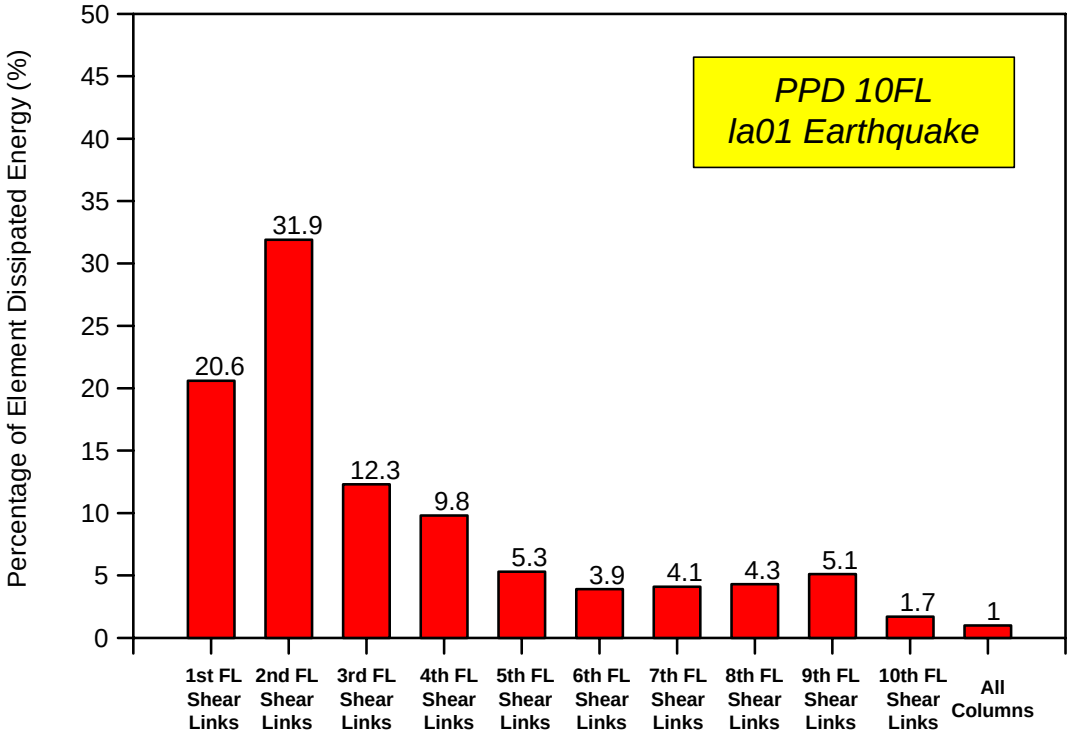

(b)

Figure 5.22 Dissipated hysteretic energy in 10-story (a) IBC EBF and (b) PPD EBF subjected LA 01 event

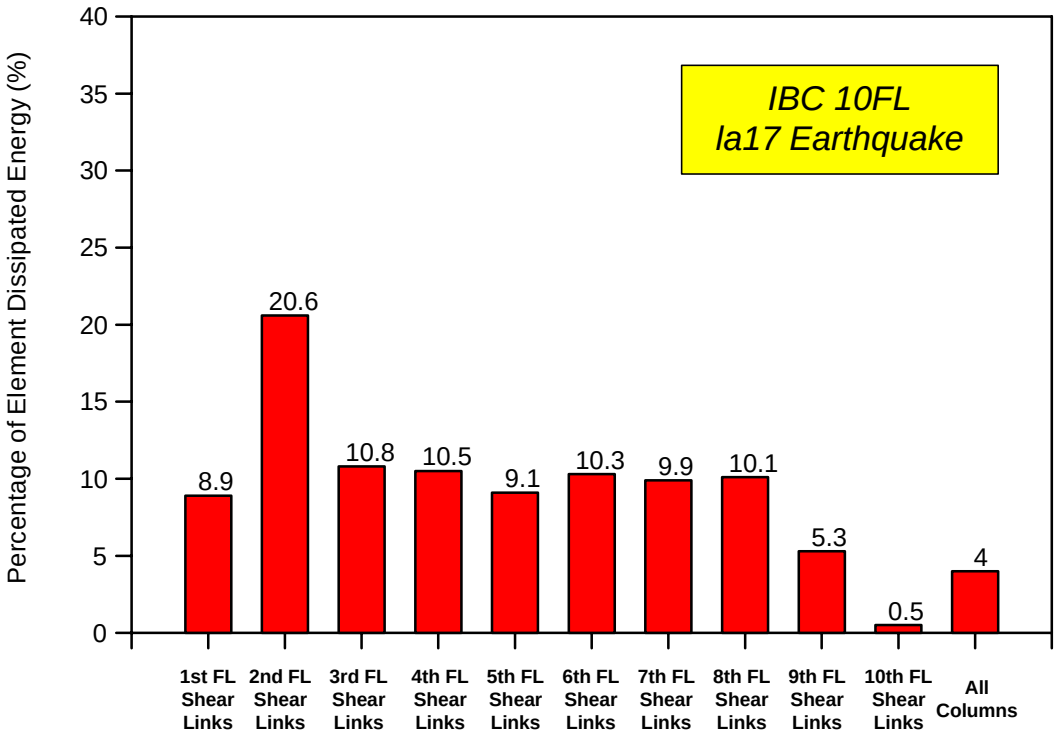

(a)

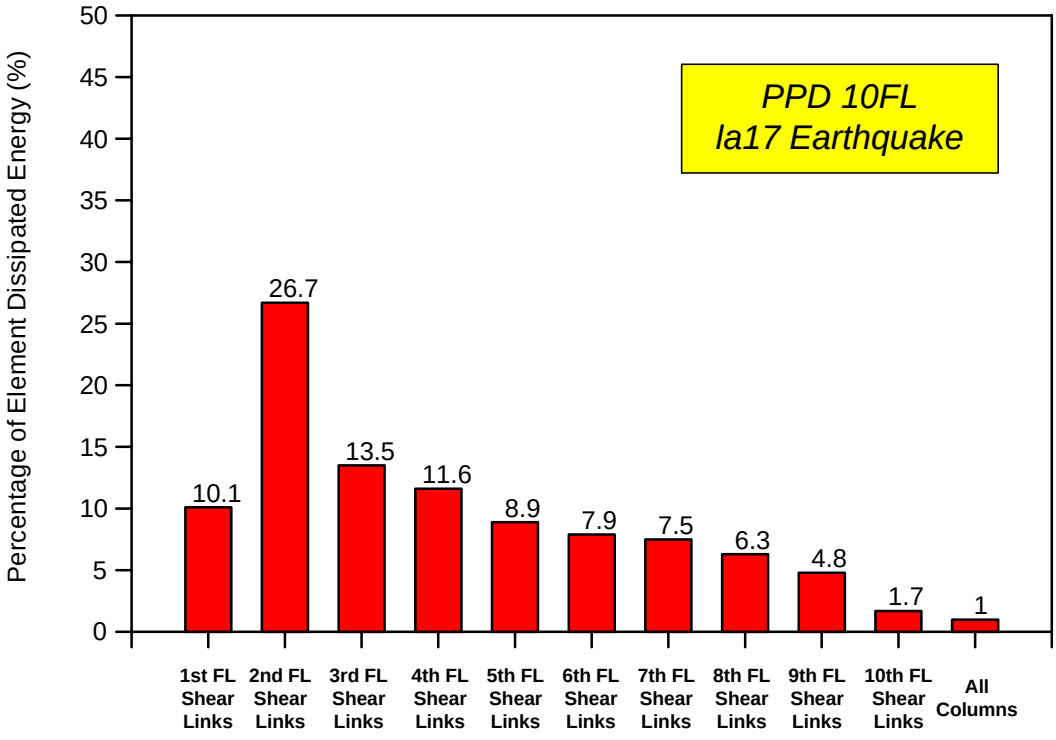

(b)

Figure 5.23 Dissipated hysteretic energy in 10-story (a) IBC EBF and (b) PPD EBF subjected LA 17 event

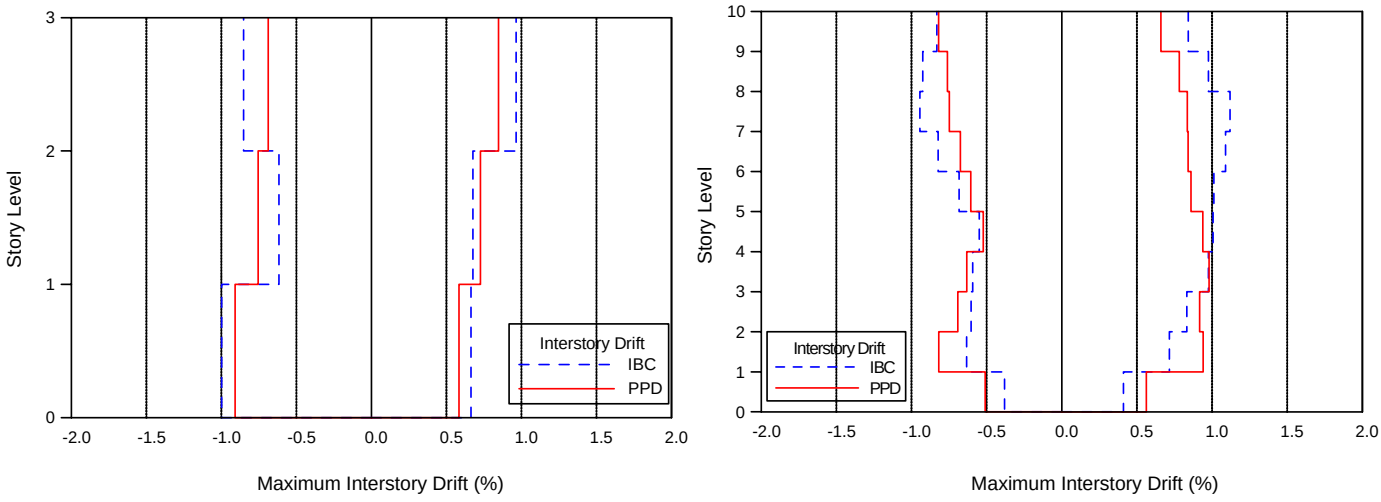

(a) (b)

Figure 5.24 Maximum interstory drift during LA 01 event: (a) 3-story frames (b) 10-story frames

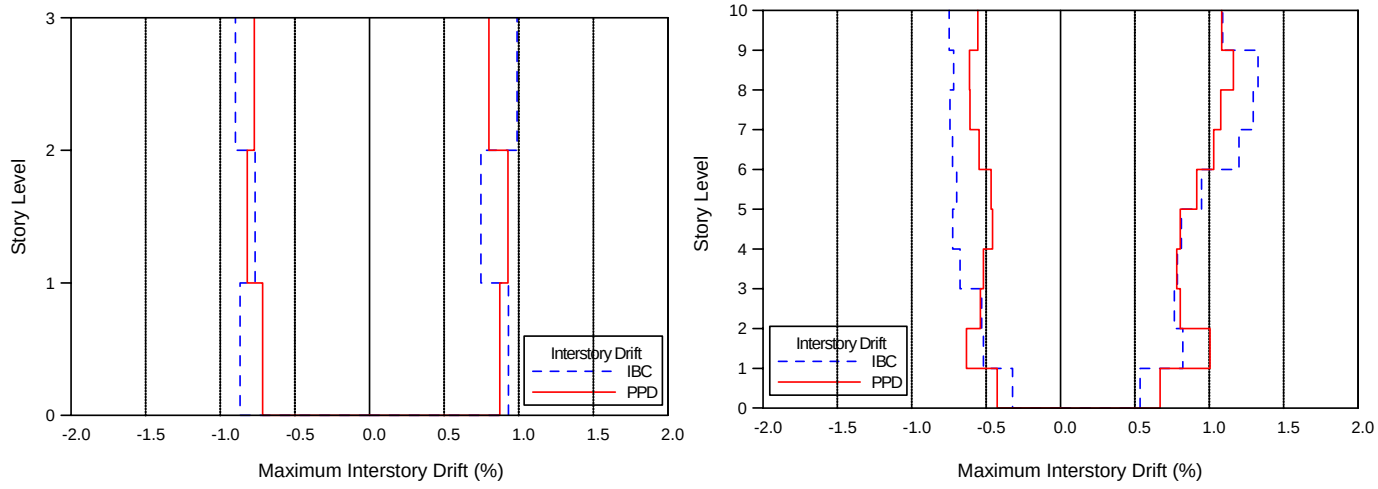

(a) (b)

Figure 5.25 Maximum interstory drift during LA 02 event: (a) 3-story frames (b) 10-story frames

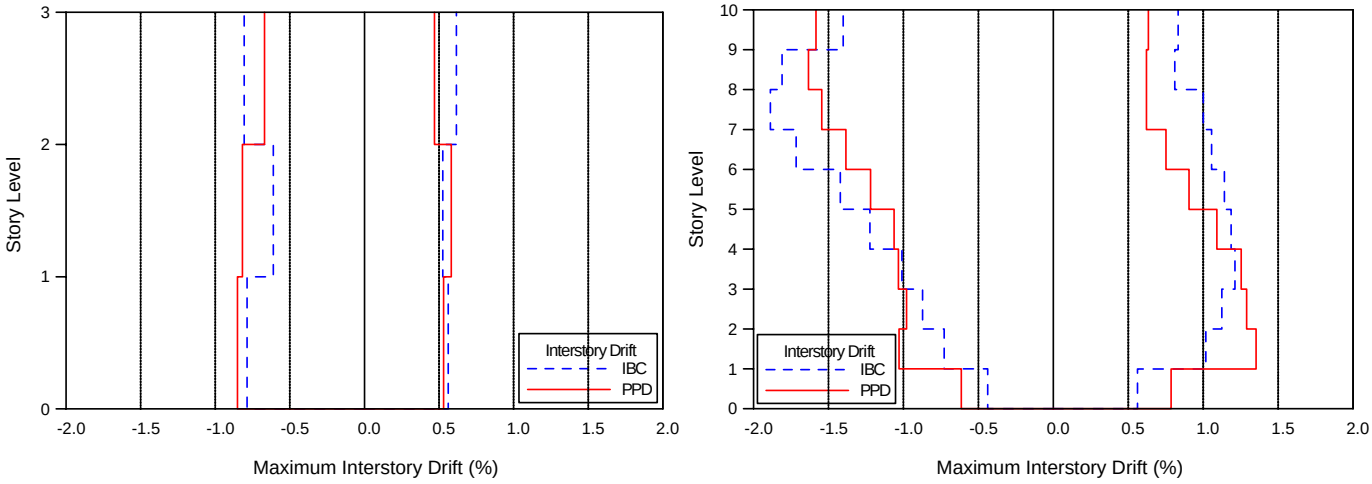

(a) (b)

Figure 5.26 Maximum interstory drift during LA 09 event: (a) 3-story frames (b) 10-story frames

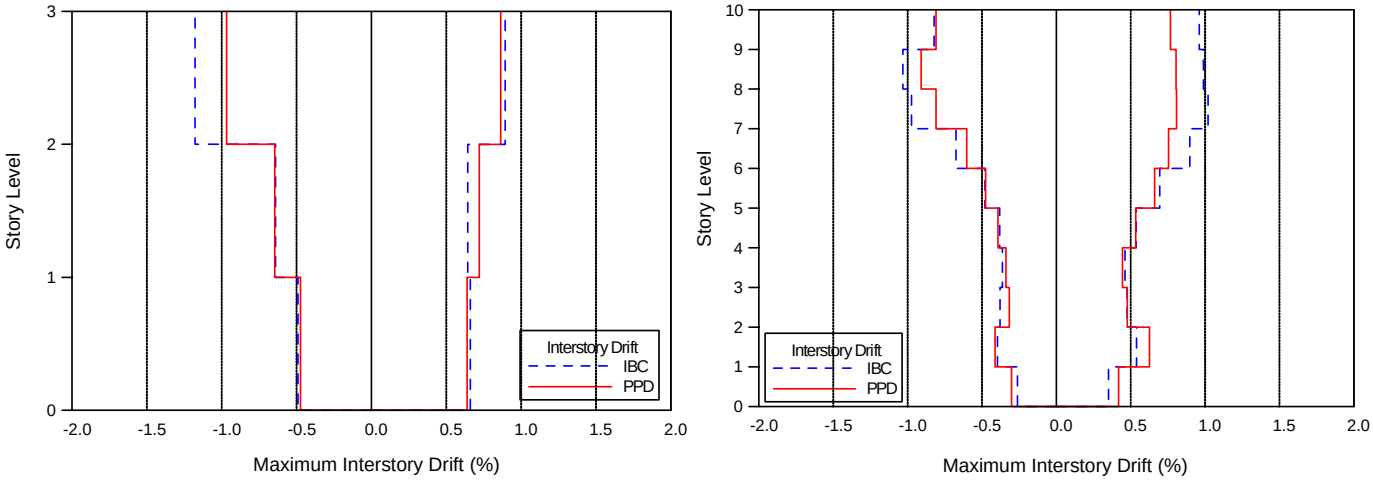

(a) (b)

Figure 5.27 Maximum interstory drift during LA 12 event: (a) 3-story frames (b) 10-story frames

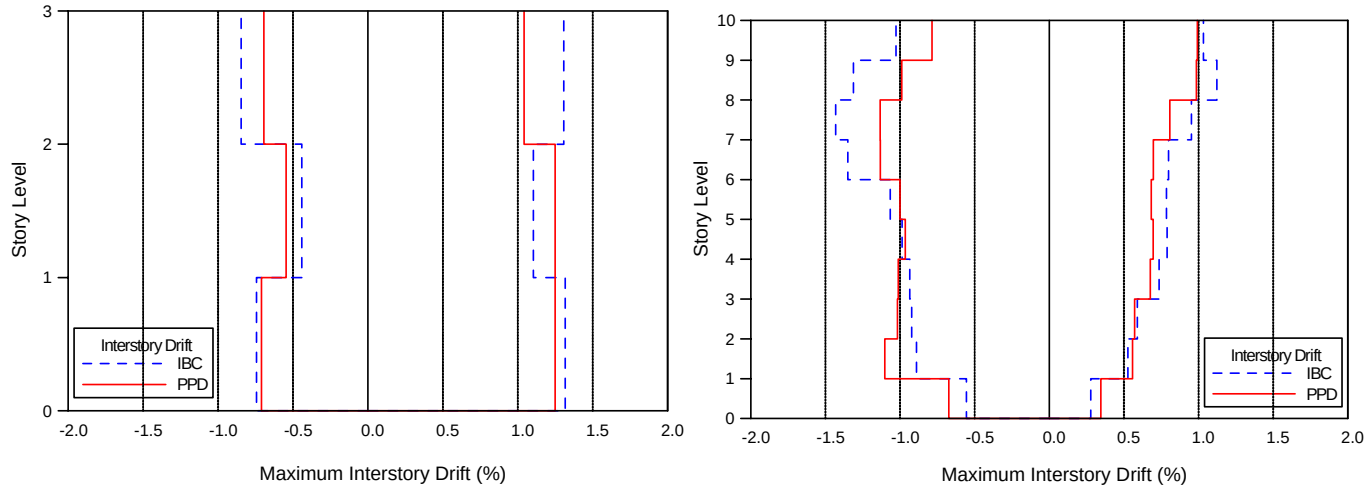

Figure 5.28 Maximum interstory drift during LA 13 event: (a) 3-story frames (b) 10-story frames

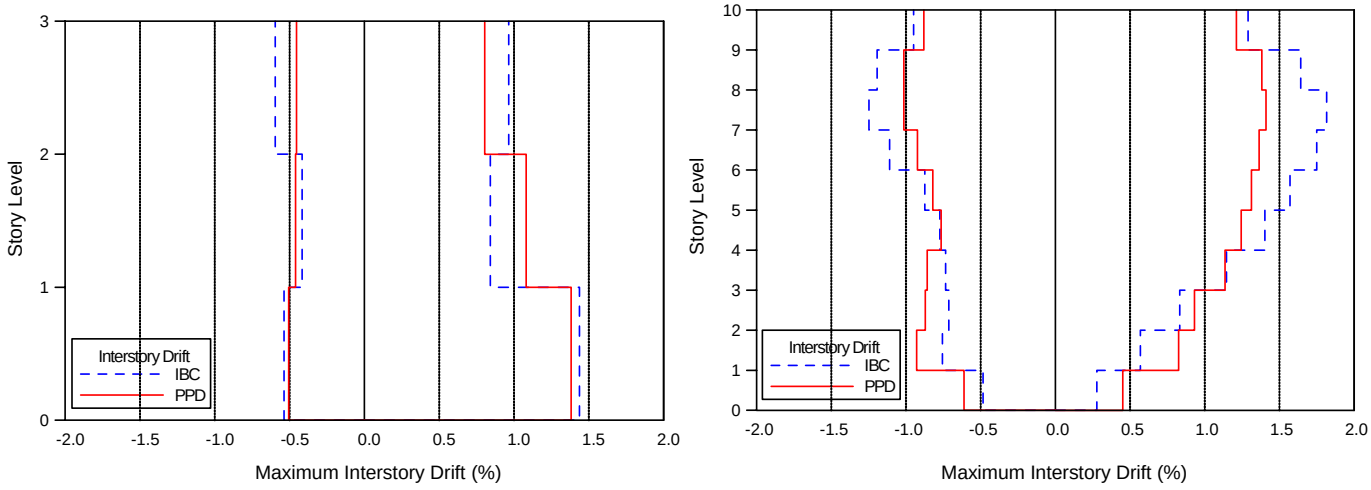

Figure 5.29 Maximum interstory drift during LA 16 event: (a) 3-story frames (b) 10-story frames

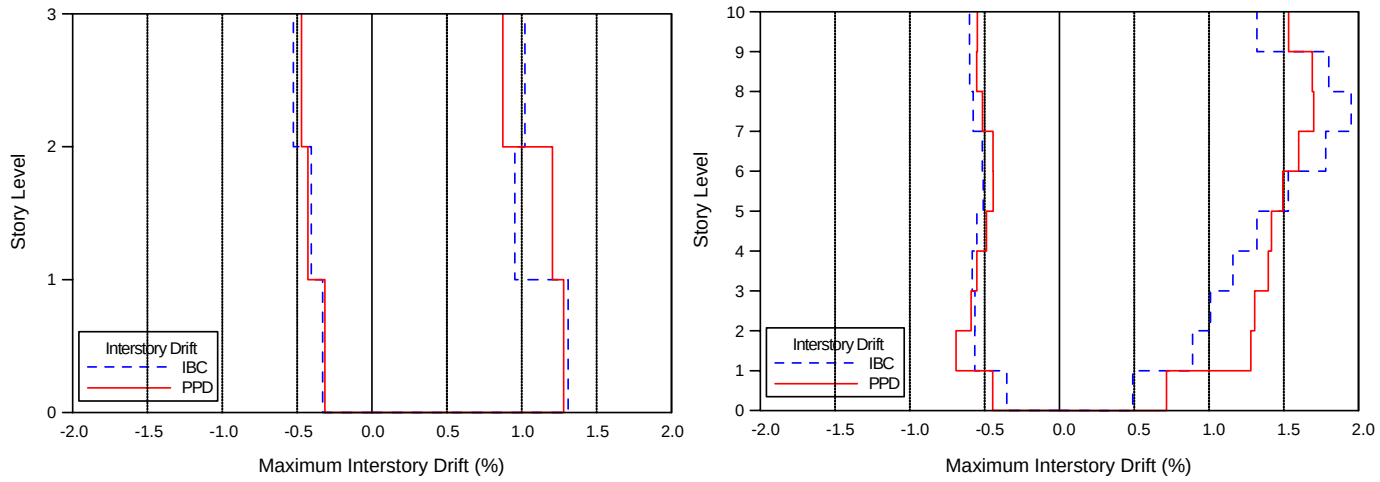

(a) (b)

Figure 5.30 Maximum interstory drift during LA 17 event: (a) 3-story frames (b) 10-story frames

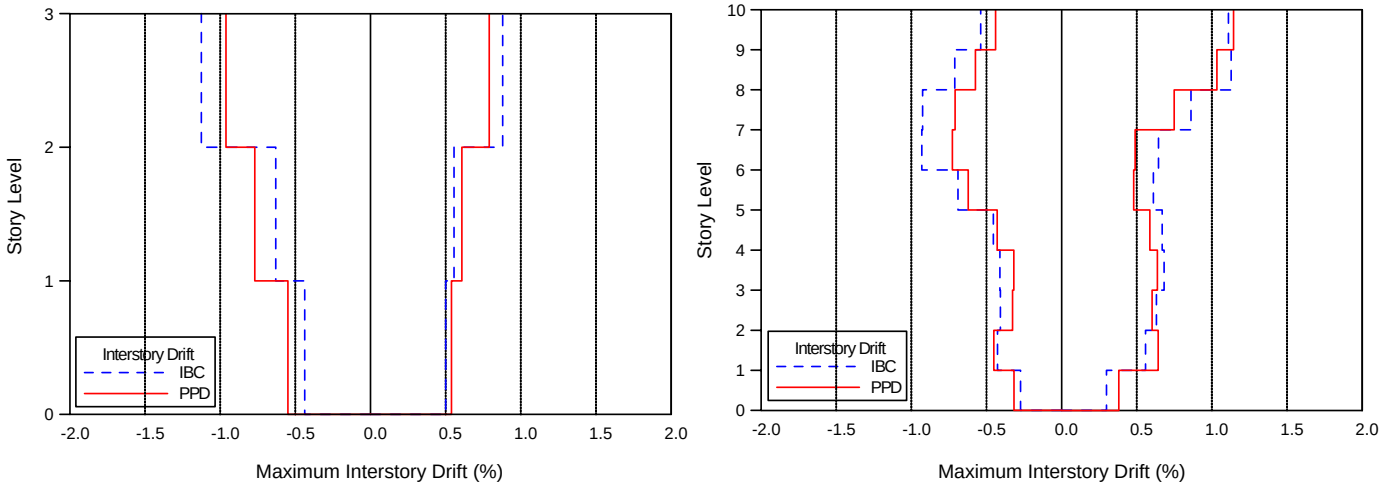

(a) (b)

Figure 5.31 Maximum interstory drift during LA 19 event: (a) 3-story frames (b) 10-story frames

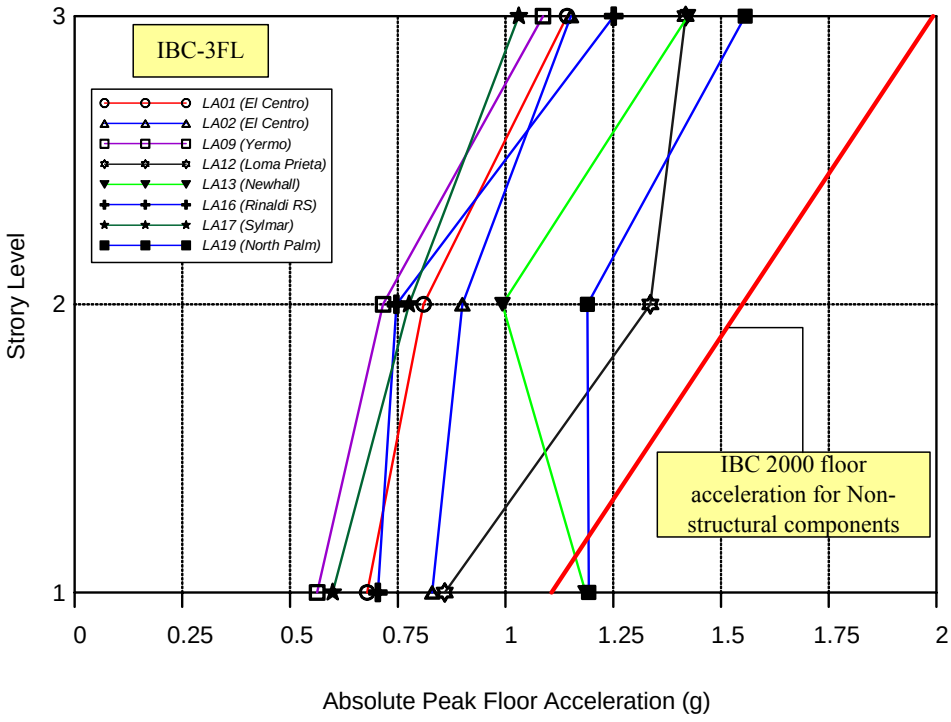

(a)

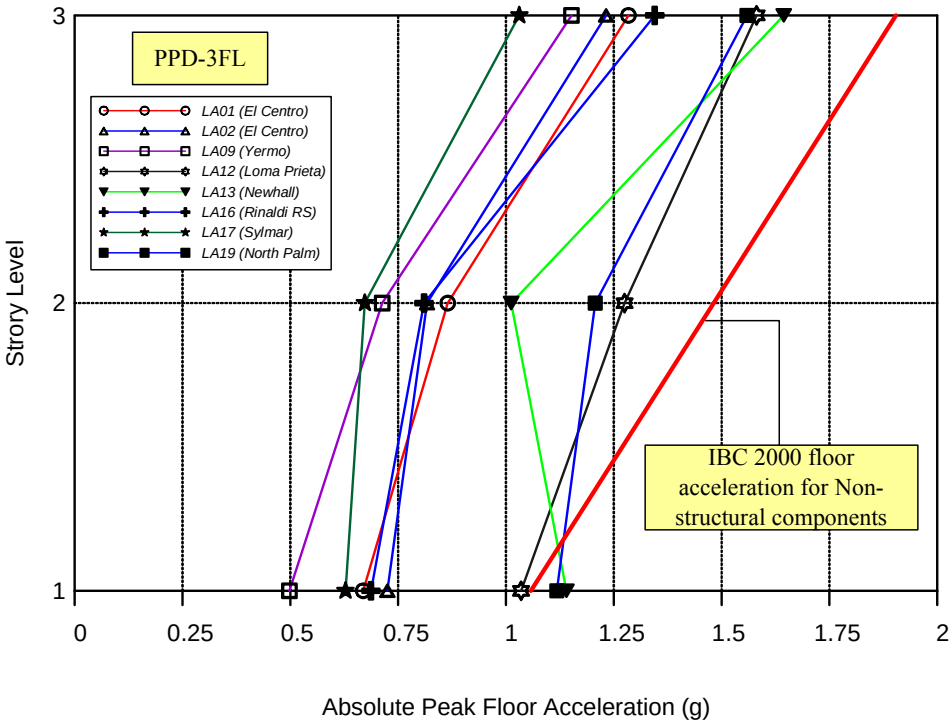

(b)

Figure 5.32 IBC 2000 design acceleration for acceleration-sensitive nonstructural components and peak floor acceleration (10% in 50 years) occurred : (a) 3-story IBC frame (b) 3-story PPD frame

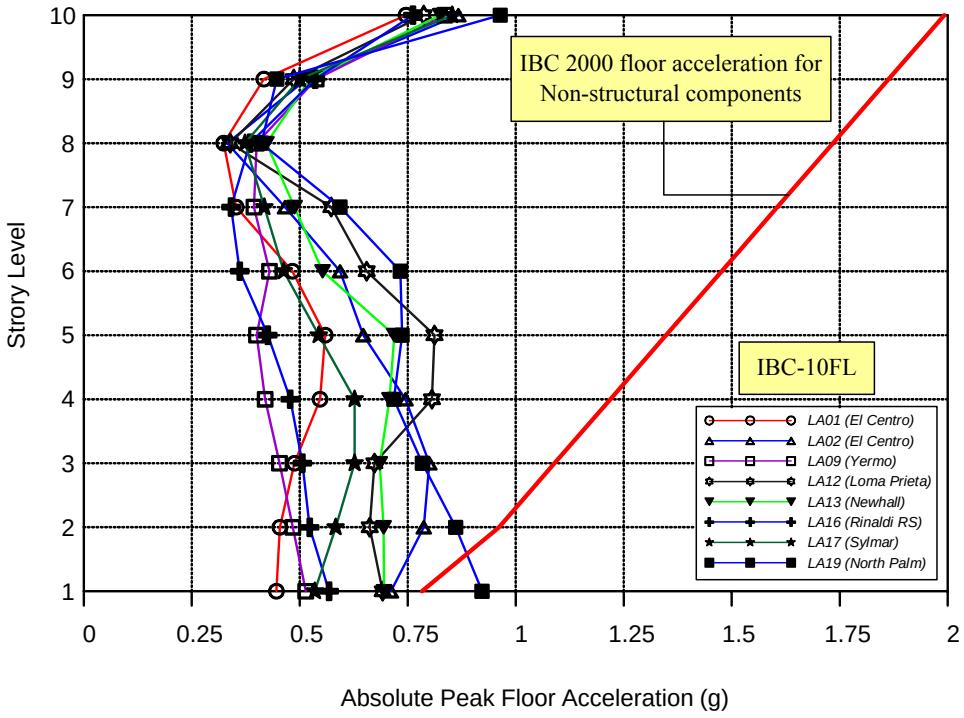

(a)

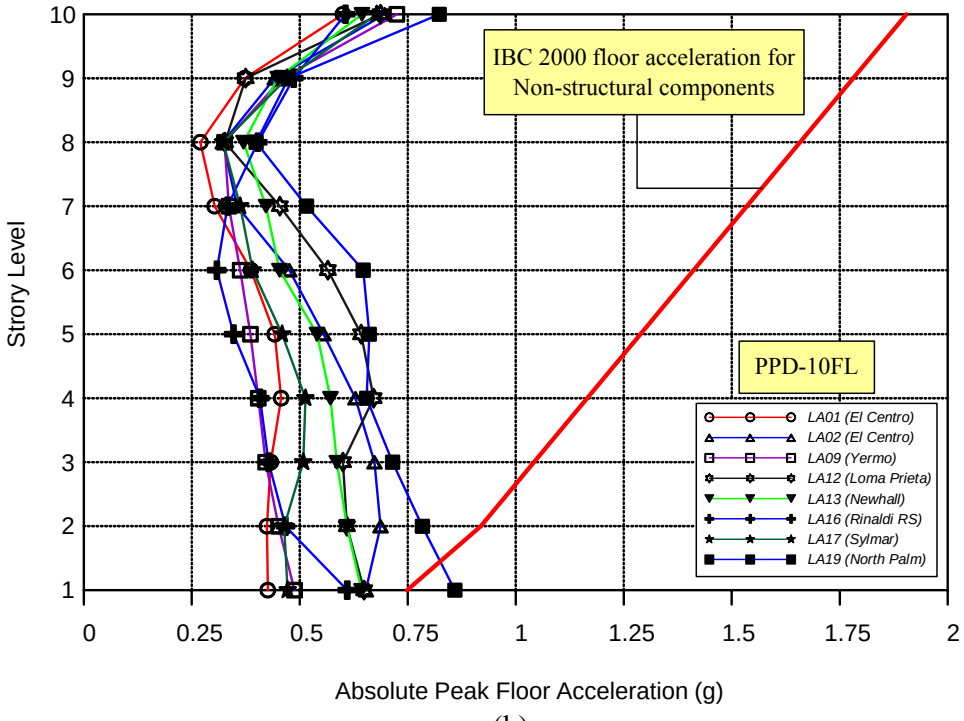

(b)

Figure 5.33 IBC 2000 design acceleration for acceleration-sensitive nonstructural components and peak floor acceleration (10% in 50 years) occurred : (a) 10-story IBC frame (b) 10-story PPD frame

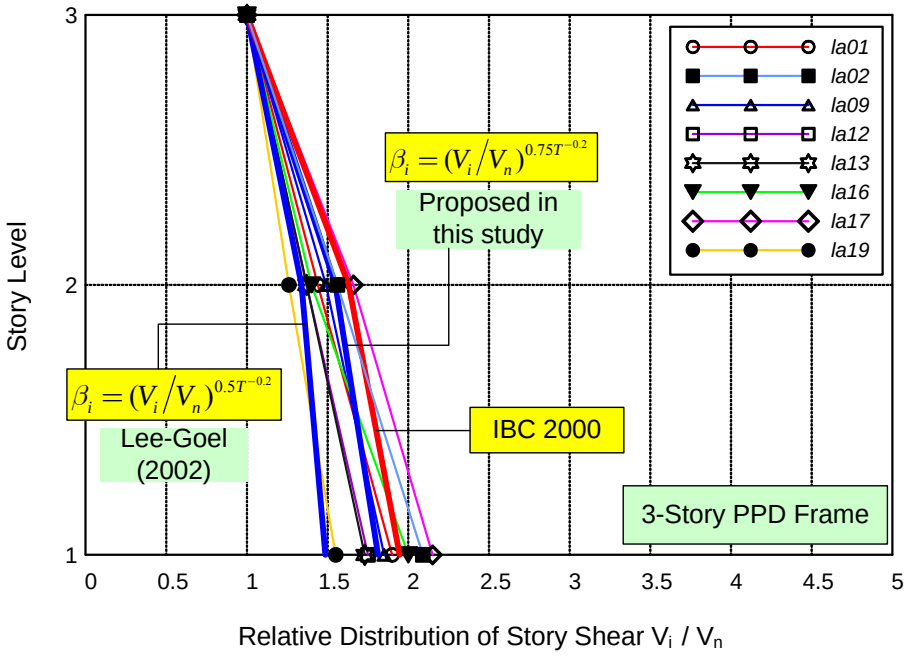

(a)

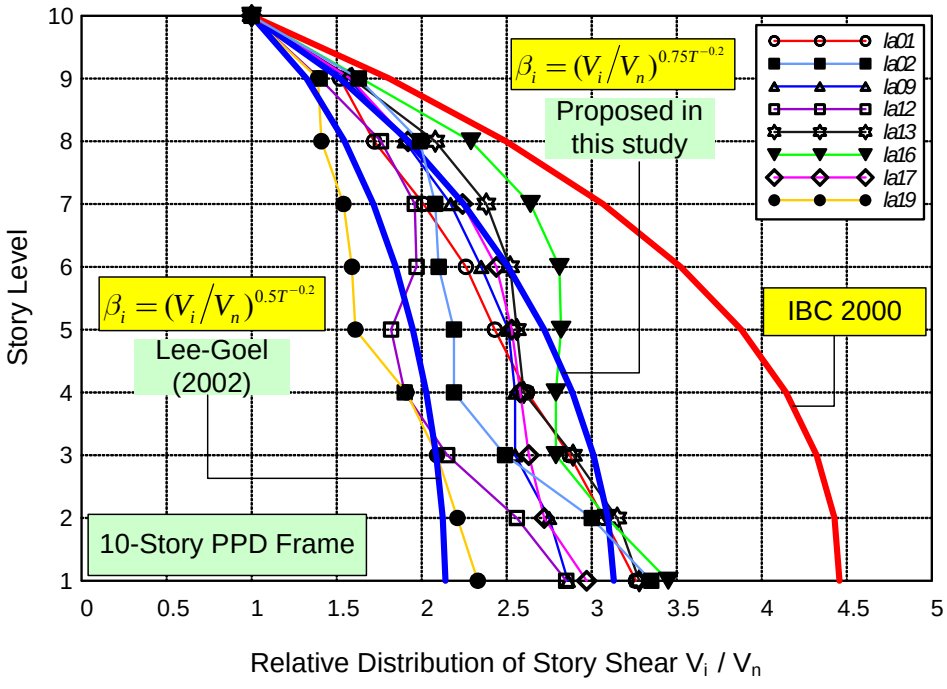

(b)

Figure 5.34 Relative story shear distributions based on nonlinear dynamic analyses: (a) 3-story PPD frame; (b) 10-story PPD frame
Note: V_i is the story shear at *i*th level, and V_n is the story shear at top level

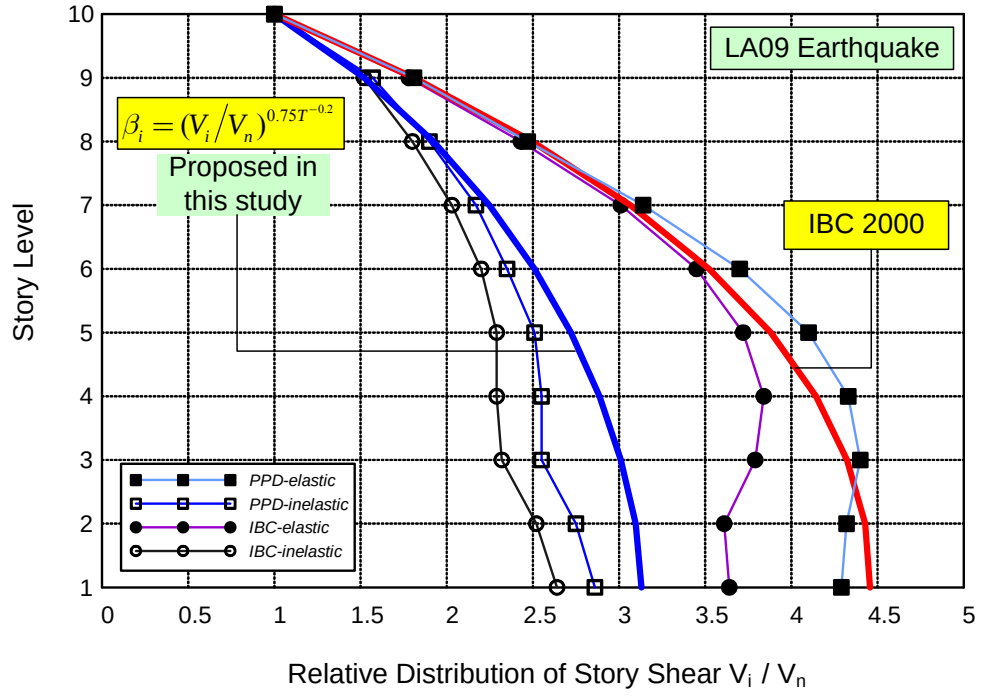

(a)

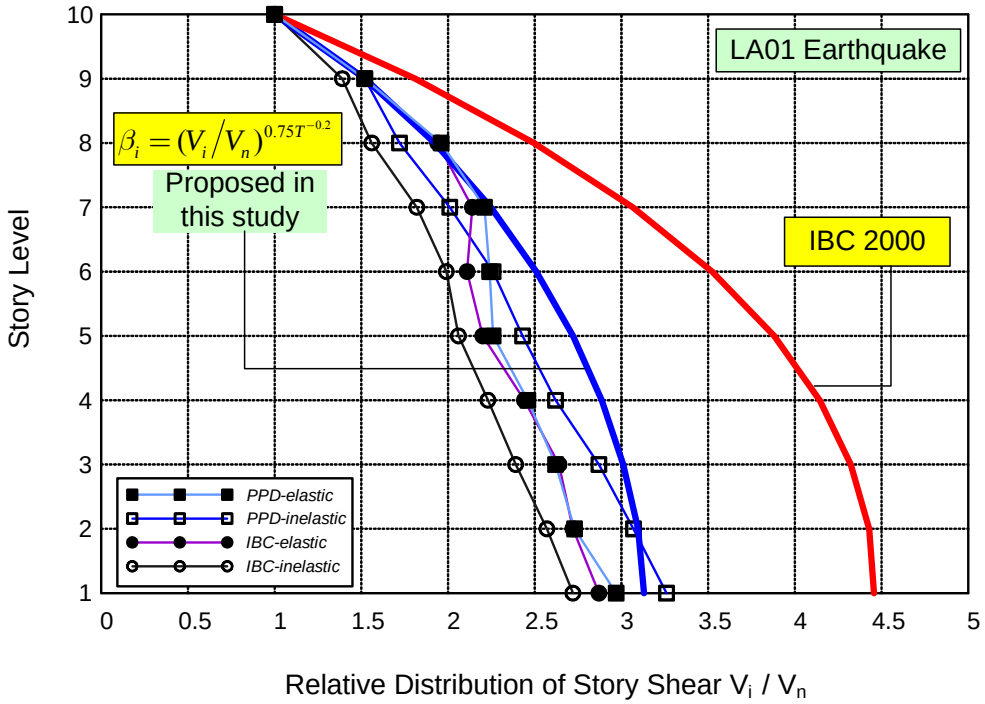

(b)

Figure 5.35 Relative story shear distributions based on linear and nonlinear dynamic analyses: (a) LA09 event; (b) LA01 event

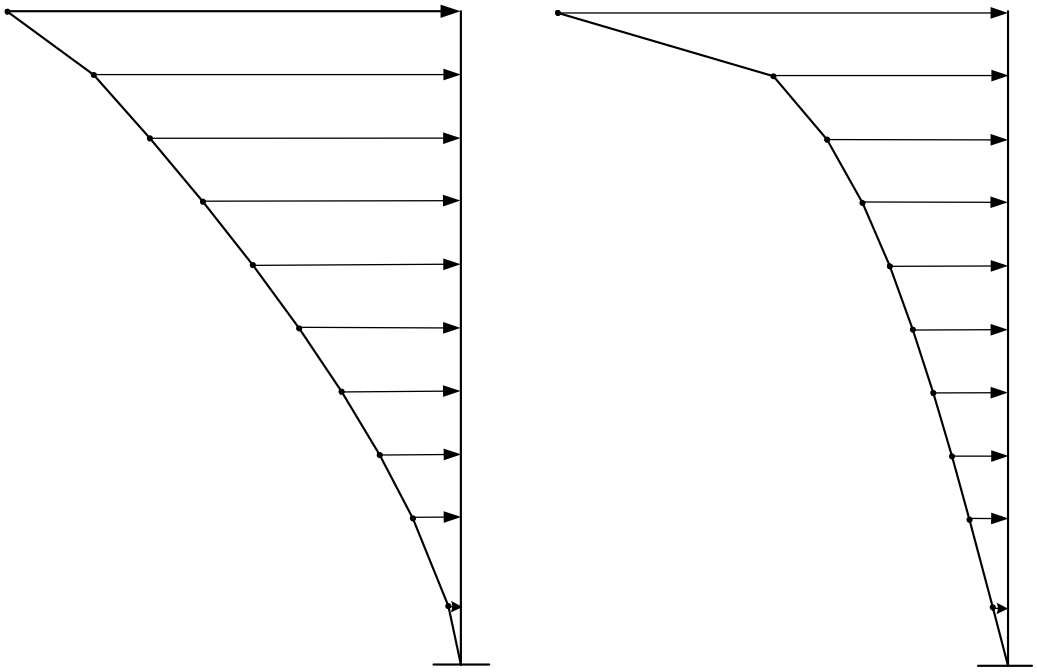

(a) IBC (b) Porposed

Figure 5.36 Seismic force distribution for study 10-story EBF: (a) IBC 2000; (b) Proposed

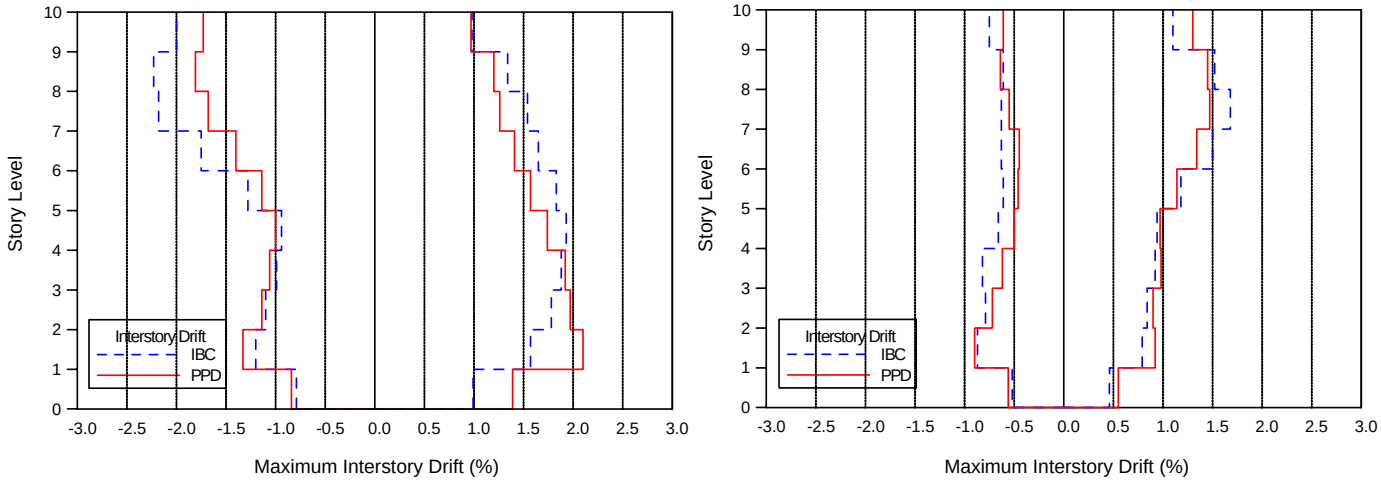

(a) LA21 event (b) LA23 event

Figure 5.37 Maximum interstory drift occurred in 10-story EBFs during 2% in 50 years earthquakes: (a) LA21 event; (b) LA23 event

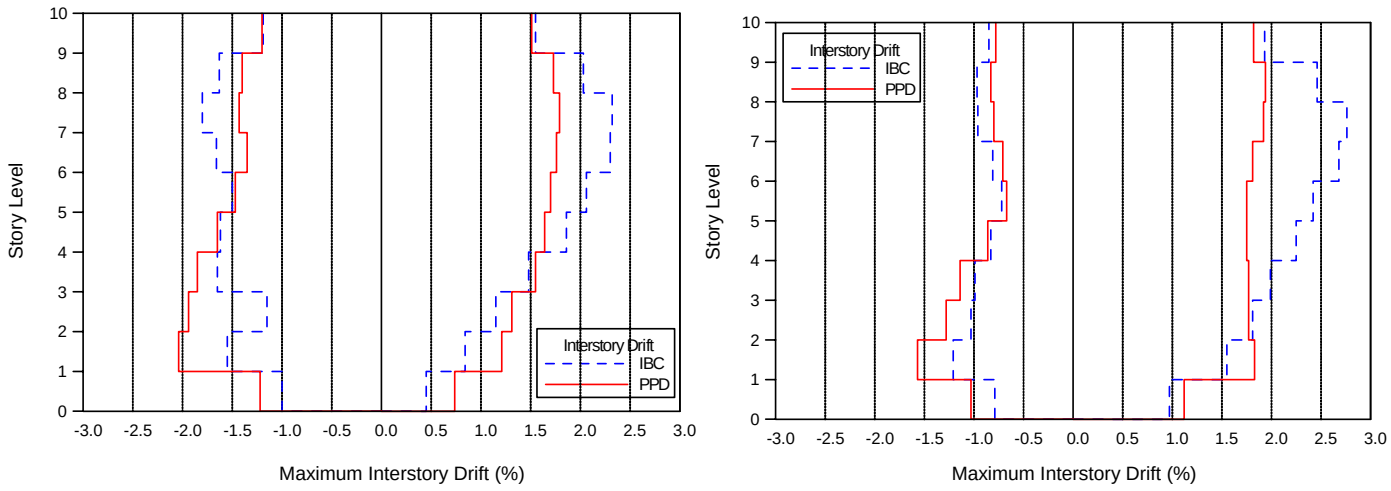

(c) LA26 event (d) LA27 event

Figure 5.37 Maximum interstory drift occurred in 10-story EBFs during 2% in 50 years earthquakes: (a) LA26 event; (b) LA27 event (con't)

CHAPTER 6
Summary and Conclusions

6.1 Summary

In current practice, the performance-based seismic design for a new structure is carried out in somewhat indirect manner. It usually starts with an initial design according to conventional elastic design procedure using applicable design codes, then perform a nonlinear static assessment analysis. Usually, iterative process between design and assessment is inevitable. Moreover, as mentioned in FEMA 440, this procedure still has difficulty in predicting reasonably accurate structural behavior during a major earthquake when compared with the results from a nonlinear dynamic analysis.

While further improvement is needed in the current practice to move towards a more reliable performance-based design philosophy, this study proposes a direct performance-based design approach which basically requires no assessment such as nonlinear static or dynamic analysis after initial design. Based on energy-balance criterion, the proposed approach gives a design base shear by using the code-specified elastic design spectral value for a given hazard level, a pre-selected global structural yield mechanism, and a pre-designated target drift. In addition, the design lateral force distribution employed in the proposed method is based on nonlinear dynamic analysis results for a number of far-field and near-field ground motions. The shear links are designed according to plastic design approach, while the members outside the links are designed by using capacity design concept. The complete detailed design procedure was

developed and various design steps were summarized in a flowchart. The entire design procedure can be easily computerized.

Four EBFs were used in this study: two EBFs (3-story and 10-story) were designed in accordance with current practice using the IBC 2000 procedure (IBC frames); the other two were obtained by redesigning those frames by using the proposed performance-based plastic design method (PPD frames). A method to take care of the stiffness irregularity in the EBFs was also presented. In order to validate the proposed design method, extensive nonlinear dynamic analyses were conducted using eight 10% in 50 years and four 2% in 50 years SAC Los Angeles region ground motions. The seismic performance of the four study frames was examined in terms of location of yielding activity, maximum link plastic rotations, maximum relative story shear distributions, maximum interstory drifts, and peak floor accelerations.

6.2 Conclusions

The following conclusions and recommendations can be drawn from the study:

1) Overall, the EBFs designed by the proposed method can be expected with good confidence to satisfy the target performance objectives when subjected to a major earthquake, and need no further assessment after the first design. This is because the performance objectives in terms of the yield mechanism and maximum drift are explicitly built into the determination of design lateral forces and design of the frame members.

2) A 0.5% yield drift for EBFs is generally reasonable to use for the proposed design method. A somewhat higher value can be used to be on the conservatism side since it will generally result higher design base shear.
3) All the inelastic activity was confined to the shear links and the column bases in PPD frames as intended. On the other hand, the inelastic activity in the IBC frames was more scattered, depending on the ground motions.
4) The maximum link plastic rotations in PPD frames were generally within the AISC limitation, and well below the maximum rotations reached in the UTA tests. Moreover, the 10-story PPD frame showed more uniformly distributed plastic rotations along the height. On the other hand, in the IBC frame, although most maximum link plastic rotations at each floor were well below the AISC limitation, the plastic rotations at upper floors tended to increase suddenly and exceeded the 0.08 radian limitation during some of ground motions. The roof level links exhibited only minor yielding.
5) The maximum interstory drifts in the PPD frames were within the 2% pre-selected target drift for all the selected 10% in 50 years ground motions, signifying that the seismic performance of the deformation-sensitive components can be controlled by the proposed design procedure.
6) The maximum absolute floor accelerations were generally below the code-specified floor design acceleration, indicating that the seismic performance of the acceleration-sensitive components can also be assumed to be satisfactory. It is also evident that the acceleration-sensitive components in a low-rise EBF are more vulnerable than in a high-rise EBF.
7) Generally, the proposed design story shear distribution represents the envelope story shear distribution of the structure due to the ground motion records used in this study very well,

because it is based on inelastic behavior. On the contrary, the code-specified force distribution, although it includes the higher mode effect, does not represent the realistic maximum story shear distribution during a major earthquake which causes the structures to respond inelastically.

8) It was clearly shown that the proposed procedure can be easily used to achieve the multilevel design goals as required in PBEE.

9) The results also showed that the EBFs can be designed by using the proposed methodology to result in the pre-selected target performance without any increase in the material weight.

BIBLIOGRAPHY

AISC. (2000), "Load and Resistance Factor Design Specification for Steel Hollow Structural Sections," American Institute of Steel Construction, Chicago, Illinois.

AISC. (2001), "Load and Resistance Factor Design Specification for Structural Steel Buildings," 3rd edition, American Institute of Steel Construction, Chicago, Illinois.

AISC. (2002), "Seismic Provisions for Structural Steel Building ," American Institute of Steel Construction, Chicago, Illinois.

Akiyama, H. (1985), "Earthquake-Resistant Limit-State Design of Buildings." University of Tokyo Press, Japan.

Arce, G. (2002), "Impact of Higher Strength Steels on Local Buckling and Overstrength of Links in Eccentrically Braced Frames," Master's Thesis, Department of Civil Engineering, University of Texas at Austin, Austin, TX.

Arce, G., Okazaki, T., and Engelhardt, M. D. (2003), "Experimental Behavior of Shear and Flexural Yielding Links of ASTM A992 Steel," STESSA 2003, Behavior of Steel Structures in Seismic Areas, 107-113.

ASCE. (2000), "Prestandard and Commentary for the Seismic Rehabilitation of Buildings," FEMA 356 Report, prepared by the American Society of Civil Engineers, published by Federal Emergency Management Agency, Washington, D. C.

ATC. (1996), "Seismic Evaluation and Retrofit of Concrete Buildings," ATC-40 Report, Vol. 1&2, Applied Technology Council, Redwood City, California.

ATC. (2004), "Improvement of Nonlinear Static Seismic Analysis Procedures (Draft)," FEMA 440 Report, Applied Technology Council, Redwood City, California and Federal Emergency Management Agency, Washington, D. C.

Becker, R., and Ishler, M. (1996), "Seismic Design Practice For Eccentrically Braced

Frames—Based on The 1994 UBC," Steel Tips, American Institute of Steel Construction, Chicago, Illinois.

Bolt, B. A. (2004), "Engineering Seismology," Earthquake Engineering—from engineering seismology to performance-based engineering, Bozorgni, Y., and Bertero, V. V. ed., CRC Press,

Bruneau, M., Uang, C. -M., and Whittaker, A. (1998), "Ductile Design of Steel Structures", McGraw-Hill.

Engelhardt, M. D. and Popov, E. P. (1989a), "Behavior of Long Links in Eccentrically Braced Frames," Report No. UCB/EERC-89/01, Earthquake Engineering Research Center, University of California at Berkeley.

Engelhardt, M. D. and Popov, E. P. (1989b), "On Design of Eccentrically Braced Frames," Earthquake Spectra, Vol. 5, No. 3, 495-511.

Engelhardt, M. D. and Popov, E. P. (1992), "Experimental Performance of Long Links in Eccentrically Braced Frames," Journal of Structural Engineering, ASCE, 118 (11), 3067-3088.

Englekirk, R. (1994), "Steel Structures, Controlling Behavior Through Design," John Wiley & Sons.

Foutch, D. A. (1989), "Seismic Behavior of Eccentrically Braced Steel Building," Journal of Structural Engineering, ASCE, 115 (8), 1857-1876.

Gálvez, P. (2004), "Investigation of Factors Affecting Web Fractures in Shear Links," Master's Thesis, Department of Civil Engineering, University of Texas at Austin, Austin, TX

Ghobarah, A. and Ramadan, T. (1990), "Effect of Axial Forces on the Performance of links in eccentrically braced frames," Engineering Structures, v 12, April, 106-113.

Goel, S. C., and Leelataviwat, S. (1998), "Seismic Design by Plastic Method," Engineering Structures, Elsevier Science, 20 (4-6), 465-471.

Hamburger, R., Rojahn, C., Moehle, J., Bachman, R., Comartin, C., and Whittaker, A. (2004), "The ATC-58 Project: Development of Next-Generation Performance-Based Earthquake

Engineering Design Criteria for Buildings, 13th World Conference on Earthquake Engineering, Paper No. 1819, Vancouver, B. C., Canada.

Hassan, O. and Goel, S. C. (1991), "Seismic Behavior and Design of Concentrically Braced Steel Structures," Report No. UMCEE 91-1, Department of Civil and Environmental Engineering, University of Michigan, Ann Arbor, MI.

Hjelmstad, K. D. and Popov, E. P. (1983a), "Seismic Behavior of Active Beam Links in Eccentrically Braced Frames," Report No. UCB/EERC-83/15, Earthquake Engineering Research Center, University of California at Berkeley.

Hjelmstad, K. D. and Popov, E. P. (1983b), "Cyclic Behavior and Design of Link Beams," Journal of Structural Engineering, ASCE, 109 (10), 2387-2403.

International Code Council (ICC) (2000), "International Building Code," ICC, Birmingham, AL.

International Code Council (ICC) (2003), "International Building Code," ICC, Birmingham, AL.

Kasai, K. and Popov, E. P. (1986a), "A Study of Seismically Resistant Eccentrically Braced Steel Frame Systems," Report No. UCB/EERC-86/01, Earthquake Engineering Research Center, University of California at Berkeley.

Kasai, K. and Popov, E. P. (1986b), "General Behavior of WF Steel Shear link Beams," Journal of Structural Engineering, ASCE, 112 (2), 362-382.

Krawinkler, H. and Miranda, E. (2004), "Performance-Based Earthquake Engineering," Earthquake Engineering—from Engineering Seismology to Performance-Based Engineering, Edited by Bozorgnia, Y. and Bertero, V. V., CRC Press.

Lee, H. S. (1996), "Revised Rule for Concept of Strong-Column Weak-Girder Design," Journal of Structural Engineering, ASCE, 122 (4), 359-364.

Lee, S. S. and Goel, S. C. (2001), "Performance-Based Design of Steel Moment Frames Using Target Drift and Yield Mechanism," Report No. UMCEE 01-17, Department of Civil and Environmental Engineering, University of Michigan, Ann Arbor, MI.

Lee, S. S., Goel, S. C., and Chao, S. H. (2004), "Performance-Based Design of Steel Moment Frames Using Target Drift and Yield Mechanism," Proceedings, 13th World Conference on Earthquake Engineering, Paper No. 266, Vancouver, B. C., Canada.

Leelataviwat, S., Goel, S. C., and Stojadinović, B. (1998a), "Drift and Yield Mechanism Based Seismic Design and Upgrading of Steel Moment Frames," Report No. UMCEE 98-29, Department of Civil and Environmental Engineering, University of Michigan, Ann Arbor, MI.

Leelataviwat, S., Goel, S. C., and Stojadinović, B. (1998b), "Seismic design by plastic method," Engineering Structures, v 20 n 4-6 Apr-Jun, 465-471

Leelataviwat, S., Goel, S. C., and Stojadinović, B. (1999), "Toward Performance-Based Seismic Design of Structures," Earthquake Spectra, Vol. 15, No. 3, 435-461.

Malley J. O. and Popov, E. P. (1983), "Design Considerations for Shear Links in Eccentrically Braced Frames," Report No. UCB/EERC-83/24, Earthquake Engineering Research Center, University of California at Berkeley.

Malley J. O. and Popov, E. P. (1983), "Shear Links in Eccentrically Braced Frames," Journal of Structural Engineering, ASCE, 110 (9), 2275-2295.

Manheim, D. N. (1982), "On the Design of Eccentrically Braced Frames," Thesis, D. Eng, Department of Civil Engineering, University of California at Berkeley.

McDaniel, C. C., Uang, C. M., and Seible, F. (2003), "Cyclic Testing of Built-Up Steel Shear Links for the New Bay Bridge," Journal of Structural Engineering, ASCE, 129 (6), 801-809.

Naeim, F. (1995), "On Seismic Design Implication of the 1994 Northridge Earthquake Records," Earthquake Spectra, EERI, 11 (1), 91-109.

NEHRP (2001), "Recommended Provisions for the Development of Seismic Regulations for New Buildings (FEMA 368)," Federal Emergency Management Agency, Washington, D. C.

NEHRP (2001), "Commentary on Recommended Provisions for the Development of Seismic Regulations for New Buildings (FEMA 369)," Federal Emergency Management Agency, Washington, D. C.

Okazaki, T., Arce, G., Ryu, H. C., and Engelhardt, M. D. (2004), "Recent Research on Link Performance in Steel Eccentrically Braced Frames," 13th World Conference on Earthquake Engineering, Vancouver, B. C., Canada, August 1-6, Paper No. 302.

Paulay, T. and Priestley, M.J.N. (1992), "Seismic design of reinforced concrete and masonry buildings," Wiley, New York.

Popov, E. P., Ricles, J. M., and Kasai, K. (1992), "Methodology for optimum EBF Link Design," Proceedings, Tenth World Conference of Earthquake Engineering, Vol. 7, Balkema, Rotterdam, 3983-3988.

Popov, E. P., Kasai, K., and Engelhardt, M. D. (1987), "Advances in Design of Eccentrically Braced Frames," Earthquake Spectra, Vol. 3, No. 1, 43-55.

Rai, D. C. (2000), "Future Trends in Earthquake-Resistant Design of Structures," special section: seismology, Current Science, Vol. 79, No. 9, 10 Nov. 1291-1300.

RAM International. (2003), "Perform-3D User Guide"

Richards, P. W. and Uang, C. M. (2003), "Development of Testing Protocol for Short Links in Eccentrically Braced Frames," Report No. SSRP-2003/08, Department of Structural Engineering, University of California, San Diego, La Jolla, CA.

Richards, P. W. (2004), "Cyclic Stability and Capacity Design of Steel Eccentrically Braced Frames," Ph. D Dissertation, Department of Structural Engineering, University of California, San Diego, La Jolla, CA.

Ricles, J. M. and Popov, E. P. (1987), "Experiments on Eccentrically Braced Frames with Composite Floors," Report No. UCB/EERC-87/06, Earthquake Engineering Research Center, University of California at Berkeley.

Ricles, J. M. and Popov, E. P. (1994), "Inelastic Link Element for EBF Seismic Analysis," Journal of Structural Engineering, ASCE, 120 (2), 441-463.

Roeder, C. W. and Popov, E. P. (1977), "Inelastic Behavior of Eccentrically Braced Steel Frames

Under Cyclic Loadings," Report No. UCB/EERC-77/18, Earthquake Engineering Research Center, University of California at Berkeley.

Roeder, C. W., Foutch, D. A., and Goel, S. C. (1987), "Seismic Testing of Full-Scale Steel Building—Part II," Journal of Structural Engineering, ASCE, 113 (11), 2130-2145.

Schneider, S. P., Roeder, C. W., and Carpenter, J. E. (1993), "Seismic Behavior of Moment-Resisting Steel Frames: Experimental Study," Journal of Structural Engineering, ASCE, 119 (6), 1885-1902.

SEAOC (1999), "Recommended Lateral Force Requirements and Commentary," Seismology Committee of Structural Engineers Association of California, Sacramento, California, Seventh Edition.

SEAOC (2000), "Seismic Design Manual—Building Design Examples: Steel, Concrete, and Cladding," Volume III, Seismology Committee of Structural Engineers Association of California, Sacramento, California.

Somerville, P. G., Smith, M., Punyamurthula, S., and Sun, J. (1997), "Development of Ground Motion Time Histories for Phase 2 of the FEMA/SAC Steel Project, Report No. SAC/BD-97/04, SAC Joint Venture, Sacramento, CA.

Tang, X. and Goel, S. C. (1989), "Seismic Analysis and Design Considerations of Braced Steel Structures," Report No. UMCEE 87-4, Department of Civil and Environmental Engineering, University of Michigan, Ann Arbor, MI.

Uang, C.-M. and Bertero, V.V. (1988), "Use of Energy as a Design Criterion in Earthquake-Reistant Design." Report No. UCB/EERC-88/18, Earthquake Engrg. Res. Ctr., University of California, Berkeley, CA, USA.

Uang, C. M., Bruneau, M., Whittaker, A. S., and Tsai, K. C. (2001), "Seismic Design o Steel Structures," The Seismic Design Handbook, 2nd edition, Kluwer Academic Publishers, 409-462.

Villaverde, R. (2004), "Seismic Analysis and Design of Nonstructural Elements," Earthquake Engineering—from Engineering Seismology to Performance-Based Engineering, Edited by Bozorgnia, Y. and Bertero, V. V., CRC Press.

Yang, M.- S. (1982), “Seismic Behavior of An Eccentrically X-Braced Steel Structure,” Report No. UCB/EERC-82/14, Earthquake Engineering Research Center, University of California at Berkeley.

Zoruba, S. and Grubb, K. A. (2003), “Do you 992?” Modern Steel Construction, AISC, January, 43-44.